INVESTIGATION ON THE CELLULAR AND NEUROPROTECTIVE FUNCTIONS OF NOGO-A/RETICULON 4A

TENG YU HSUAN FELICIA
(B.Sc. (Hons.)), NUS

A THESIS SUBMITTED
FOR THE DEGREE OF DOCTOR OF PHILOSOPHY
DEPARTMENT OF BIOCHEMISTRY
NATIONAL UNIVERSITY OF SINGAPORE
2010

Acknowledgements

My most sincere thanks goes to my supervisor, A/P Tang Bor Luen, for his guidance, encouragement, criticisms and also financial support throughout these years.

I like to also express my appreciation to A/P Marie-Veronique Clement and Dr Deng Lih Wen for being my thesis advisory committee members.

Heartfelt thanks goes to the pioneers of this project, Dr Liu Haiping and Dr Cherry Ng Ee Lin, and also my ex-labmates who have worked alongside with me in this project, especially Ms Belinda Ling Mei Tze who has generated some of the Nogo-A truncation constructs, and Ms Low Choon Bing and Ms Selina Aulia who assisted in maintaining our Nogo-deficient mouse colony.

I am truly grateful to my fellow colleagues, especially Dr Ng Ee Ling and Ms Chen Yanan for their inspiration, friendship and discussions.

I would also like to extend my thanks to my neighbouring lab's colleagues, especially Dr Sharon Lim, Ms Luo Le, Ms Teong Huey Fern and Dr Michelle Chang Ker Xing, for sharing their expertise and reagents with me.

Lastly but most importantly, my deepest gratitude goes to my fantastic husband, my adorable son and my dearest family for their endless support and encouragement.

Table of Contents

Summary

Nogo/RTN4 belongs to the Reticulon (RTN) family, which comprises of four members, RTN 1-4. There are three major splice isoforms of *Nogo/Rtn4*, namely Nogo-A, -B and -C. Nogo is first discovered as a myelin-associated neurite outgrowth inhibitor localized at the oligodendrocytes where it interacts with its neuronal receptor, NgR, to elicit its neurite growth inhibitory effect. However, the endogenous physiological role of Nogo has remained unknown.

In our studies, we have generated specific antibodies against Nogo-A, showed that it is enriched in the paranodal region, and that it interacts with the neuronal axon-glial junction protein Caspr. Nogo-A's interaction with Caspr implied a function at the axon-glial junction, but comparative analysis did not reveal significant changes in the structural organization of the node in Nogo-deficient mice. Nogo-A also interacts with RTN3, another member of the RTN family. We demonstrated that this interaction is stronger than Nogo-A's low affinity to RTN1 and RTN2, and have molecularly dissected the interaction domains involved in Nogo-A-RTN3 interaction.

As Nogo-A levels are elevated in neurons (but not oliodendrocytes) in brain injuries and ischemia, we investigated if elevated Nogo-A could have a neuroprotective effect. Moderate Nogo-A expression could protect SH-SY5Y neuroblastoma cells against a myriad of pro-apoptotic stimuli such as H_2O_2, serum deprivation, staurosporine and etoposide. Tunicamycin-induced cell death, however, is enhanced by Nogo-A expression. The same effects are also observed by Nogo-B expression. On the other hand, while Nogo-C and RTN3 confer some degree of protection against serum deprivation, staurosporine and etoposide, they are not effective against apoptosis induced by H_2O_2.

Stable Nogo-A expression does not intrinsically induce upregulation of anti-apoptotic proteins such as Bcl-2 and Bcl-xL, but instead causes downregulation of pro-apoptotic Bid truncation and AIF. Nogo-A expression also increases the basal levels of total and activated Bax. This correlates with increased basal levels of activated caspase-3. Indicators of the unfolded protein response (UPR), one type of ER stress responses, are, however, not significantly elevated. Focusing on H_2O_2 induction of cell death, we investigated on the possible neuroprotective mechanisms of Nogo-A. We show that Akt and Erk are not necessary for Nogo-A's protective effect against H_2O_2. Any UPR-based preconditioning is also found not to be accountable for Nogo-A's protection. Interestingly, Nogo-A expression is able to attenuate caspase-3 and -9 activation upon H_2O_2 treatment. This implies that Nogo-A may protect by the attenuation of the intrinsic pathway and the subsequent caspase-dependent apoptosis. We also observe some differences in terms of nuclear translocation of p65/RelA subunit of NF-κB between the Nogo-A expressing and control cells, which may, at least partly, contribute to Nogo-A's neuroprotective function.

The work presented in this thesis provided insights into possible cell autonomous functions of Nogo-A other than its role in neurite outgrowth inhibition. In line with earlier observations that Nogo-A is elevated during brain injury, Nogo-A may thus have a role as a component of the neuron's injury response and survival preservation mechanism.

List of Publications

Teng F.Y. and Tang B.L. (2010) Rtn3 and Nogo/Rtn4 isoforms expression protects SH-SY5Y cells against multiple death insults. *(manuscript in preparation)*

Teng F.Y. and Tang B.L. (2008) Cell autonomous function of Nogo and reticulons – the emerging story at the endoplasmic reticulum. J. Cell. Physiol., 216: 303-308.

Teng F.Y. and Tang B.L. (2006) Axonal regeneration in adult CNS neurons – signaling molecules and pathways. J. Neurochem., 96: 1501-1508.

Teng F.Y., Lim B.M.T. and Tang B.L. (2004) Inter- and intracellular interactions of Nogo: new findings and hypothesis. J. Neurochem., 89: 801-806.

List of Figures

List of Abbreviations

aa	amino acid
AD	Alzheimer's disease
AIF	apoptosis inducing factor
AFC	7–amino–4–trifluoromethylcoumarin
ALS	Amyotrophic lateral sclerosis
APP	amyloid precursor protein
ATCC	American Type Culture Collection
ATP	adenosine triphosphate
Aβ	β-amyloid
BACE1	β-site amyloid precursor protein cleaving enzyme 1
Bcl-2	B-cell lymphoma protein-2
bp	base pair
BSA	bovine serum albumin
cDNA	complementary DNA
CDS	coding sequence
c-FLIP	cellular FLICE-like inhibitory protein
CHO	Chinese hamster ovary
CNPase	2', 3'-cyclic nucleotide 3'-phosphodiesterase
CNS	central nervous system
CO_2	carbon dioxide
co-IP	co-immunoprecipitation
CREB	cAMP response element-binding protein
CRELD1	cysteine rich with EGF like domains 1

CSF	cerebrospinal fluid
CSPGs	chondroitin sulphate proteoglycans
CST	corticospinal tract
DG	dentate gyrus
DIV	days *in vitro*
DMEM/F12	Dulbecco's Modified Eagle Medium: Nutrient Mixture F-12
DNA	deoxyribonucleic acid
dNTPs (A, T, G ,C)	deoxyribonucleotide triphosphates (adenine, thymine, guanine, cytosine)
DP1	deleted in polyposis
DR5	death receptor 5
DRG	dorsal root ganglion
Drs	downregulated by v-*src*
DTT	dithiothreitol
E7	embryonic day 7
E.coli	*Escherichia coli*
EAE	experimental autoimmune encephalomyelitis
EDTA	ethylenediaminetetraacetic acid
EGFR	epidermal growth factor receptor
EOR	ER overload response
ER	endoplasmic reticulum
EST	expressed sequence tag
FADD	Fas-associated death domain protein
FBS	fetal bovine serum
FITC	fluorescein isothiocyanate

GFAP	glial fibrillary acidic protein
GPCR	G protein-coupled receptor
GPI	glycosylphosphatidylinositol
GRP94	glucose regulated protein 94
GST	glutathione S-transferase
H_2O_2	Hydrogen peroxide
HA	hemagglutinin
HEK	Human embryonic kidney
HRP	horse radish peroxidase
Hsp	heat shock protein
IACUC	Institutional Animal Care and Use Committee
ICC	immunocytochemistry
Ig	immunoglobulin
IHC	immunohistochemistry
IP_3	inositol 1,4,5-triphosphate
IPTG	isopropyl-β-D-thiogalactopyranoside
JNK	Janus N-terminal kinase
kDa	kilodaltons
LB	Luria-Bertani Broth
LGI1	LRR protein leucine-rich glioma inactivated
LILRB2	leukocyte immunoglobulin (Ig)-like receptor B2
LINGO-1	LRR and Ig domain-containing, Nogo Receptor-interacting Protein
LRR	leucine-rich-repeat
MAG	myelin-associated glycoprotein

MANI	Myelin-Associated Neurite-outgrowth Inhibitor
MBP	myelin basic protein
MEM	minimum essential medium
MGC	Mammalian Gene Collection
mRNA	messenger RNA
MS	Multiple sclerosis
NE	nuclear envelope
NF 155	155-kDa isoform of neurofascin
NF-kB	nuclear factor κB
NIH	National Institutes of Health
NSCs	neural stem cells
NSP	neuroendocrine-specific protein
NUS	National University of Singapore
O.C.T.	Optimum Cutting Temperature
OMgp	oligodendrocyte myelin glycoprotein
P1-2	postnatal day 1-2
PARP	Poly (ADP-ribose) polymerase
PBS	phosphate buffered saline
PCR	polymerase chain reaction
PDI	protein dismutase isomerase
PERK	protein kinase R-like ER kinase
PF	paraformaldehyde
PI	propidium iodide
PI3K	phosphoinositol-3-kinase
PKC	protein kinase C

PLL	poly-L-lysine
PMSF	phenylmethylsulphonyl fluoride
PNS	peripheral nervous system
PTEN	phosphatase-and-tensin homolog
RE	restriction enzyme
RFU	relative fluorescence units
RHD	reticulon homology domain
Rho-GDI	Rho GDP dissociation inhibitor
ROCK	Rho-associated protein kinase
ROS	reactive oxygen species
RNA	ribonucleic acid
RPMI	Roswell Park Memorial Institute
RTN	reticulon
SALMs	synaptic adhesion-like molecules
sd	standard deviation
SDS	sodium dodecyl sulphate
SDS-PAGE	sodium dodecyl sulphate polyacrylamide gel electrophoresis
siRNA	small interfering ribonucleic acid
SOD	Cu-Zn superoxide dismutase
SPF	specific pathogen free
TACE	TNFα converting enzyme
tBid	truncated Bid
TEMED	N, N, N, N-Tetramethy-Ethylenediamine
TM	transmembrane
TNF	tumour necrosis factor

TRAIL	TNF-related apoptosis-inducing ligand
Tx-100	Triton X-100
TxR	Texas Red
UPR	unfolded protein response
V	volt

Chapter 1 Introduction

1.1 Discovery of Nogo-A: an inhibitor of neuronal regeneration

1.1.1 Neuronal regeneration is limited in adult CNS

Adult mammalian central nervous system (CNS) has been notoriously known by its inefficiency to regenerate and self-repair. This inability is especially crucial in situations where the CNS is ‘damaged', like in physical injuries such as spinal cord injuries and brain trauma, or in non-physical ones such as neurodegenerative diseases. As axons are usually severed or degenerated in these instances, recovery of function is therefore greatly dependent on the ability of the axons to regenerate. Patients who suffer from physical severing of axons may have to endure with paralysis for the rest of their lives, while those who suffer from neurodegenerative disorders will gradually lose either or both of their sensory and motor functions, and eventually premature death. Exceptions may only be observed in specific pathways, such as those in the hippocampus (Chauvet *et. al.*, 1998) and olfactory bulb (Monti *et. al.*, 1980; Morrison and Costanzo, 1995). In contrast, the adult peripheral nervous system (PNS), the other nervous system in the body, is more than capable of regeneration. When a PNS neuron is severed, its axon is able to regenerate, and in many cases, able to reinnervate target tissues.

There are two possibilities for the differing regenerative capacities of the two nervous systems. One reason could be that CNS neurons are intrinsically incapable of regeneration as compared to PNS ones. However, this notion appears not to be entirely true. Ramón y Cajal, commonly regarded as ‘the father of neuroscience’ and the one who coined the term ‘neuronal plasticity’, observed that CNS neurons were not intrinsically unable to regenerate but exhibited only limited regeneration (Ramón,

1928). Another report showed that the CNS branch of dorsal root ganglion (DRG) axons had better growth capacity after preconditioning lesions were carried out, which also suggests that CNS neurons are intrinsically capable of regenerating (Neumann and Woolf, 1999).

A second plausible reason for the lack of regeneration in the CNS is that the environment in CNS is growth-inhibitory and not growth-promoting. It became evident that the tissue environment indeed played a crucial role during regeneration, with studies showing injured CNS neurons, although unable to regenerate when in a CNS environment, being able to do so in the presence of a peripheral nerve environment when PNS grafts were inserted into different regions of the CNS (Dam-Hieu et. al., 2002; David and Aguayo, 1981; Richardson *et. al.*, 1980; Schwab and Thoenen, 1985). Schwab and Thoenen (1985) observed that newborn rat sympathetic or sensory neurons, when placed in the middle of a three-compartment chamber with sciatic and optic nerve explants on either side, were able to grow out of the former but not the latter. This observation convincingly demonstrated the non-permissive substrate conditions that pervade the CNS. This was performed in the presence of optimal amounts of nerve growth factor, which suggested that a lack of trophic factors in CNS was at least not the major reason for the lack of regeneration in CNS.

1.1.2 The adult CNS environment is non-permissive to neuronal growth and regeneration

It has been suggested that after CNS injury, glial scars which serve to contain the wound site and confine inflammation and cellular degeneration (Faulkner *et. al.*, 2004), also inevitably act as a mechanical barrier that prevents axonal growth and reconnection (Ramón, 1928; Reier *et. al.*, 1983; Silver and Miller, 2004). Neurite

outgrowth was inhibited in studies using *in vitro* glial scar models, thus confirming that the presence of glial scars formed during CNS injury does play a role in limiting axonal regeneration (Rudge and Silver, 1990; Wanner *et. al.*, 2008). When injury is inflicted in the CNS, proliferation and activation of astrocytes (astrogliosis) in the vicinity of the injury site occur, together with the recruitment of other cell types such as the microglia, oligodendrocyte precursors and meningeal cells to the injury site. This eventually resulted in the formation of a glial scar (Fig 1.1).

The reactive astrocytes present at the glial scar become hypertrophic and secrete extracellular matrix molecules collectively known as chondroitin sulphate proteoglycans (CSPGs) (including molecules such as aggrecan, brevican, versican and NG2). These CSPGs are known to be inhibitory to neuronal regeneration (McKeon *et. al.*, 1991; Asher et. al., 2001). Removal of CSPGs by treatment with glycan trimming chondroitinase ABC resulted in improved regeneration (Bradbury *et. al.*, 2002; Moon *et. al.*, 2001; Yick *et. al.*, 2000). This indicated that these molecules play an important role in contributing to the growth-inhibitory environment in CNS.

Another contributor to the non-permissive growth conditions in CNS is the oligodendrocytes themselves (Schwab and Caroni, 1988). Oligodendrocytes are responsible for myelination of axons in CNS, analogous to the myelination of PNS axons by Schwann cells. Upon CNS injury, debris that originated from the myelin structures ensheathing the neurons before lesion remains at the vicinity of the injury site (Fig 1.1). This means that the severed axons are exposed to the myelin debris present. Myelin produced by oligodendrocytes has been reported to have an inhibitory effect on neuronal regeneration.

The first important hint that myelin could play a major role in the inhibition of neuronal regeneration was from the studies performed by Schwab and Thoenen

described above, where a CNS (optic nerve) explant but not one from PNS (sciatic nerve) inhibited axonal regeneration (Schwab and Thoenen, 1985). More evidence came from the report where newborn rat DRG neurons and NG-108-105 cells were plated onto human CNS myelin patches coated on 96-well plates. Myelin patches were found to strongly inhibit neurite outgrowth, with this inhibition requiring direct contact between myelin and the neurites (Ng *et. al.*, 1996). Embryonic chick sympathetic neurons also showed poor neuronal outgrowth on white matter regions compared to the grey matter ones when cultured on freshly frozen adult rat brain or spinal cord sections (Crutcher, 1989), or on adult spinal cord sections subjected to injury by *ex vivo* crushing prior to freezing (Pettigrew *et. al.*, 2001). The same conclusion was reached in animal studies, where an increase in regeneration of lesioned neurons was observed in myelin-free spinal cord (Savio and Schwab, 1990) or optic nerve (Weibel *et. al.*, 1994), or for myelin-immunized mice that had circulating antibodies to myelin (Huang *et. al.*, 1999).

Subsequently, several myelin-associated inhibitory molecules that are able to inhibit neuronal regeneration are identified. These include Nogo (Chen *et. al.*, 2000; GrandPré *et. al.*, 2000; Prinjha *et. al.*, 2000), myelin-associated glycoprotein (MAG) (McKerracher *et. al.*, 1994; Mukhopadhyay *et. al.*, 1994) and oligodendrocyte myelin glycoprotein (OMgp) (Kottis *et. al.*, 2002; Wang *et. al.*, 2002b). Exposure of these myelin-associated inhibitors present in the myelin debris to severed axons at the injury site may explain the loss of, or limited, neuronal regeneration in these damaged axons, and hence a lack of function recovery after CNS injury.

1.1.3 Nogo-A present in myelin acts as a neurite outgrowth inhibitor

Nogo-A is first identified as a myelin-associated neurite outgrowth inhibitor

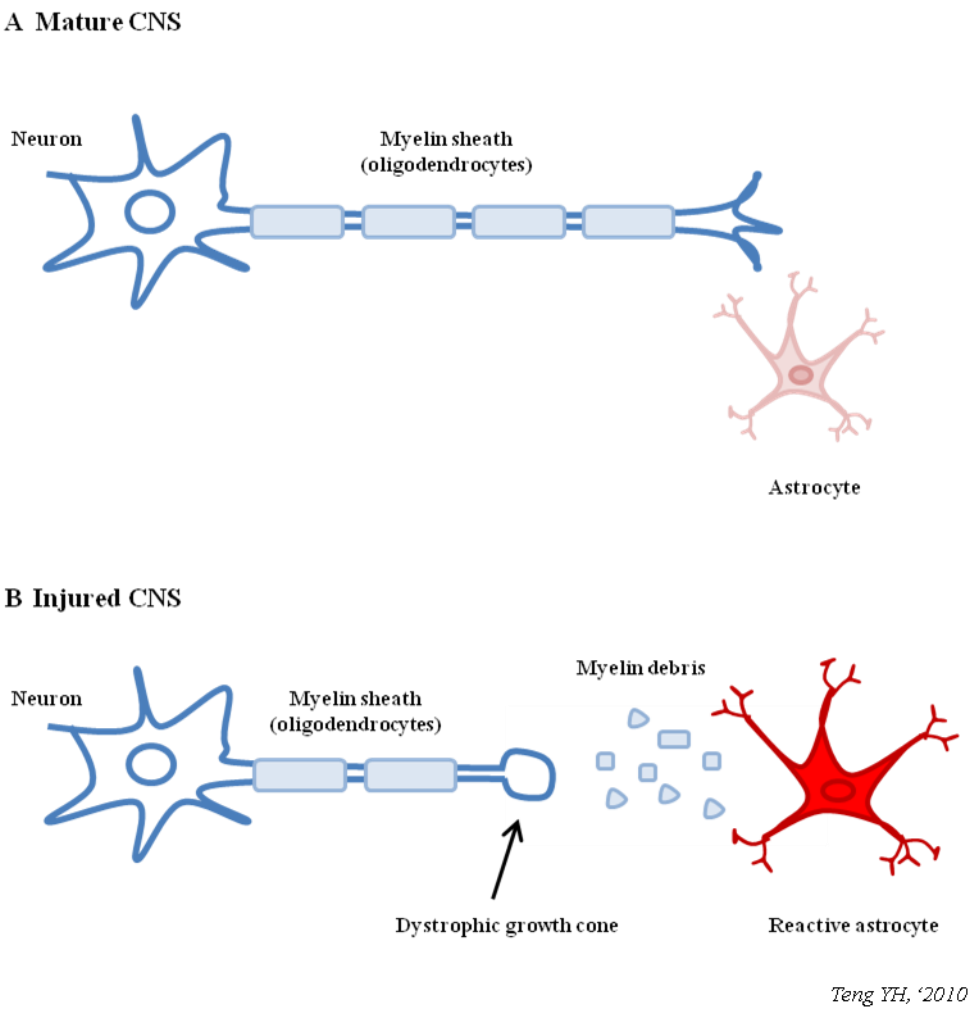

Fig 1.1 Inhibition of axonal regeneration upon CNS injury. ***(A)*** In mature CNS, myelin-associated inhibitors from oligodendrocytes and CSPGs from astrocytes act on the axons to limit plasticity and sprouting. ***(B)*** Upon injury, the distal end of the severed axon degenerates while the proximal end forms a dystrophic growth cone. Recruitment of reactive astrocytes, oligodendrocyte precursors, microglia and meningeal cells to the injury site forms a glial scar that acts as a barrier for axonal growth. In addition, myelin-associated inhibitors present in the myelin debris also act on the axons to prevent regeneration.

when it is found to be the antigenic target of IN-1, a monoclonal antibody raised against rat myelin that could neutralize CNS myelin's inhibitory effect on neurite outgrowth. Caroni and Schwab (1988a) had extracted CNS myelin from rats and isolated crude fractions from this myelin extract which contained two membrane proteins of molecular sizes 250 and 35 kilodaltons (kDa) (NI-250 and NI-35), which accounted for most of CNS myelin's inhibitory effect on neurite outgrowth and

fibroblast spreading. The group proceeded to raise antibodies against these two membrane protein fractions, and found that the IN-1 monoclonal antibody raised against NI-250 (likely the longest isoform of Nogo, Nogo-A), as well as IN-2 antibodies which was against NI-35 (suggested to be Nogo-B), were able to neutralize CNS myelin's inhibitory effect and allowed neurites to extend into optic nerve explants (Caroni and Schwab, 1988b).

Importantly, the IN-1 antibody, when applied to experimental spinal cord injury models, was able to enhance neuronal regeneration and functional recovery in the injured animals (Bregman *et. al.*, 1995; Fouad *et. al.*, 2001; Thallmair *et. al.*, 1998). Conversely, transgenic expression of Nogo-A in Schwann cells, which were devoid of Nogo-A, was able to override the growth-promoting and permissive PNS environment to result in prevention of regeneration (Pot *et. al.*, 2002). This strengthened the notion that Nogo-A in CNS myelin plays an important role in the inhibition of neurite outgrowth.

1.2 Molecular characterization of Nogo-A

1.2.1 Nogo: part of the Reticulon family

Identification and characterization of the gene encoding IN-1 antigen, Nogo-A, was aided by the report from Spillmann *et. al.* (1998), where the group published sequence information of six peptides obtained from a bovine ortholog of NI-250, bNI-220, purified from extracted bovine myelin. In 2000, three groups concurrently identified and cloned Nogo-A (Chen *et. al.*, 2000; GrandPré *et. al.*, 2000; Prinjha *et. al.*, 2000) from cDNA libraries using this valuable information.

Nogo belongs to the Reticulon (RTN) family that has three previously known mammalian paralogs, RTN1-RTN3 (Oertle *et. al.*, 2003b; Yang and Strittmatter,

2007). Nogo, the latest of the RTNs to be reported, is therefore termed RTN4. RTNs are variable in their N-terminal regions but share a highly conserved C-terminal domain. This reticulon homology domain (RHD; Pfam PF02453) is about 200 amino acids (aa) long and comprises of two putative transmembrane (TM) domains sandwiching a hydrophilic loop (about 60-70 aa) followed by a short C-terminal tail. The latter harbors an endoplasmic reticulum (ER) retention signal - a dilysine motif (KXKXX). RTNs are termed reticulons as a majority of the proteins (>95%) are localized at the ER (van de Velde *et. al.*, 1994).

RTN1, also called neuroendocrine-specific protein (NSP), was the first reticulon to be discovered and exhibited specific expression in neural tissues (Wieczorek and Hughes, 1991; Roebroek *et. al.*, 1993; van de Velde *et. al.*, 1994). RTN2 was isolated based on its homology to RTN1 (Roebroek *et. al.*, 1998). RTN3 was isolated during a subtractive cloning project to look for transcripts differentially expressed between macula and peripheral retina (Moreira *et. al.*, 1999). Each of the RTNs has several splice isoforms, which are divergent in terms of exon usage at the N-terminus.

1.2.2 The *Nogo* gene and its splice isoforms

Nogo has been mapped to human chromosome 2 (2p16.1→16.3 (Nagase *et. al.*, 1998) and 2p14→p13 by radiation hybrid mapping (Yang *et. al.*, 2000)). The gene locus spans approximately 75 kb, contains at least two promoter regions, 14 exons and 8 introns, and gives rise to three major splice isoforms (Nogo-A, -B and -C) and several other minor splice isoforms (Oertle *et. al.*, 2003a). Amongst these, an isoform was found to be expressed specifically in the testis (Zhou *et. al.*, 2002).

Nogo-A and -B are generated by alternative splicing using the first Nogo gene promoter and both contain exon 1A, which covers the 5'UTR and the N-terminal 184 aa of Nogo-A and -B. This N-terminus contains an acidic domain and a proline-rich domain. Nogo-A, in addition, contains the 2.4 kb exon 3 that is uniquely present in this isoform only. The exon 3 has consensus sequences for PEST domains, SH3-ligands and WW-ligands. Indeed, Nogo-A has been shown to be able to bind to a SH3-containing adaptor protein, Nck2 (Liu *et. al.*, 2006), and a WW domain-containing E3 ubiquitin ligase, WWP1 (Qin *et. al.*, 2008). Nogo-C is produced by a differential promoter usage and contains exon 1C, which has the 5' UTR of Nogo-C and the N-terminal 11 aa residues specifically found in Nogo-C. All three isoforms contain exons 4-9 that encode the RHD domain common to them, with exons 4 and 5 encoding a stretch of hydrophobic sequence constituting a putative TM domain 1 (TM1) and a 66-aa hydrophilic loop (Nogo-66). This is followed by exons 6-7 encoding a second putative TM domain (TM2) that contains a leucine zipper-like motif, and exons 8 and 9 encoding the C-terminus with the ER retention signal and the 3' UTR. An illustration of the domain structures of Nogo-A, -B and -C is shown in Fig 1.2A.

Nogo-A is the longest of the three major isoforms, with a coding region of 3579 base pairs (bp)/ 1192 aa (estimated molecular size of 220 kDa). Nogo-B has a coding region of 1122 bp/ 373 aa (est. 50 kDa) while Nogo-C is the shortest, with 600 bp/ 199 aa (est. 25 kDa).

1.2.3 Subcellular localization, topology and structure of Nogo

As mentioned in section 1.2.1, the majority of Nogo proteins are localized at the ER (GrandPré *et. al.*, 2000). The lack of a canonical signal peptide at the N-

terminus for directing the proteins to ER suggested that internal ER targeting signals may be present. Their subsequent ER retention could be due to the presence of the dilysine motif situated at the C-terminus of Nogo proteins. However, it was suggested that TM2 was enough for ER localization since its deletion, but not that of the dilysine motif, disrupted Nogo's ER localization (Oertle *et. al.*, 2003c). Besides the ER, Nogo proteins have also been shown to be present on the plasma membrane (Dodd et. al., 2005; GrandPré *et. al.*, 2000) and Golgi complex (Oertle *et. al.*, 2003d).

Nogo-A could adopt at least two membrane topologies (Fig 1.2B). The first predicted topology has a horse-shoe like orientation, with both the N and C termini facing the cytoplasmic region and the Nogo-66 loop being extracellular/lumenal. This topology was supported by data showing that antibodies targeting both termini of Nogo-A were unable to detect Nogo-A by immunocytochemistry (ICC) on surface of unpermeabilized cells, while that against Nogo-66 were able to do so (GrandPré *et. al.*, 2000). A second topological prediction has the N-terminus facing the extracellular/lumenal region, as a result of the putative TM1 flip-flopping in the membrane without transversing the lipid bilayer. The looping back of the putative TM domain is possible as this hydrophobic sequence is longer (approximately 35 aa) than a typical 20 aa TM domain. This topology was suggested when similar ICC experiments were performed with cultured oligodendrocytes (Oertle *et. al.*, 2003d). It is proposed that the first topology is typically adopted by majority of Nogo-A, especially at the ER, while a fraction of Nogo-A at the cell surface may adopt the second one (Oertle *et. al.*, 2003d). The second topology could explain how the N-terminus of Nogo-A, which itself contains two growth inhibitory domains, works hand in hand with Nogo-66 to inhibit neurite outgrowth (Oertle *et. al.*, 2003d). Additional evidence for the N-terminus of Nogo facing extracellularly came from the

study of the topology of Nogo-B on the surface of endothelial cells (Acevedo *et. al.*, 2004). Nogo-A has also been postulated to adopt other topologies (Voeltz *et. al.*, 2006). The exact membrane topology of which Nogo-A adopts on the various membranous compartments it traverses or resides in its lifetime remains debatable.

Studies on the structure of Nogo-A have been carried out in the hope of understanding its function, and more importantly, discovering important structural domains for the design of antagonists that might aid in neuronal regeneration. However, it seems that Nogo-A domains are generally unstructured in solution (Li and Song, 2007; Zander *et. al.*, 2007), except for perhaps the fragments Nogo-40, -54 and -60, which are truncated forms of Nogo-66 (Li *et. al.*, 2004a; Li *et. al.*, 2006; Li *et. al.*, 2008). A recent report in which the group employed a membrane-like environment to show that Nogo-66 forms a unique structure only upon binding to a phosphocholine surface, has allowed structural insights for the design of antagonists that might disinhibit Nogo-A's inhibitory effect on neuronal regeneration (Vasudevan *et. al.*, 2010).

1.2.4 Tissue distribution of Nogo

The expression pattern of Nogo proteins, especially Nogo-A, in various tissues has been extensively studied by others and us (see chapters 3 and 4). Nogo-A is highly enriched, and has a widespread expression, in the CNS. It is also found to be expressed at lower levels in the cochlea, heart, testis, gastrointestinal tract and visual system (Caelers *et. al.*, 2009; Huber *et. al.*, 2002; Osborne *et. al.*, 2004; Xiao *et. al.*, 2009). Analysis at RNA and protein levels have pinpointed the expression of Nogo-A largely to oligodendrocytes and neurons. Nogo-B is more ubiquitously expressed, with presence in CNS as well as other tissues such as the lung, spleen and kidney.

Nogo-C is mainly found in the skeletal muscle, with lower expression in the brain, heart and adipocytes (Huber *et. al.*, 2002; Morris *et. al.*, 1999).

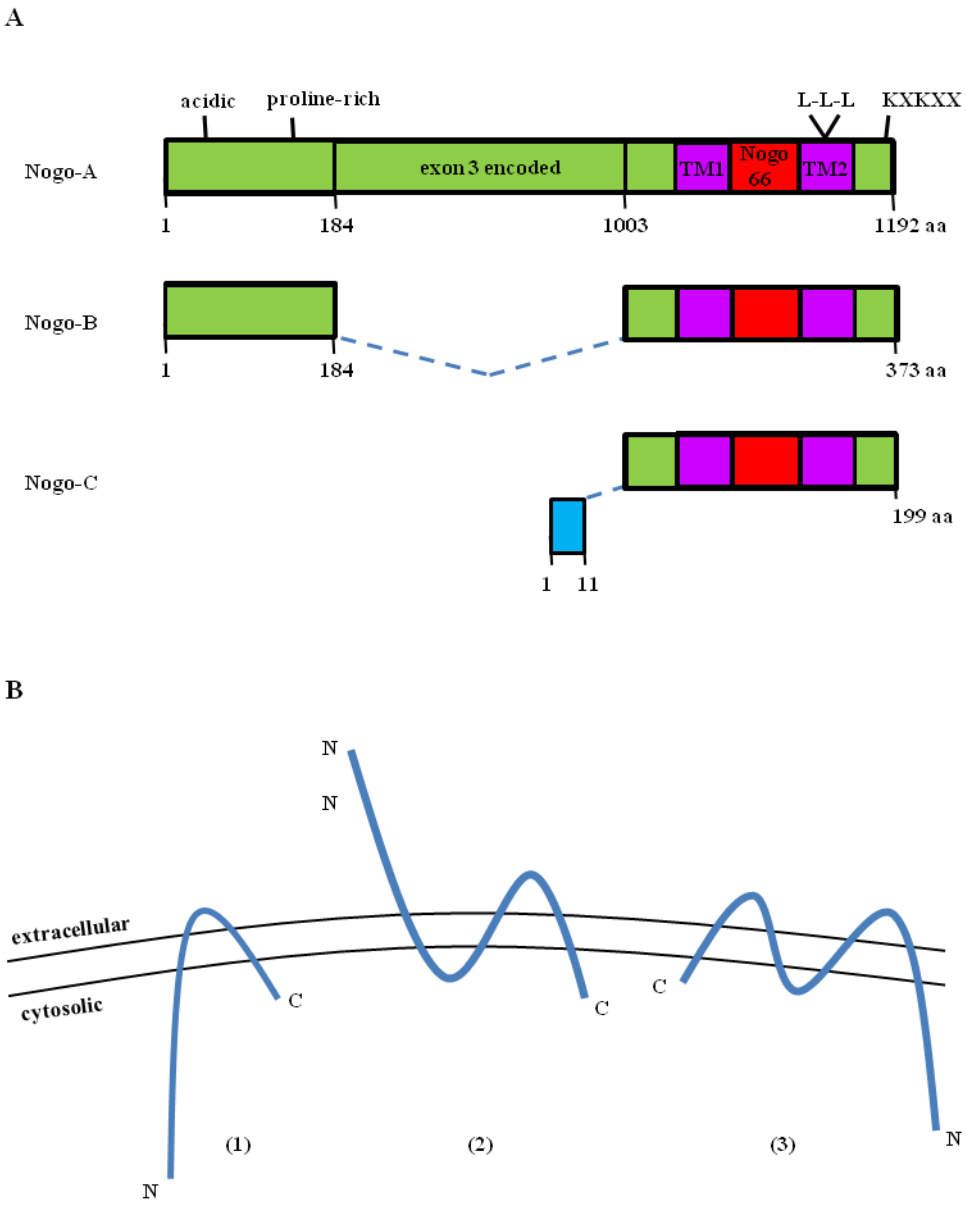

Fig 1.2 Domain structure and topology of Nogo. ***(A)*** A schematic diagram of the three major splice isoforms of *Nogo* (Nogo-A, -B and -C) and their domain structures, with their aa sizes indicated. Nogo-A and -B share the same 1-184 aa N-terminus domain, while Nogo-C has a different N-terminus domain (blue box) that is generated by differential promoter usage. acidic = acidic domain. proline-rich = proline-rich domain. L-L-L = leucine zipper-like motif. KXKXX = ER retention signal. ***(B)*** Three of the proposed topologies of Nogo-A. Topology (1) is proposed by GrandPré *et. al.* (2000), topology (2) is suggested by Oertle *et. al.* (2003d) while topology (3) is proposed by Voeltz *et. al.* (2006).

The high expression of Nogo-A in oligodendrocytes is expected because of its known association with myelin and its inhibitory role on neurite outgrowth. Nogo-A was found to be expressed in the cell bodies and processes of oligodendrocytes, including the outer myelin sheath surrounding myelinated axons, and at the inner adaxonal sheath where myelin and axon came into contact with each other (Wang et. al., 2002). This role of Nogo-A at the axoglial junction has not been elucidated. However, it is possible that it could have similar function as that of OMgp, whose enrichment at the same location stabilized the node and prevented axonal sprouting (Huang *et. al.*, 2005). Association of Nogo-A with tubulin and myelin basic protein (MBP) suggested another possible function of Nogo-A in oligodendrocytes, which is to aid in the maturation of the myelin sheath (Taketomi *et. al.*, 2002).

In addition, Nogo-A was also present in several types of neurons, such as motor neurons, sympathetic neurons, Purkinje cells, DRG neurons and cortical neurons (Liu *et. al.*, 2002b; Hunt *et. al.*, 2003). Expression of Nogo-A in neurons was found to precede that in oligodendrocytes during early stages of mouse development, and it was suggested to play a role in axonal guidance and architecture organization of neural networks (Meier *et. al.*, 2003). Within the neuron, the protein was localized to multiple substructures, including growth cones (Tozaki *et. al.*, 2002) and postsynaptic active zone (Liu *et. al.*, 2003). The function of Nogo-A in neurons is still unclear at present, and results presented in this thesis shall attempt to address an aspect of this function.

Interestingly, Nogo-A has very recently been reported to be expressed on the surface of neural stem cells (NSCs) derived from cerebral cortex and spinal cord of newborn rats (Hou *et. al.*, 2010). NSCs are self-renewing, multipotent and can differentiate into the different cell lineages in the nervous system. Nogo-66 was

shown to promote differentiation of these cells into astrocytes (Wang B *et. al.*, 2008). Whether Nogo-A expression influences the type of cell lineage that NSCs may differentiate into, and whether this expression in NSCs is the reason for the failure of transplanted NSCs to improve CNS regeneration, require further exploration.

1.3 Functions of Nogo-A

1.3.1 Role of Nogo-A, after physical injury in adult CNS, as a myelin-associated inhibitor of neuronal regeneration

1.3.1.1 Growth inhibitory domains of Nogo-A

Inhibitory activity of Nogo-A is exhibited by both its N terminal as well as the Nogo-66 domains. A more widespread, non-cell type specific inhibitory activity was associated with the N-terminal domain, while Nogo-66's inhibitory activity appeared fairly specific for neurons (Fournier *et. al.*, 2001; GrandPré *et. al.*, 2000). The fact that antibodies against the N-terminus were able to neutralize the inhibitory effect of CNS myelin *in vitro* (Chen *et. al.*, 2000) and enhance adult rat Purkinje axonal sprouting *in vivo* (Buffo *et. al.*, 2000) implies the important role of this region in Nogo-A's inhibitory function in neuronal regeneration.

There are at least two regions in the N-terminus of Nogo-A that were found to exert growth inhibitory effects. Together with Nogo-66, these three domains acted to restrict growth by different mechanisms (Oertle *et. al.*, 2003d). The first inhibitory region in the N-terminus, aa 59-172, is present in both Nogo-A and -B. It was shown to be able to inhibit spreading of 3T3 fibroblasts. The second domain in the N-terminus, aa 544-725 (also known as NogoΔ20), is found in the Nogo-A specific region encoded by exon 3, and this could strongly inhibit neurite outgrowth, cell spreading and induce growth cone collapse in both neuronal and non-neuronal cells.

Importantly, the soluble dimeric form of this region, but not its monomeric form, caused growth cone collapse in DRG neurons. Nogo-66 was able to induce growth cone collapse and neurite outgrowth in DRG neurons as well as differentiated rat pheochromocytoma PC12 cells. Nogo-66 was also shown to be able to prevent adhesion and migration of human glioma cells (Liao *et. al.*, 2004). GrandPré *et. al.* (2000) has further narrowed down the inhibitory region in Nogo-66 to aa 31-55. Interestingly, aa 1-40 of Nogo-66 (Nogo-40, or NEP1-40) was shown to be antagonistic to Nogo-66's binding to its receptor (GrandPré and Strittmatter, 2002) (see section below). It is possible that the Nogo-A specific inhibitory domain and Nogo-66 play different roles *in vivo*, with the former more involved in limiting outgrowth, regeneration and the latter functioning in axonal guidance.

1.3.1.2 Nogo-A and its neuronal receptors

Oligodendroglial Nogo-A requires a neuronal receptor that it could interact with to cause inhibition of regeneration in the neurons. While the Nogo-66 domain has been clearly shown to be extracellular, the orientation of the N-terminus of Nogo-A is still unclear. The former region would most likely convey an 'inhibitory message' from oligodendrocytes to neurons via a receptor. Yet-to-be-discovered receptors that bind to the N-terminus of Nogo-A may also transduce the growth-inhibitory signal of Nogo-A. Two neuronal receptors for Nogo-66 have been discovered to date. One is the Nogo-66 receptor, NgR (Fournier *et. al.*, 2001), and the second one being paired immunoglobulin-like receptor B (PirB) (Atwal *et. al.*, 2008).

1.3.1.2.1 NgR

NgR is a brain-enriched glycosylphosphatidylinositol (GPI)-linked cell surface protein that is 473 aa long and contains eight leucine-rich-repeat (LRR) domains. It belongs to the superfamily of LRR domain-containing proteins, and has two other paralogues NgR2 (or NgRH1) and NgR3 (or NgRH2) (Barton *et. al.*, 2003; Lauren *et. al.*, 2003; Pignot *et. al.*, 2003), which are also brain-enriched. NgR was first identified by a Nogo-66 affinity based screen (Fournier *et. al.*, 2001). In situ hybridization and IHC showed widespread expression of NgR in the adult brain, with observed levels in neurons of the cerebral cortex, hippocampus, cerebellum, substantia nigra, amygdala and pons (Fournier *et. al.*, 2001; Hunt *et. al.*, 2002; Nyatia and Lang, 2007). NgR was exclusively detected in neurons (cell surface, cell bodies, growth cones and processes) but not in oligodendrocytes or astrocytes (Josephson *et. al.*, 2002). Interestingly, mRNA of NgR was initially detected in the spinal cords of human and mouse fetus but its levels were downregulated in adulthood (Josephson *et. al.*, 2002).

In addition to the Nogo-66 domain, a stretch of 24 aa on the N-terminus of Nogo-A specific to this isoform (aa 995-1018), which is situated just N-terminus to TM1, was shown to bind to NgR (Hu *et. al.*, 2005). This region was able to bind to the receptor with high affinity, but could not inhibit neurite outgrowth or cell spreading. Covalent linkage of this domain with Nogo-66 enabled better binding affinity with NgR than Nogo-66 alone, and its fusion with a truncated form of Nogo-66 (1-32), an antagonist of Nogo-66, resulted in agonistic neurite outgrowth inhibition in DRG neurons. These two Nogo-A inhibitory domains may therefore bind NgR in a co-operative manner. NgR interacts with Nogo-66 via its LRR domains (Fournier *et. al.*, 2002; He *et. al.*, 2003), with several residues between LRR3 and LRR5 having been identified to directly bind to Nogo-66 (Schimmele and Plückthun, 2005).

It is evident that Nogo-66 functions through NgR to elicit its inhibition on neurite outgrowth. Expression of NgR in embryonic day (E) 7 retinal ganglion cells, originally insensitive to Nogo-66's inhibitory effect, was able to cause Nogo-66-induced growth cone collapse in these cells (Fournier *et. al.*, 2001). The LRR domains in NgR is important in eliciting the inhibitory signal since a truncated form of NgR containing only the region C-terminus of the LRR domains was unable to induce growth cone collapse, suggesting an involvement of LRR domain-required conformational change, or receptor aggregation, in activating downstream signals.

Interestingly, NgR also interacts with the other two known myelin-associated neurite outgrowth inhibitors, MAG (Liu *et. al.*, 2002a; Domeniconi *et. al.*, 2002) and OMgp (Wang *et. al.*, 2002b), and these molecules effect their growth inhibitory signalling through NgR. Additionally, NgR binds gangliosides (Williams *et. al.*, 2008) and a neuronal membrane protein, Myelin-Associated Neurite-outgrowth Inhibitor (MANI) (Mishra *et. al.*, 2010), to convey their neurite outgrowth inhibitory signals. Interaction of NgR with the secreted LRR protein leucine-rich glioma inactivated (LGI1), which antagonizes myelin-based growth inhibition, has also been reported (Thomas *et. al.*, 2010).

1.3.1.2.2 PirB

As NgR knockout did not show complete disinhibition of axonal regeneration after injury (which shall be discussed in detail in section 1.3.4), presence of alternative receptors for Nogo-A and the other myelin-associated inhibitors was hypothesized. Indeed, another molecule, PirB was later found to be a second receptor for Nogo-66. It could also bind MAG and OMgp, with binding affinities similar to that of NgR (Atwal *et. al.*, 2008). PirB is a mouse ortholog for the human leukocyte

immunoglobulin (Ig)-like receptor B2 (LILRB2), with ~50% similarity between them. It is a typical type 1 transmembrane protein which localizes mainly on the plasma membrane, and contains six Ig-like repeats in its extracellular domain and four immunoreceptor tyrosine-based inhibitory motifs in the cytoplasmic region. The region that interacts with Nogo-66 lies in the ectodomain of PirB, as a soluble ectodomain of PirB was able to prevent Nogo-66's inhibition of neurite outgrowth in postnatal day (P) 7 cerebellar granule cells (Atwal *et. al.*, 2008). However, it was also shown that only partial disinhibition of neurite outgrowth was achieved with neurons from PirBTM mice (containing a loss-of-function *PirB* allele). PirB may work in concert with NgR to mediate neurite outgrowth inhibition.

PirB is expressed widely in the neurons in the brain, with significant levels observed in the cerebral cortex, cerebellum, hippocampus and olfactory bulb. It has been shown to have an inhibitory role in receptor signalling within B cells, mast cells and dendritic cells, via its binding to the protein tyrosine phosphatases (SHP-1 and -2) and the polyphosphate inositol 5-phosphatase (SHIP) via its cytoplasmic inhibitory domains (Bléry *et. al.*, 1998), or upon phosphorylation and activation by the src family kinases Hck and Fgr (Zhang *et. al.*, 2005). It could also negatively regulate integrin signalling, thereby reducing adhesion and spreading of neutrophils and macrophages (Pereira *et. al.*, 2004), and limit plasticity in the visual cortex both during and after a critical developmental period (Syken *et. al.*, 2006). It is hypothesized that these inhibitory signalling pathways may also be activated upon binding with myelin-associated inhibitors to cause inhibition of neurite outgrowth.

1.3.1.3 The growth-inhibitory signalling pathways elicited by Nogo-A to induce neuronal regeneration inhibition

The best known inhibitory signalling pathway associated with myelin inhibitors is the Nogo-66-NgR axis. Being a GPI-linked protein, NgR does not transverse the plasma membrane and therefore needs to recruit membrane spanning co-receptors in order to engage cytoplasmic signalling intermediates for its growth inhibition signalling. In fact, a co-receptor complex of two molecules may be necessary to interact with NgR for activation of growth inhibitory signalling pathways. The two proteins are p75, which binds directly with NgR (Wang *et. al.*, 2002a; Wong *et. al.*, 2002), and the LRR and Ig domain-containing, Nogo Receptor-interacting protein (LINGO-1) that binds to both NgR and p75 (Mi *et. al.*, 2004). p75, the low affinity neurotrophin receptor, belongs to the tumour necrosis factor (TNF) receptor superfamily and has a restricted expression pattern in adult CNS, with only a few subpopulations of mature neurons expressing it. It could interact and activate RhoA to modulate axonal and dendritic growth (Yamashita *et. al.*, 1999), and also play additional roles in apoptosis and myelination besides neurotrophin signalling and neurite outgrowth. LINGO-1 is a transmembrane protein containing twelve LRR motifs and an Ig domain, and is CNS-specific, with expression in neurons and oligodendrocytes but not astrocytes. Absence of either of the two co-receptors would prevent inhibition effected by NgR binding to the myelin-associated inhibitors from occurring.

An alternative co-receptor for NgR that belongs to the same family as p75 has also been discovered. This molecule, TAJ/TROY, shows wider expression than p75 in adult brain and is able to bind both NgR and LINGO-1 as well to form the ternary complex responsible for activating downstream signalling pathways to inhibit neurite

outgrowth (Park *et. al.*, 2005; Shao *et. al.*, 2005). The presence of a second co-receptor for NgR possibly explains the inefficient CNS neuronal regeneration observed in p75 knockout mice (Song *et. al.*, 2004).

The downstream mechanism upon binding of Nogo-A to NgR leading to neurite outgrowth inhibition appears to involve more than one signalling pathway (Fig 1.3). Nogo-66's interaction with the tripartite receptor complex led to activation of RhoA and its substrate, Rho-associated protein kinase (ROCK), and a concomitant antagonistic inhibition of Rac1 (Madura *et. al.*, 2004; Niederöst *et. al.*, 2002). This could be due to the release of RhoA from its inhibitor, Rho GDP dissociation inhibitor (Rho-GDI), by the binding of p75 to Rho-GDI (Yamashita and Tohyama, 2003). RhoA activation was known to cause growth cone collapse and axon guidance repulsion (Luo, 2000). LIM kinase, a downstream effector of ROCK, and the phosphatase Slingshot have been shown to be regulated by Nogo-66 that led to an inactivation of cofilin and hence actin depolymerisation (Hsieh *et. al.*, 2006). Reagents targeting RhoA and ROCK, such as C3 transferase (which causes ADP ribosylation of the effector domain on RhoA) and Y27632 (which inhibits ROCK), allowed enhanced regeneration of corticospinal tract (CST) axons and improved recovery of function (Dergham *et. al.*, 2002; Fournier *et. al.*, 2003).

Nogo-A may also inhibit growth signalling by affecting/negatively regulating the cAMP pathway, which is induced by neurotrophins. cAMP could abrogate RhoA activation and Rac1 inactivation by Nogo-A, thereby disinhibiting neurite outgrowth inhibition (Bandtlow, 2003). Signalosomes (signalling-active endosomal structures) containing NogoΔ20 generated by pincher-dependent endocytosis were retrogradely transported from neurites to cell bodies. These were able to activate RhoA along the way and also inhibit cAMP-dependent activation of cAMP response element-binding

protein (CREB) (Joset *et. al.*, 2010). It is likely that Nogo-A could act analogously to MAG, which inhibited cAMP accumulation by activating G protein-coupled receptors (GPCRs) via p75, and their Gi proteins (Cai *et. al.*, 1999).

Another GPCR related signalling pathway involving that of Ca^{2+} and protein kinase C (PKC) may also be engaged by the Nogo-NgR interaction. Nogo-A was shown to trigger an intracellular elevation of Ca^{2+} and PKC activation (Hasegawa *et. al.*, 2004). The balance between inositol 1,4,5-triphosphate (IP_3)/Ca^{2+} and PKC seems crucial in determining the regulation of axon regeneration by the myelin-associated inhibitors.

Several other possible mechanistic inhibitory pathways are also implicated in NgR-mediated downstream signalling. A particularly prominent one is the epidermal growth factor receptor (EGFR) pathway. EGFR inhibitors were able to block the neurite outgrowth inhibitory effects of myelin-associated inhibitors including Nogo-A to promote regeneration of injured optic nerve fibers (Koprivica *et. al.*, 2005). A recent study has shown that LINGO-1 exhibited enhanced interaction with WNK1, a serine-threonine kinase, upon Nogo-66 treatment, and this interaction led to activation of RhoA supposedly via WNK1's interaction with Rho-GDI (Zhang *et. al.*, 2009). Nogo-66 was also shown to interact with necdin to sequester it in the cytoplasm, thereby suppressing its role in enhancing neurite outgrowth (Liu *et. al.*, 2009). Additionally, the N-terminus of Nogo-A has been reported to inhibit integrin signalling (Hu and Strittmatter, 2008) and may also inhibit Akt1 activation (Deng *et. al.*, 2010), thereby inhibiting neurite outgrowth and cell adhesion.

Some mechanisms that further regulate Nogo-A's inhibitory signals have been reported. Cholesterol depletion could effectively inhibit Nogo-66 signalling, since it disrupted the structure of lipid rafts where NgR and p75 were segregated (Yu *et. al.*,

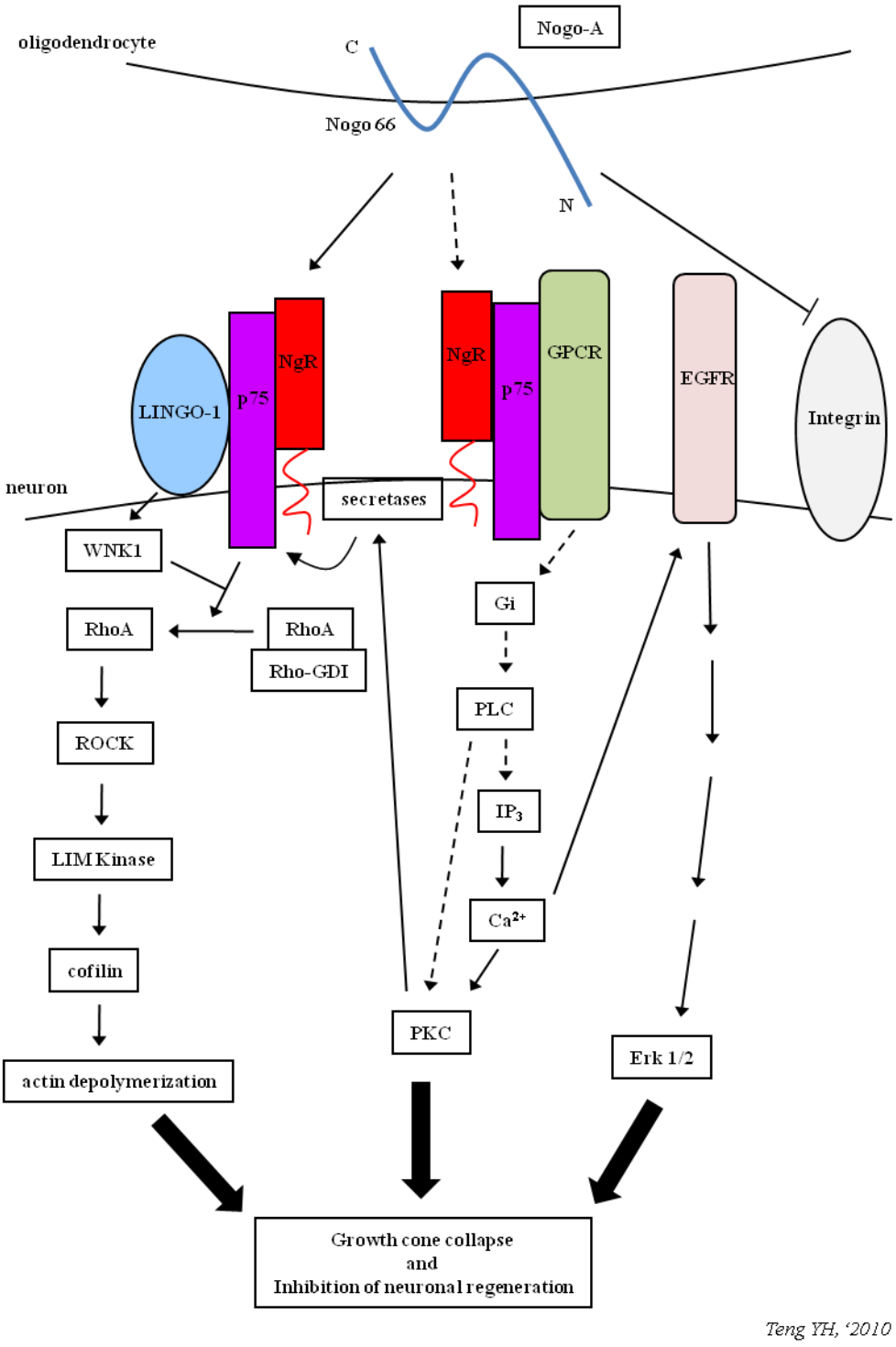

Fig 1.3 Neuronal regeneration inhibitory signalling pathways activated by Nogo-A. Some of the reported pathways described in the text are illustrated in this schematic diagram. Nogo-66 binding to NgR-p75-LINGO-1 ternary receptor complex leads to activation of RhoA via the interaction of p75 with Rho-GDI and release of RhoA. Rac1 inactivation is also resulted (not shown here). LINGO-1 is also able to mediate RhoA release by interacting with WNK1 which then binds to Rho-GDI. RhoA activates ROCK, which activates LIM kinase that phosphorylates cofilin, leading to actin depolymerisation and neurite outgrowth inhibition and growth cone collapse. PKC and IP_3-Ca^{2+} are also activated by Nogo-66 but the upstream molecules

involved are unclear (dotted lines). PKC activation leads to inhibition. Apparently, intramembrane cleavage of p75 by secretases is PKC-dependent. Transactivation of EGFR by Ca^{2+} induced activation of Erk1/2 which also seemingly causes inhibition. The N-terminus of Nogo-A is able to inhibit integrin signalling, thereby preventing growth.

2004). Also, the ectodomain of NgR, which was essentially the entire LRR domains, could be shed from the plasma membrane via cleavage by zinc metalloproteinases and could be detected in the human brain cortex and cerebrospinal fluid (CSF) (Walmsley *et. al.*, 2004). Shedded NgR ectodomains could act in a dominant-negative manner, and this shedding may be regulated to allow axonal regeneration to occur. NgR could also be regulated by phosphorylation, and Nogo-66's binding to NgR was inhibited when it was phosphorylated by extracellular casein kinase II (Takei, 2009). Cleavage of p75 by α- and γ-secretase in a PKC-dependent manner upon ligand-binding was found to be necessary for RhoA activation and neurite outgrowth inhibition (Domeniconi *et. al.*, 2005). A different form of cleavage of p75 and NgR, this time by TNFα converting enzyme (TACE), has however the opposite effect (Ahmed *et. al.*, 2006).

1.3.1.4 Therapeutic interventions targeting the Nogo-A-NgR signalling axis

Although the Nogo-A-NgR signalling pathway is proposed to be a major cause for neurite growth inhibition in the adult CNS, knockout studies of Nogo-A and NgR have not been very supportive of this notion. Deletion of Nogo or NgR achieved at most a moderate enhancement of neuronal regeneration in some cases, but no improvement at all in other cases upon spinal cord injury. Nogo knockout animal strains with different modes of targeted gene disruption of Nogo isoforms have been generated. Kim *et. al.* (2003) observed significant fiber sprouting in young Nogo-A/

$B^{-/-}$ mice, Simonen *et. al.* (2003) saw only moderate CST neuronal regeneration in Nogo-$A^{-/-}$ mice while a third group did not obtain any improvement in all their three lines of knockout mice (Lee *et. al.*, 2009; Zheng *et. al.*; 2003). The second group of investigators, by backcrossing their Nogo-A deficient mice to two different parent genetic backgrounds, achieved better regeneration in the backcrossed 129X1/SvJ Nogo-A mice compared to their original C57BL/6 ones (Dimou *et. al.*, 2006), suggesting genetic background differences to be a reason for the varied regeneration capabilities shown by the different knockout mice. NgR knockout studies did not yield much enhancement of CST regeneration either (Kim *et. al.*, 2004; Zheng *et. al.*, 2005), although Kim *et. al.* (2004) did report observing some regeneration in raphespinal and rubrospinal axons.

In optic nerve injury, however, both Nogo-A/B/$C^{-/-}$ or $NgR^{-/-}$ mice were shown to exhibit enhanced axonal growth (Su *et. al.*, 2008; Su *et. al.*, 2009). An interesting and counterintuitive result was obtained in traumatic brain injury, where Nogo-A/$B^{-/-}$ mice showed impaired recovery from neurological and cognitive deficits as compared to the wild type (Marklund *et. al.*, 2009), suggesting that Nogo-A may play a protective role in these type of injuries.

As there may be redundancy and synergism in the inhibitory functions of Nogo-A, MAG and OMgp that could possibly explain the negative results from Nogo knockout studies, two groups have recently attempted to delete all three of these, and have obtained contrasting results after spinal cord injury. One group of investigators showed enhanced axonal growth and locomotive function in the triple mutant mice compared to Nogo-A mutant (Cafferty *et. al.*, 2010), while the other group did not observe improvement in axonal growth even after deleting all three inhibitors (Lee *et. al.*, 2010).

Despite the surprising observations from the knockout studies targeting deletion of the Nogo-A-NgR axis which may not significantly improve axonal regeneration and recovery of function in spinal cord injuries, various reagents against Nogo-A, NgR and other components in their implicated signalling pathways have thus far achieved very positive results *in vitro*. Most importantly, these also enhance regeneration and function in CNS injuries *in vivo*. These reagents include antibodies against Nogo-A (IN-1 (Emerick and Kartje, 2004; Liebscher *et. al.*, 2005; Seymour *et. al.*, 2005), 11C7 and 7B12 (Müllner *et. al.*, 2008; Wiessner *et. al.*, 2003)), NgR (7E11) (Li *et. al.*, 2004c) and LINGO-1 (Lv *et. al.*, 2010); the NgR antagonist, NEP1-40 (Gou *et. al.*, 2010; GrandPré *et. al.*, 2002; Li and Strittmatter, 2003); soluble proteins containing the ectodomains of NgR (Fournier *et. al.*, 2002; Lee *et. al.*, 2004; Li *et. al.*, 2004b; Peng *et. al.*, 2010) and LINGO-1 (Ji *et. al.*, 2006); protein vaccines of Nogo-A/MAG (Sicotte *et. al.*, 2003) and NgR (Yu *et. al.*, 2008); RNA aptamers binding to NgR (Wang *et. al.*, 2010); and reagents against RhoA and ROCK (Dergham *et. al.*, 2002; Fournier *et. al.*, 2003). Combinatory treatments, such as NEP1-40 with the anti-inflammatory drug methylprednisolone achieved better survival of neurons and oligodendrocytes, and locomotion function in spinal cord injury (Wu *et. al.*, 2010), and may be more effective in dealing with CNS injuries. More clinically relevant studies have been extended to adult primates. Monkeys treated with IN-1 antibodies upon spinal cord injury exhibited enhanced axonal fiber sprouting and functional recovery (Fouad *et. al.*, 2004; Freund *et. al.*, 2006).

In fact, a humanized anti-Nogo-A antibody (AI355) has been tested in phase I clinical trial that started in 2006. Excitingly, no side effects were observed in the subjects tested and phase II trials would commence this year (2010) to check for the

efficiency of the antibody treatment in patients after spinal cord injury (Zörner and Schwab, 2010).

1.3.2 Role of Nogo-A in pathological conditions of CNS

Nogo-A and NgR have both been connected to neurological disorders. Findings in this regard are highlighted in this section.

1.3.2.1 Alzheimer's disease (AD)

Alzheimer's disease (AD) is the most common neurodegenerative disease affecting subjects above 65 years old, and it is characterized by the presence of senile plagues and neurofibrillary tangles in brain. The aggregation of hydrophobic β-amyloid peptides (Aβ) leads to the formation of extracellular plagues, which is a pathological hallmark of AD. Aβ is formed after the sequential cleavage of amyloid precursor protein (APP), first by the type 1 membrane-bound aspartyl protease β-site APP cleaving enzyme 1 (BACE1), followed by the γ-secretase complex (Cole and Vassar, 2007). Soluble Aβ oligomers are now known to initiate AD, impairing cognitive function through synaptic mechanisms.

The first evidence implicating a possible role for Nogo in AD was from the report by He *et. al.* (2004), where Nogo-B, along with RTN3, was shown to interact with BACE1 and inhibit its enzymatic activity, thereby reducing $A\beta_{1\text{-}40}$ generation. Another study has obtained the same conclusion, and in addition, showed binding of Nogo-C with BACE1 (Murayama *et. al.*, 2006). As Nogo-A and BACE1 are both brain-enriched, the above evidence suggests that Nogo-A could also possibly interact with BACE1. It was further found that BACE1 bound preferably to monomeric RTN3 and the interaction required the C terminus of BACE1 and a highly conserved triplet

aa QID motif on the reticulons (He *et. al.*, 2006). The tertiary structure formed by the two TM domains of reticulons seemed important for their binding with BACE1 as well (Kume *et. al.*, 2009).

Nogo-A's receptor, NgR, has also been shown to interact with APP (via the central 15-28 aa of Aβ), and prevent its binding with BACE1 and therefore reducing Aβ secretion (Park *et. al.*, 2006a). Importantly, subcutaneous administration with the soluble ectodomain of NgR reduced amyloid plague deposition in APPswe/PSEN-1(Δ9) double-transgenic mice (an AD mouse model) while increasing serum Aβ levels and improved spatial memory in the mice (Park *et. al.*, 2006b).

Nogo-A has been found to be overexpressed in hippocampal neurons in post-mortem human AD brains and was associated with the Aβ deposits in senile plagues (Gil *et. al.*, 2006). Interestingly, Nogo-A may possibly play a role opposite to that of RTN3 and NgR, as suggested by the evidence that Nogo-A's inhibition on neurite sprouting aided the progression of AD (Masliah *et. al.*, 2010).

1.3.2.2 Amyotrophic lateral sclerosis (ALS)

Amyotrophic lateral sclerosis (ALS) is a fatal neurodegenerative disease characterized by motor neuron loss and muscle wasting. Finding a biomarker for the disease would allow early diagnosis and also development of effective treatments. Nogo isoforms have been implicated as potential biomarkers for ALS, since the expression level of Nogo-A was found to be increased in muscle biopsies of ALS patients, with a concomitant decrease in Nogo-C, the muscle-enriched Nogo isoform. Importantly, Nogo-A levels varied according to the severity of the disease (Dupuis *et. al.*, 2002). Nogo-A expression could be used to predict the progression of lower motor neuron syndrome to full ALS with an accuracy of 91% (Pradat *et. al.*, 2007). Invasive

procedures may be needed to obtain CSF for analysis of Nogo-A's levels since serum Nogo-A level was found not to be increased in ALS patients (Harel *et. al.*, 2009). One contrasting report, however, showed that Nogo-A may not be an accurate biomarker for ALS, as an increase in Nogo-A expression level was observed in several muscle diseases with diverse etiology (Wojcik *et. al.*, 2006).

It has been suggested that Nogo-A aids in disease progression in ALS, since deleting Nogo-A in a mouse model of ALS (SOD1(G93A)) improved survival and reduced muscle denervation, while overexpression of the protein resulted in shrinkage of the postsynapse and retraction of the presynaptic motor ending (Jokic *et. al.*, 2006). Nogo-A may act to induce repulsion and destabilization of motor nerve terminals, leading to the eventual degeneration of the motor neurons. However, Nogo-A has also been implicated in the survival of motor neurons when Nogo-A and NgR levels were found to increase transiently only in these neurons from an ALS model (Miyazaki *et. al.*, 2009). A mechanism underlying Nogo-A activity in ALS was recently proposed. Nogo-A expression redistributed the ER chaperone protein disulphide isomerase (PDI) from the ER to a yet-to-be-identified punctuated membrane compartment (Yang *et. al.*, 2009). The investigators also showed a strong correlation between Nogo-A expression and survival against ALS, as deleting a single copy of Nogo-A/B gene in SOD1(G93A) mice sped up disease onset and progression while deleting both copies further worsened the disease. Understanding the exact role of Nogo-A in ALS would be crucial for it to be recognized as a novel therapeutic target for this devastating disease.

1.3.2.3 Multiple sclerosis (MS)

Multiple sclerosis (MS) is a neuroinflammatory disease partly caused by an auto-immune response to CNS myelin, leading to demyelination and other symptoms. Nogo-A was first implicated in MS when serum IgM antibodies against its N-terminal inhibitory domain were detected in MS and also other acute inflammatory and non-inflammatory neurological diseases (Reindl *et. al.*, 2003). Inconsistent results have however indicated that CSF Nogo-A may not be useful as a biomarker for MS (Lindsey *et. al.*, 2008; Jurewicz *et. al.*, 2007).

Despite this, Nogo-A may still play an important causative role in MS. Its expression was upregulated in surviving oligodendrocytes at chronic demyelinating lesions, where it was suggested to interact with NgR on reactive astrocytes and microglia (Satoh *et. al.*, 2005). Immunization with a peptide from the N-terminus of Nogo-A (aa 623-640) induced a strong T cell response that promoted recovery in rats with spinal cord injury (Hauben *et. al.*, 2001), and also attenuated demyelination, axonal damage and other clinical signs associated with experimental autoimmune encephalomyelitis (EAE), a rodent model of MS (Karnezis *et. al.*, 2004). DNA vaccination (using plasmid driven Nogo-A expression) in a bid to generate antibodies against Nogo-A also did not exacerbate EAE (Bourquin *et. al.*, 2008). Immunization with peptides from the Nogo-66 domain in EAE-susceptible mice suggested that a specific antibody response generated could spread to other encephalitogenic myelin antigens, and that some Nogo-66 epitopes could ameliorate established EAE while others may be encephalitogenic (Fontoura *et. al.*, 2004). Importantly, improved functional recovery as a result of axonal growth and /or sprouting was observed upon silencing of Nogo-A via siRNA (Yang *et. al.*, 2010). This indicates that targeting Nogo-A may ameliorate and even improve the condition of MS.

1.3.2.4 Epilepsy

Epilepsy is a chronic neurological disorder characterized by recurrent unprovoked seizures. Nogo-A was found to be upregulated in the hippocampus of mouse at the same time with the re-expression of the regeneration associated GAP-43 protein after kainite-induced seizures (Meier *et. al.*, 2003), and in hippocampus of human patients suffering from temporal lode epilepsy (Bandtlow *et. al.*, 2004).

The role of Nogo-A in epilepsy is unclear as yet. In a recent paper, where the authors showed increased expression of Nogo-A in the ipsilateral but not the contralateral hippocampus of amygdale kindling rats, suggested that seizures did not by themselves induce Nogo-A, and that Nogo-A may partially control aberrant synaptic reorganization during epilepsy (Takeda *et. al.*, 2007).

1.3.2.5 Schizophrenia

Correlation between Nogo and schizophrenia was first established by the work of Tallerico and colleagues (Novak *et. al.*, 2002), where they reported an elevation of Nogo mRNA in schizophrenia samples. A more recent paper by the investigators suggested that the different Nogo isoforms may have different consequences. Nogo-C upregulation may have a role in schizophrenia, decreased Nogo-B contributing to the clinical condition of depression, while Nogo-A did not seem to play a significant role in schizophrenia or depression (Novak and Tallerico, 2006). The CAA insert polymorphism at the 3'-untranslated region of Nogo was initially thought to be correlated to the disease (Novak *et. al.*, 2002), but others have reported otherwise (Chen *et. al.*, 2004; Covault *et. al.*, 2004; Gregório *et. al.*, 2005; Xiong *et. al.*, 2005). Implications of NgR in schizophrenia were made after genetic variants of NgR were discovered which may influence the patients' response to drug treatment (Sinibaldi *et.*

al., 2004) and failure to induce myelin-associated axonal inhibition (Budel *et. al.*, 2008). This suggests that the NgR signalling pathway plays a part in schizophrenia. In addition, Nogo-A knockout mice exhibited schizophrenia-related endophenotypes but neutralizing Nogo-A with antibodies in adult wild type mice did not generate the same schizophrenia-related phenotype, hinting that Nogo-A was functioning in neurodevelopment that may result in schizophrenia (Willi *et. al.*, 2010).

1.3.3 Nogo-A and its cell autonomous functions

1.3.3.1 Apoptosis

Nogo-B was initially regarded as a tumour suppressor, when its mRNA level was found to be reduced in small cell lung carcinomas (Qin *et. al.*, 2001). Its ectopic expression led to apoptosis especially in cancer cells. However, the classification of Nogo-B as a tumour suppressor for all cancers were disputed after high levels of endogenous Nogo-B was found in several other cancer cell-lines (Oertle *et. al.*, 2003). Nogo-B was thought to interact with B-cell lymphoma protein-2 (Bcl-2) and Bcl-xL, thereby localizing them to the ER and reducing their anti-apoptotic activities (Tagami *et. al.*, 2000). Its interaction with downregulated by v-*src* (Drs), a tumour suppressor, increased apoptosis more than Drs alone (Tambe *et. al.*, 2004).

Three other reticulons have also been shown to have pro-apoptotic activities. Nogo-C was observed to be downregulated in human hepatocellular carcinoma samples and overexpression in a cell-line of the same cancer type promoted apoptosis, presumably by translocating p53 to the cytoplasm and decreasing expression of c-Fos and heat shock protein 70 (Hsp70) (Chen *et. al.*, 2005). Its overexpression in human embryonic kidney (HEK) 293 cells also induced cell death by activating caspase-3 and p53 through the Janus N-terminal kinase (JNK)-c-Jun-dependent pathway (Chen

et. al., 2006). RTN3 was able to deplete ER Ca^{2+} stores, thereby inducing ER stress and mitochondrial dysfunction and eventually cell death (Kuang *et. al.*, 2005). RTN3 may induce cell death by recruiting the death adaptor protein, Fas-associated death domain protein (FADD), to the ER, thereby activating the caspase-8 cascade (Xiang *et. al.*, 2006). Alternatively, RTN3 may induce death by upregulating death receptor 5 (DR5) and downregulating of cellular FLICE-like inhibitory protein (c-FLIP) to enhance TNF-related apoptosis-inducing ligand (TRAIL)-mediated apoptosis (Lee *et. al.*, 2009). Interaction of RTN3 with a cell adhesion protein, cysteine rich with EGF like domains 1(CRELD1), was shown to localize RTN3 to the cell surface and its apoptotic effect was therefore reduced (Xiang and Zhao, 2009). RTN-1C was able to sensitize cells to ER stress inducers while protecting them against genotoxic drugs (Di Sano *et. al.*, 2007). The former effect was due to acetylation modification on RTN-1C which was proposed to affect its binding to DNA (Fazi *et. al.*, 2009).

There are hints that reticulons could have anti-apoptotic effects as well. Nogo-B was able to reduce sensitivity of cells to tunicamycin treatment, where cells stably expressing Nogo-B showed lower cell death as compared to wild type or cells stably expressing RTN3 (Oertle *et. al.*, 2003). Activation of ER stress as a result of Nogo-B's stable expression was suggested to be involved in its protective response (Kuang *et. al.*, 2006).

1.3.3.2 Organization of endoplasmic reticulum (ER) and formation of nuclear envelope (NE)

Nogo-A, its isoforms and fellow reticulons are largely localized to the ER and a function on this organelle has long been suspected. Indeed, Nogo-A was discovered to play an important role in shaping the tubular ER (Voeltz *et. al.*, 2006). The

elaborate ER membrane consists of the nuclear envelope (NE) and the peripheral ER. The NE has two continuous membranes, the outer and the inner nuclear membrane, which are connected by nuclear pores. The peripheral ER, on the other hand, is made up of high curvature tubules and flat sheets. Nogo-A was found to localize exclusively in the tubular ER. The group used an *in vitro* system of *Xenopus* membranes to demonstrate ER reticular network formation regulated by Nogo-A. They showed that blocking of Nogo-A by its antibodies abolished this network formation while overexpressing Nogo-A resulted in longer tubules in COS cells. Interaction of Nogo-A with itself, its isoforms or other fellow reticulons and another tubular ER-localized protein, deleted in polyposis (DP1), was essential for the maintenance of the high membrane curvature tubular ER, with the proteins probably adopting an "ω" orientation where the first TM domain and likely the second one forming hairpin structures in the membrane. Voeltz and colleagues went further to show that oligomerization resulted in lower immobility of the proteins, and was essential in their localization in the tubular ER and their ability to form tubules (Shibata *et. al.*, 2008). A recent paper which characterized five plant reticulons also suggested ER membrane shaping properties for these (Sparkes *et. al.*, 2010).

The importance of maintaining the tubular ER was evident in the observation that positioning of the mitotic division plane was defective in cells that lacked this ER network (Zhang *et. al.*, 2010). This implies that the tubule ER aids in limiting the region for actomyosin ring assembly at exactly the cell equator.

The ability of Nogo-A to stabilize the tubular ER also has implications on NE formation. The same antibodies used in Voeltz *et. al.* (2006) could inhibit growth of the nucleus and prevent NE assembly (Kiseleva *et. al.*, 2007). Another study

suggested that Nogo-A may be involved in the assembly of nuclear pore complex and de novo nuclear pore formation (Dawson *et. al.*, 2009).

1.4 Rationale of my current work

Nogo-A has been identified about a decade ago as an inhibitor of neuronal regeneration associating with oligodendrocytes and myelin. Most investigation has been on the non-cell autonomous inhibitory function of Nogo-A, as indicated by the vast literature on this topic. However, Nogo-A's function in the cell, especially in neurons, has remained relatively unexplored. Hence, my thesis aims to elucidate some of the cell autonomous functions of Ngo-A.

In order to perform investigations on the molecule, the first thing that we did was to generate Nogo-A specific antibodies. The antibodies that we have generated were proven to be specific for Nogo-A and essential in all of the subsequent experiments that we performed. Nogo-A was detected in cells and various parts of the CNS by these antibodies with high specificity. Interestingly, Nogo-A was found to be expressed in both oligodendrocytes and neurons. Additionally, Nogo-A was found to be specifically concentrated at the paranodal region at the Node of Ranvier. These results on Nogo-A expression and localization are presented in chapter 3.

We asked if paranodal Nogo-A from the oligodendrocyte membranes could interact with the paranodal protein Caspr. We also checked if Nogo-A played a role in the formation of the architectural organization at the Node of Ranvier. Nogo-A's binding to another neuronal reticulon, RTN3, was also investigated, with the interacting domains between the two proteins delineated. These studies are described in chapter 4.

We and others have previously observed that Nogo-A expression was upregulated in CNS neurons upon injury. We hypothesized that this upregulation may be part of the cell's response to injury. The role of Nogo isoforms and RTN3 in protecting neural cells against various cell death-inducing treatments is therefore investigated. Interestingly, Nogo-A and -B could efficiently protect these cells against diverse forms of apoptotic insults, including oxidative stress by hydrogen peroxide (H_2O_2). The possible mechanisms behind this protection were explored, and we have in this connection examined possible pro-survival signalling, mitochondrial-associated proteins, ER stress response, and other pathways. These investigations are detailed in chapters 5 and 6.

Chapter 2 Materials and Methods

2.1 General reagents

All fine chemicals were from Sigma-Aldrich (Saint Louis, Missouri, USA) or BDH Chemicals Ltd (Poole, Dorset, UK) unless otherwise stated. Primers (listed in Appendix 1) were synthesized by 1st Base Pte Ltd (Singapore). All enzymes (restriction enzymes, polymerase, phosphatase and ligase) used for cloning were obtained from Promega (Madison, Wisconsin, USA) or New England BioLabs (Ipswich, Massachusetts, USA). The apparatus and reagents employed in sodium dodecyl sulphate polyacrylamide gel electrophoresis (SDS-PAGE) and western transfer were mostly obtained from Bio-Rad Laboratories (Hercules, California, USA). Antibodies were bought from Santa Cruz Biotechnology Inc. (Santa Cruz, California, USA) unless stated otherwise.

2.2 DNA manipulation

2.2.1 Design of constructs

2.2.1.1 Nogo-A constructs

Full-length human Nogo-A coding sequence (CDS) was obtained from the KIAA0886 complementary DNA (cDNA) clone (Kazusa original clone product ID: ORK00673) (Kazusa DNA Research Institute, Chiba, Japan). The clone contained a 4053 bp cDNA inserted into pBluescript II SK (+) vector (pBSK) at the Sal1 and Not1 restriction enzyme (RE) sites via a Sal1 adaptor (5' TCGACCCACGCGTCCG 3') at the 5’ end.

To clone Nogo-A into pCIneo vector (Promega) for protein expression in mammalian cells, the cDNA insert was retrieved from the KIAA0886 clone using Xho1 and Not1, and directly inserted into the pCIneo vector at the Xho1-Not1 site.

Myc-Nogo-A was obtained by cloning only the CDS of Nogo-A (3579 bp) into pDmyc vector. pDmyc was generated by a modification of pCIneo, with an insertion of two tandem myc epitope coding sequences at the Nhe1-Xho1 site. The cloning resulted in Nogo-A fusing at its 5' terminus with two myc tags (EQKLISEEDL), which is a polypeptide protein tag derived from the c-myc gene product. As amplification of the long Nogo-A CDS would increase chances of point mutations during polymerase chain reaction (PCR), a shorter fragment (bp 4-347) of the N-terminus designed to be fused in-frame with the myc tag was first generated instead. The primer set used was A-P1/A-P2. This fragment was cloned into the KIAA0886 construct at the Xho1-Sal1 site, replacing the original sequence present at that site. Xho1 site was present at the 5' end of the Nogo-A CDS while Sal1 was an internal site available at bp 342 of Nogo-A. The now myc-tagged full-length Nogo-A was then retrieved from this construct by Xho1 and Not1 and inserted into pDmyc.

Several myc-Nogo-A truncation constructs were also generated to investigate the interaction between Nogo-A and RTN3 (section 4.2). These constructs are: (1) myc-Nogo-A (-cyto), (2) myc-Nogo-A (-TM1), (3) myc-Nogo-A (-TM2), and (4) myc-Nogo-A (-TMS). Full-length myc-Nogo-A was used as a PCR template in the generation of these truncation constructs. Besides being a template for PCR, myc-Nogo-A was cut with Sac1 (at bp 2504 of Nogo-A CDS) and Not1 (behind the stop codon) to be linearized and acted as the vector backbone for subsequent insertion of the truncation sequences. This cut vector (termed 5' Nogo-A (pDmyc)) contained only bp 1-2504 of Nogo-A. The strategy was to minimize point mutations generated

during PCR of long sequences, as explained earlier. For myc-Nogo-A (-cyto), a DNA fragment of bp 2505-3489 that excluded the cytoplasmic tail after the putative TM2 was amplified by PCR using A-P3/A-P4 and cloned into 5' Nogo-A (pDmyc) at the Sac1-Not1 site. Myc-Nogo-A (-TM1) did not contain the putative TM1 and the 3' KAE motif, and was produced by cloning two DNA fragments sequentially into 5' Nogo-A (pDmyc). The first fragment (amplified using A-P3/A-P5) was from bp 2505-3051, and was inserted into the vector at the Sac1-Xba1 site while the second one (amplified using A-P6/A-P7) was from bp 3163-3567 and was inserted at the Xba1-Not1 site. As for myc-Nogo-A (-TM2), the putative TM2 and cytoplasmic tail of Nogo-A were absent in the construct and only consisted of bp 1-3360, with the DNA fragment of bp 2505-3360 inserted into 5' Nogo-A (pDmyc) at the Sac1-Not1 site after amplification with A-P3/A-P8. Myc-Nogo-A (-TMS) contained only the N-terminus region of Nogo-A, with the whole RHD being truncated, and the amplified N-terminus fragment was inserted at the Sac1-Xba1 site. The primer set A-P3/A-P9 was employed for this construct.

Ng1V2 (pGEX4T1) was constructed to generate a glutathione S-transferase (GST) fused Nogo-A specific peptide to be used in the production of specific antibodies for Nogo-A. The Ng1V2 region, bp 667-1196 (aa 223-399), was selected to be the epitope for antibody generation since it was specifically found in Nogo-A only, and not Nogo-B or -C. An amplified product of this region was obtained by PCR using A-P10/A-P11 and cloned into pGEX4T1 vector (GE Healthcare, Buckinghamshire, UK), which contained a GST sequence 5' of its multiple cloning site, via the EcoR1-Xho1 site.

To delineate the region of Nogo-A that interacted with Caspr, the whole Nogo-66 domain and two other shorter forms of it, Nogo-35 and -40, were fused to

GST and used for GST pull-down assays (section 4.1.3). Nogo-35 (bp 3133-3167), Nogo-40 (bp 3133-3182) and Nogo-66 (bp 3133-3360) were amplified by primer sets A-P12/A-P13, A-P12/A-P14 and A-P12/A-P15 respectively, and cloned into pGEX4T1 at the EcoR1-Xho1 site.

2.2.1.2 Nogo-B constructs

The first construct of Nogo-B generated was myc-Nogo-B. As Nogo-B contained the same bp 1-555 as that of Nogo-A, myc-Nogo-A was used as a PCR template. Two human Nogo-B fragments (bp 1-555 and bp 556-1122) were obtained by PCR using primer sets B-P1/B-P2 and B-P3/B-P4 respectively, and pieced together by sticky end ligation at one end with pDmyc, and blunt end ligation at the alternative splicing site at the center. The first fragment was cloned into the vector at the EcoR1 site at its 5' end, while the 3' end of the second fragment was cloned into Not1 site on the vector.

HA tagged Nogo-B used in the generation of SH-SY5Y HA-Nogo-B stable cell-lines was constructed by simply retrieving the Nogo-B insert out from pDmyc and ligating it into pDHA vector (also modified from pCIneo, containing two hemagglutinin (HA) epitopes (YPYDVPDYAS) instead of myc tags in pDmyc) at the EcoR1-Not1 site.

Untagged Nogo-B was constructed by performing PCR with B-P4/B-P5 to generate a Nogo-B open reading frame that contained a start codon at the N-terminus, followed by cloning into pCIneo at the EcoR1-Not1 site.

For checking of the role of the N-terminus of Nogo-B in protection against cell death, two additional Nogo-B truncation constructs, Nogo-B (1-200) and Nogo-B (N-TM1), were created. For both, the amplified DNA fragment was directly ligated

into pCIneo at the EcoR1-Not1 site. Nogo-B (1-200) fragment (600 bp) was amplified by B-P5/B-P6 while Nogo-B (N-TM1) (717 bp) was by B-P5/B-P7.

2.2.1.3 Nogo-C constructs

Full-length human Nogo-C was obtained by PCR using Nogo-A (pCIneo) as a template. The primer set employed here was B-P5/C-P1. The PCR product was inserted into pCIneo at the EcoR1-Not1 site. This untagged Nogo-C construct was used to generate SH-SY5Y Nogo-C stable cell-lines. N-terminus myc tagged Nogo-C was also generated by inserting Nogo-C into pDmyc vector. This construct was useful as a control while checking for antibodies that could detect Nogo-C. This construct was made by ligating in-frame Nogo-C PCR product (amplified by B-P5/C-P2) into the vector at the EcoR1-Not1 site.

2.2.1.4 Reticulon 1 and 2 constructs (RTN1 and 2)

Expressed sequence tags (ESTs) of mouse RTN 1 (GenBank accession no: BU152315; IMAGE clone ID: 6334636) and 2 (GenBank accession no: BG296036; IMAGE clone ID: 4507150) were obtained from Invitrogen (Carlsbad, California, USA) and found to contain full-length CDS by DNA sequencing. Both RTNs were fused with myc tags at the N-terminus to facilitate detection of expressed proteins by anti-myc antibodies. PCR was performed using the ESTs as templates. The primer sets used for RTN1 and 2 were 1-P1/1-P2 and 2-P1/2-P2 respectively. The amplified DNA fragments obtained were cloned into pDmyc vector at the Xho1-Sal1 site to obtain myc-RTN1 and myc-RTN2.

2.2.1.5 Reticulon 3 constructs (RTN3)

Mouse RTN3 EST clone (GenBank accession no: BM461074; IMAGE clone ID: 5503813) was obtained from Invitrogen. Unlike RTN1 and 2 ESTs, sequencing results of RTN3 EST clone showed that it lacked the first twelve bases (which encoded the first four aa). In the construction of HA- and myc- RTN3, these bases were added in by PCR. RTN3 was tagged with HA and myc via cloning into pDHA and pDmyc respectively at the EcoR1-Sal1 site. The primer set for generating full-length RTN3 in-frame with the tags in these vectors was 3-P1/3-P2.

An untagged RTN3 construct was also generated which was used to generate SH-SY5Y RTN3 stable cell-lines. A direct transfer of the full-length RTN3 CDS from the myc-RTN3 construct to pCIneo vector was carried out via digestion and ligation using EcoR1 and Sal1 RE. This was possible since the RTN3 gene in the former construct already contained a Kozak sequence and a start codon.

To investigate which domains of RTN3 were important for its interaction with Nogo-A, four HA tagged RTN3 truncation constructs were generated: (1) HA-RTN3 (-N), (2) HA-RTN3 (-TM1), (3) HA-RTN3 (-TM2), and (4) HA-RTN3 (-TMS). For (1), the N-terminus of RTN3 was removed from the full-length gene by performing PCR with 3-P2/3-P3 and the amplified DNA fragment (bp 172-714) was inserted into pDHA at the EcoR1-Sal1 site. For (2) to (4), two or three DNA fragments were produced by PCR and first inserted into pQE30 vector (Qiagen, Valencia, California, USA) to piece them together to produce the specific RTN3 truncation genes. This strategy made use of a RE site (Sac1) that was absent in the RTN3 gene but conveniently present between the EcoR1 and Sal1 sites in the vector (and also in pDHA where the gene would eventually be cloned into). Upon confirming that the sequences of the truncation genes were correct after sequential cloning into pQE30,

they were re-cloned into pDHA at the EcoR1-Sal1 site. (2) was formed by two DNA fragments, fragment 1 (bp 1-183) and fragment 2 (bp 222-714) which were amplified by 3-P1/3-P4 and 3-P2/3-P5 respectively. (3) was also the product of two DNA pieces ligated, with the first fragment (bp 1-492) amplified by 3-P1/3-P6 and the second fragment (bp 610-714) being amplified by 3-P2/3-P7. (4) required three parts, the first being the first DNA fragment of (2), the second being bp 222-492 (amplified by 3-P5/3-P6) and the third being the second DNA fragment of (3).

2.2.1.6 Caspr and Caspr 2 constructs

Human Caspr cDNA was generously provided by Dr Elior Peles (Weizmann Institute of Science, Rehovot, Israel). The construct contained CDS of Caspr cloned into pRK5 vector at the Xba1 site. A construct whereby GST was fused to aa 1308-1377 (bp 3922-4131) of human Caspr was generated for the production of specific Caspr antibodies. The fragment was amplified by the primer set Caspr-P1/Caspr-P2 and cloned into pGEX4T1 at EcoR1-Xho1 site.

Full-length human Caspr 2 cDNA was obtained from the KIAA0868 clone (Kazusa original clone product ID: ORK04596) (Kazusa DNA Research Institute). A digestion of the KIAA clone was performed to obtain the cDNA for direct ligation into pCIneo at the Sal1-Not1 site. As for the generation of a GST fusion protein containing aa 1284-1331 (bp 3850-3993) of Caspr 2 for use in antibody production, the DNA fragment was amplified with the primers Caspr2-P1/Caspr2-P2 and cloned into pGEX4T1 at the EcoR1-Xho1 site.

2.2.2 Molecular cloning procedure

The expression constructs described in section 2.2.1 were obtained by first performing PCR with a TPersonal Thermocycler (Biometra, Goettingen, Germany) to amplify the DNA fragment of interest, in a reaction containing KIAA or EST clones as templates, the high fidelity *pfu* DNA polymerase, a specific pair of forward and reverse primers (final concentration of 20 µM) and dNTPs (dATP, dGTP, dTTP and dCTP each at a final concentration of 10 mM; Promega). A typical PCR program was: (1) 95°C, 5 min (2) 95°C, 1 min (3) 50°C, 2 min (4) 72°C, 3 min (5) 72°C, 10 min, with the reaction cycling from steps (2)→(4) for 45 times.

Amplified products were checked by DNA gel electrophoresis on 1% agarose gels (agarose from BioWhittaker Molecular Applications, Rockland, Maine, USA) that contained 0.5 µg/ml of ethidium bromide (Bio-Rad Laboratories). The 2-log DNA marker (New England BioLabs) was used to confirm the fragments' sizes. The gels were run for 30 min at a constant voltage of 120 V in a Tris-acetate-EDTA buffer (40 mM Tris, 20 mM Na-acetate and 1 mM EDTA; pH 8.2) before they were viewed using the image analysis software, KODAK 1D LE v3.6, under UV light with a KODAK EDAS 290 (Eastman Kodak Company, Rochester, NY, USA).

Observed bands of amplified products were excised and purified by QIAquick Gel Extraction Kit (Qiagen). The amplified products, together with required vectors, were digested with appropriate REs overnight at 37°C. The linearized vectors were additionally incubated with Calf Intestinal Alkaline Phosphatase for 45 min at 37°C to remove the phosphate group at the 5' end so as to lower the chances of self-ligation. After purification using the QIAquick Gel Extraction Kit, the amplified DNA and vectors were ligated by T4 DNA ligase overnight at 16°C.

The ligation mixture was then transformed into *Escherichia coli* (*E. coli*) DH5α strain competent cells (Subcloning Efficiency™ DH5α™ Competent Cells; Invitrogen) by the following steps. It was first incubated with the bacterial cells for 30 min on ice, followed by heat-shock for 1 min at 42°C. Following that, the cells were placed on ice for another 1 min, before 1 ml of SOC medium (2% Bacto™ Tryptone (Difco Laboratories Inc., Detroit, Michigan, USA), 0.5% Bacto™ Yeast Extract (Difco), 2.5 mM NaCl, 10 mM $MgCl_2$, 10 mM $MgSO_4$ and 0.4% glucose) was added and recovery of the cells was allowed for 45 min at 37°C. Finally, the cells were plated onto Luria-Bertani Broth (LB) agar (Bio Basic Inc., Markham Ontario, Canada) containing 100 µg/ml of ampicillin (Sigma-Aldrich) and incubated overnight at 37°C. Cells transformed with the plasmid would survive in the presence of ampicillin due to an ampicillin resistance gene found on the vector and would form colonies observable on the next day.

After expanding these colonies in ampicillin-containing LB, plasmid DNA were extracted from these bacterial cells using Wizard® *Plus* SV Minipreps DNA Purification System (Promega). Insertion of gene in the plasmid was checked by analytical restriction digestion and DNA gel electrophoresis, before sequencing of the constructs was carried out. This step was to confirm that the inserted gene contained the correct sequence. Large-scale preparation of the plasmids, whenever necessary, was performed using Pureyield™ Plasmid Midiprep System (Promega).

2.3 Protein work

2.3.1 Sodium dodecyl sulphate polyacrylamide gel electrophoresis (SDS-PAGE)

SDS-PAGE was carried out using a Mini-PROTEAN 3 system, with the discontinuous polyacrylamide gels casted using its gel casting frames. 8-15%

resolving gels were accordingly prepared with 8-15% of an acrylamide/bisacrylamide mixture (30%, with a ratio of 29:1) in 0.375 M Tris-Cl and 0.1% sodium dodecyl sulphate (SDS) (pH 8.8). The stacking gel was made up of 5% acrylamide/bisacrylamide in 0.125 M Tris-Cl and 0.1% SDS (pH 6.8). For both gels, ammonium persulphate (Sigma-Aldrich) and N, N, N, N-Tetramethy-Ethylenediamine (TEMED) (Invitrogen) were added at a final concentration of 0.025% and 1:400 ratio respectively to aid in the polymerization of acrylamide.

Protein samples were prepared as described. Cells and tissue samples were lysed in ice-cold lysis buffer (50 mM Tris, 1 mM EDTA and 150 mM NaCl; pH 8) containing 1% Triton X-100 (Tx-100), 0.1 mM phenylmethylsulphonyl fluoride (PMSF) (Sigma-Aldrich) and 1X protease inhibitor cocktail (Roche Diagnostics, Indianapolis, Indiana, USA). For experiments where phosphorylated proteins were being investigated, the phosphatase inhibitors, sodium orthovanadate (Sigma-Aldrich) and sodium fluoride (Sigma-Aldrich), were added at a final concentration of 1 mM and 5 mM respectively. The lysates were rolled overnight at 4°C to allow for complete lysis. An additional homogenization step using a Dounce homogenizer after addition of lysis buffer was required for tissue samples. Cell lysates were spun at 16,000 g for 5 min at 4°C while tissue samples were ultra-centrifuged at 100,000 g for 1 hr at 4°C to spin down the debris. The lysates' concentrations were then measured with the Bio-Rad Protein Assay (Bio-Rad Laboratories) using a GeneQuant *pro* spectrophotometer (GE Healthcare). Appropriate amounts of lysates were diluted in phosphate buffered saline (PBS) (1^{st} Base) to achieve equal volumes before the addition of freshly prepared 5X SDS sample buffer (250 mM Tris-Cl (pH 6.8), 100 mM dithiothreitol (DTT) (Bio-Rad Laboratories), 10% SDS, 50% glycerol and 0.5% bromophenol blue (Sigma-Aldrich)). The protein samples were subsequently

denatured for 10 min at 70°C before loading into the gels. The protein marker, Precision Plus All Blue Standards (Bio-Rad Laboratories), was loaded into all gels to indicate protein sizes. Gels were run at a constant voltage of 120 V for 80 min in a buffer containing 0.3% Tris-base, 1.44% glycine and 0.1% SDS.

2.3.2 Coomassie Blue staining and destaining of SDS-PAGE gels

In some experiments, the gels were stained with Coomassie Blue to visualize the proteins. This was carried out by soaking the gels for 30 min at room temperature, with shaking, in a Coomassie Blue staining solution (0.2% Coomassie Brilliant Blue R-250 (Bio-Rad Laboratories) in 40% methanol and 10% acetic acid). Destaining of the gels was then performed in two steps, first for 10 min in a stronger destaining solution (50% methanol and 10% acetic acid), followed by a milder one (10% methanol and 10% acetic acid) until the background staining was removed and bands could clearly be seen.

2.3.3 Western transfer and blotting

Proteins resolved in SDS-PAGE gels were transferred to Hybond^{TM}-C Extra nitrocellulose membranes (GE Healthcare) using a Mini Trans-Blot® Electrophoretic Transfer Cell. The transfer was performed in 0.3% Tris-base and 1.44% glycine at a constant voltage of 100 V for 80 min. To check the efficiency of protein transfer to the membranes after western transfer, the membranes were reversibly stained with Ponseau S after a brief incubation with the staining solution (0.2% Ponseau S (Sigma-Aldrich) in 0.5% acetic acid). Background staining was removed by rinsing the membranes with deionized water. Complete removal of Ponseau S staining was achieved by washing in 0.05% Tween-20/PBS.

Following this, the membranes were blocked with 5% skim milk (in 0.05% Tween-20/PBS) for 1 hr at room temperature. Membranes were then incubated with specific primary antibodies (diluted in 3% bovine serum albumin (BSA) (Sigma-Aldrich) in 0.05% Tween-20/PBS) overnight at 4°C. The primary antibodies that were employed were listed in Appendix 2. γ-tubulin (1:5000; Sigma-Aldrich) was generally probed as a loading control, and for normalization purpose in protein band quantification. Secondary antibodies conjugated to horse radish peroxidase (HRP) were diluted in the blocking buffer stated above and incubation with the membranes took place for 1 hr with shaking at room temperature. Donkey anti-goat HRP (Santa Cruz) was usually diluted 1:3000 while goat anti-rabbit and -mouse HRP (Thermo Fisher Scientific, Waltham, MA, USA) were usually diluted 1:5000. Membranes were washed three times with 0.05% Tween-20/PBS at 5 min per wash after each antibody incubation. The membranes were finally incubated for 5 min with gentle rocking in a solution of a chemiluminescent substrate, SuperSignal West Pico Chemiluminescent Substrate (Thermo Fisher Scientific), before visualization of the protein bands was achieved upon developing exposed films (China Lucky Film Corporation, Hebei, China) with a Kodak X-OMAT 200 processor (Eastman Kodak Company).

2.3.4 Production of GST fusion proteins

GST tagged-Nogo 1V2, -Caspr and -Caspr 2 were produced as antigens for the generation of antibodies specific to Nogo-A, Caspr and Caspr 2 respectively. GST, GST-Nogo-35, -40 and -66 were generated for GST pull-down experiments in the determination of Nogo-A's interaction with Caspr (section 4.1.3). The required GST tagged expression plasmids were constructed as stated in section 2.2.1.

2.3.4.1 Preparation of GST-proteins for antigens

To produce GST fusion proteins as immunogens, 50 µl of fresh bacterial culture was inoculated into 200 ml of LB + 100 ug/ml ampicillin and grown overnight at 37°C with shaking. This was topped up with 600 ml of fresh medium the next day and left to grow for another 2 hr for the bacteria cells to reach logarithm phase (optical density at a wavelength of 600 nm = 0.5-1.0).

Isopropyl-β-D-thiogalactopyranoside (IPTG) (Invitrogen) was then added to a final concentration of 0.1 mM to induce protein expression via its action on the lac operon found on the vector pGEX4T1 in the bacterial cells. The culture was grown for another 4 hr before harvesting was carried out by centrifugation at 7,560 g for 10 min. The pellet was resuspended in 80 ml of ice-cold PBS containing 0.1 mM PMSF and then sonicated on ice using a Sonics Vibra-Cell^{TM} VCX 130 ultrasonicator (Sonics & Materials Inc., Newtown, Connecticut, USA) with two rounds of 4 pulses lasting 10 s each and a 15 s rest period between each pulse. The bacterial suspension was allowed to cool on ice between the two rounds to prevent degradation of proteins as a result of heat generated from sonication. Lysed cells were spun at 36,000 g for 30 min to collect the supernatant, which was then added with 800 µl of glutathione agarose beads (GE Healthcare) and subjected to rolling at 4°C for 2 hr to allow complete binding of fusion proteins with the glutathione on the beads.

After collecting and washing the beads with ice-cold PBS, elution of bound GST fusion proteins was carried out using freshly prepared ice-cold elution buffer (20 mM reduced glutathione (Sigma-Aldrich), 50 mM Tris (pH 8.0) and 0.1% Tx-100 in PBS; pH 7-7.5). Eight 1 ml fractions were collected and analyzed by SDS-PAGE followed with Coomassie Blue staining. Only fractions with high amounts of proteins

were dialysed in three rounds of 600 ml of cold PBS at 4°C, with a change of PBS every 8-15 hr, after which the proteins were stored at -20°C.

2.3.4.2 Preparation of GST-proteins for pull-down assays

A similar procedure as described above (section 2.3.4.1) was used, except that the volume of bacterial culture required was halved. Also, the fusion proteins were bound to glutathione sepharose 4B beads (GE Healthcare) and not agarose. Instead of eluting out the GST-proteins bound to the beads, the beads were collected by centrifuging at 1,700 g for 2 min to remove the supernatant and washed four times with 1 ml of ice-cold PBS, with spinning at 2,500 g for 30 s after each wash to remove the PBS. The beads were then stored at 4°C. To determine the concentration of bound fusion proteins, an aliquot of the beads was checked by SDS-PAGE and Coomassie Blue staining, using BSA as a loading control.

2.3.5 Purification of antibodies

After collection of blood from immunized rabbits (as described in section 2.5.1), the blood was first left to clot overnight at 4°C. Serum was obtained by centrifuging the clotted blood at 4,100 g for 20 min at 4°C. The serum was then diluted 1:1 with PBS before incubation with nitrocellulose membrane strips containing immobilized antigens overnight at 4°C with rolling. The membrane strips were obtained by first running SDS-PAGE with antigens loaded into 2-well gels, followed by electroblotting the antigens onto nitrocellulose membranes by western transfer, staining the membranes with Ponseau S to visualize the antigen bands and finally cutting out these bands.

After the overnight incubation with serum, the membrane strips were washed with PBS before they were cut into small pieces and placed in a snap cap vial. Antibodies bound to the membrane were then eluted out with an IgG elution buffer containing Tris-HCl and glycine (pH 2.8) (Thermo Fisher Scientific). The eluent was neutralized to pH 7.0 with 1 M Tris-HCl (pH 8.0) before storage at -20°C.

2.3.6 Nuclear-cytosol fractionation

Cells were plated onto 100 mm dishes at a cell density of 3.75 X 10^5. Fresh medium was given on the second day after plating and the cells were harvested the next day.

Fractionation was performed as described by Qu *et. al.* (2004) with some modifications. Briefly, cells were washed twice with ice-cold PBS before being pelleted at 16,000 g for 30 s. The pellet was resuspended in 100 µl of ice-cold buffer A (10 mM HEPES-KOH (pH 7.5), 10 mM KCl, 1 mM DTT, 1 mM PMSF and 1X protease inhibitor cocktail) and incubated on ice for 15 min. 10% Nonidet P-40 (final concentration of 0.3125%) was then added, the mixture vortexed briefly and incubated on ice for another 10 min. The nuclei were pelleted by centrifugation at 1,500 g for 5 min at 4°C, while the cytoplasmic extracts (supernatant) were recovered by centrifugation at 13,000 g for 15 min at 4°C. Nuclei were washed twice with 1 ml of ice-cold buffer A before resuspension in 12.5 µl of ice-cold buffer B (20 mM HEPES-KOH (pH7.5), 0.4 M NaCl, 1 mM DTT, 1 mM PMSF and 1X protease inhibitor cocktail). The mixture was incubated on ice for 30 min, with a brief vortex after every 10 min, before centrifugation at 18,000 g for 5 min at 4°C to collect the nuclei extracts (supernatant).

2.4 Cell culture

2.4.1 Mammalian cell culture

Human neuroblastoma SH-SY5Y cells, HEK293 cells and Chinese hamster ovary (CHO) cells were obtained from the American Type Culture Collection (ATCC) (Manassas, Virginia, USA). The cells were maintained in Roswell Park Memorial Institute (RPMI) medium (Caisson Laboratories Inc., North Logan, Utah, USA) with 10% fetal bovine serum (FBS) (Hyclone Laboratories Inc., South Logan, Utah, USA) and 1X antibiotics/antimycotics solution (containing 10,000 units of penicillin, 10,000 µg of streptomycin and 25 µg amphotericin B in 0.85% saline per ml) (Invitrogen) in a humidified 37°C incubator with 5% carbon dioxide (CO_2) atmosphere. Upon confluency, cells were washed once with PBS, trypsinized with 0.05% trypsin/0.0076% EDTA (Invitrogen) and split at a ratio of 1:5.

2.4.2 Transient transfection

Cells were plated onto 12 mm microscope cover glasses (Einst Technology Pte Ltd, Singapore) or in 6-wells for ICC or western blotting respectively. Transient transfection was performed using Lipofectamine™ 2000 (Invitrogen) when the cells were 60-80% confluent according to the manufacturer's instructions. In brief, Lipofectamine™ 2000 was incubated for 5 min in Opti-MEM® I Reduced Serum Medium (Invitrogen) before addition to the DNA to be transfected which was also diluted in Opti-MEM®. A further incubation of the complex for 20 min was carried out before it was added to the cells. Cells were analysed 24 and 48 hr later for protein expression by the two respective techniques mentioned above.

2.4.3 Generation of stable cell-lines

Stable cell-lines of SH-SY5Y (SH-SY5Y Nogo-A, Nogo-B, HA-Nogo-B, Nogo-B (1-200), Nogo-B (N-TM1), Nogo-C and RTN3); HEK293 Nogo-A and HA-RTN3; and CHO Nogo-A were generated as described below. The respective wild type cells were plated into 6 wells the day before transfection. On the next day, cells were transfected using Lipofectamine™ 2000. 4 µg of the respective DNA constructs was mixed with Lipofectamine™ 2000 at a ratio of 1:2.5 (DNA: Lipofectamine™ 2000) in Opti-MEM® and added to the cells. Medium was changed after 4 hr to minimize the toxicity of the transfection mixture.

24 hr later, cells were trypsinized and plated into 100 mm dishes at a very low density. Geneticin or G418 (Invitrogen) was added to the cells the day after plating at a concentration of 0.5 mg/ml. G418 was gradually increased to 1.4 mg/ml with a change of medium every 4-5 days. G418-resistant colonies appeared approximately 2 weeks later and were picked into 24 wells. After confirmation of protein expression by ICC and western blotting, the positive colonies were expanded, frozen and used for subsequent experiments. The stable cell-lines were then maintained in RPMI medium containing 0.8 mg/ml G418.

CHO expressing Caspr/F3 was generously provided by Prof. Xiao Zhi Cheng (Department of Clinical Research, Singapore General Hospital, Singapore).

2.4.4 Primary culture of cortical neurons

C57BL/6 or Nogo-deficient pregnant mice on E15 were used for the harvesting of cortical neurons. The former was obtained from the Centre of Animal Resources (Singapore) while the latter was bred as described in section 2.5.2. The pregnant mother was first anaesthetized intraperitoneally with 300 µl of a 1:1

ketamine and xylazine mixture before a cervical dislocation was performed. 70% ethanol was used to swab the abdominal region and the skin cut to allow retrieval of the uterus with embryos to the harvest medium (10 mM HEPES (pH 7.4) (Sigma-Aldrich) and 1X antibiotics/antimycotics in Hank's balanced salt solution without Ca^{2+} and Mg^{2+} (Invitrogen)). Amnia enclosing the embryos were removed, the heads decapitated and the cerebral hemispheres separated from skin and skull. Removal of the meninges layer and separation of the cortices from the other parts of the brain was performed under a microscope.

Cortices were then minced in 2 ml of harvest medium, followed by the addition of 0.2 ml of 2.5% trypsin and 20 µl of 250 ug/ml DNaseI (Sigma-Aldrich). Enzymatic digestion was allowed to take place for 15 min at 37°C, with mixing performed at every 5 min interval. 0.22 ml of FBS was added to the cortices to inhibit the trypsin and this was left to stand for 5 min at room temperature. The supernatant was carefully removed, followed by the addition of plating medium (0.05% $NaHCO_3$ (Sigma-Aldrich), 1 mM sodium pyruvate (Invitrogen), 0.6% glucose, 10% FBS and 1X antibiotics/antimycotics in minimum essential medium (MEM) (Invitrogen)) and trituration using a glass Pasteur pipette. Volume of plating medium to be added depended on each harvest but typically 1 ml of plating medium was added for each brain harvested. Cell density of the suspension was determined by counting using a hemocytometer, and the cells were then plated onto 12 mm coverslips and 100 mm dishes at a cell density of 1.25×10^5 and 8×10^6 respectively. The coverslips and 100 mm dishes were first coated with 10 µg/ml poly-L-lysine (PLL) before plating. On the following day after plating, the plating medium was replaced with maintaining medium (1X B-27 serum-free supplement (Invitrogen) and 10 mM L-glutamine (Invitrogen) in Neurobasal™ medium (Invitrogen)) and the cortical neurons were

maintained in this medium with a change of medium every 4 days until 7 days *in vitro* (DIV7) for checking of Nogo-A expression in neurons, or DIV16 for cortical neuronal morphological differentiation studies (section 3.3).

2.4.5 Primary culture of oligodendrocytes and astrocytes

Primary astrocytes were obtained from P1-2 C57BL/6 mice or Sprague Dawley rats. Primary oligodendrocytes were cultured from the latter only.

The animals were first anaesthetized on ice before they were decapitated and the brains removed from the skull and placed in Dulbecco's Modified Eagle Medium: Nutrient Mixture F-12 (DMEM/F12) (Invitrogen) containing 1 mM sodium pyruvate and 1% antibiotics/antimycotics. The brains were minced into small pieces after removing the meninges and subjected to tryptic digest for 30 min at 37°C with 0.1% trypsin/versene (0.02% EDTA/PBS). Approximately 1 ml of trypsin/versene was used for each brain. Trypsin present was then inhibited by the addition of DMEM/F12 supplemented with 10% FBS in a 1:3 trypsin:medium ratio.

The trypsinized brains were triturated with a glass Pasteur pipette before filtration through a 70 µM BD Falcon nylon cell strainer (BD Biosciences, San Jose, California, USA). The mixed glial cell suspension was then plated onto T75 flasks (2 brains per flask) precoated with 30 µg/ml of PLL in DMEM/F12 containing 10% FBS, 1 mM sodium pyruvate and 1% antibiotics/antimycotics, and medium was refreshed every 3 days. The mixed culture was also plated onto PLL-coated coverslips for ICC studies.

After 12-14 days when the culture reached confluency, the flasks were shaken in an orbital shaker at 220 rpm overnight to isolate oligodendrocytes from astrocytes. As oligodendrocytes were less adherent, they would dislodge into the medium after

vigorous shaking. The medium was centrifuged at 2,500 g for 3 min to collect the suspended oligodendrocytes which were then plated into PLL-coated 60 mm dishes for western blot analysis. The remaining astrocytes in the T75 flasks were trypsinized and re-plated onto 60 mm dishes as well. Both the oligodendrocytes and astrocytes were maintained in DMEM/F12 containing 10% FBS, 1 mM sodium pyruvate and 1% antibiotics/antimycotics, with the medium being refreshed every 3 days.

2.5 Animal work

2.5.1 Immunization of rabbits

500 µg of GST-Nogo 1V2, -Caspr or -Caspr 2 (preparation as described in section 2.3.4.1) in 2 ml of sterile PBS and mixed with 2 ml of Freund's Adjuvant (Sigma-Aldrich) to form an emulsion with 2 syringes connected through a Luer fitting. Complete Freund's Adjuvant was used for the first immunization while Incomplete Freund's Adjuvant was employed for subsequent booster injections. The mixture was then injected subcutaneously into specific pathogen-free (SPF) New Zealand White female rabbits under anaesthesia in compliance with the protocol approved by the National University of Singapore (NUS) Institutional Animal Care and Use Committee (IACUC). Booster immunizations were given at every two weeks interval after the first immunization.

Two weeks after the fourth injection, 10 ml of blood was collected from the central ear artery of anaesthetized rabbits using a 25-gauge Surflo winged infusion set (Terumo Europe, Leuven, Belgium). Rabbits with positive response continued to receive a booster injection whereby two weeks after the booster injection, 20-50 ml of blood was taken from the animals. The rabbits were rested for a month after each bleed before the next immunization.

2.5.2 Maintenance and breeding of Nogo-deficient mice

Two pairs of Nogo-deficient mice (Zheng *et. al.*, 2003) were obtained from Genentech, Inc. (South San Francisco, California, USA). These mice were deficient in all three isoforms of Nogo (termed Nogo-A/B/C mutant), as they were shown to express neither Nogo-A nor -B mRNA while expressing a shorter Nogo-C transcript (which most likely produced a non-functional protein). The knockout was designed such that the first exon of the six exons encoding the RHD was removed. After many rounds of breeding, a mouse colony was established. The mice were kept in the NUS Animal Holding Unit in individually ventilated cages in an environment in accordance to NUS IACUC policies and guidelines.

Periodic matings were carried out to maintain the mouse colony and also to provide pregnant E15 mice for primary cortical neuronal culture (section 2.4.4). For the latter, a female mouse was placed into a cage containing a male mouse overnight and on the next day, they were separated and the female mouse weighed. Three to four pairs of mating were set up each time. The day of separation was considered to be E0 (or E0.5). The female mice were weighed again on E12-13 to check for pregnancy before one pregnant mouse was sacrificed on E15 to obtain primary cortical neurons.

2.5.3 Perfusion of C57BL/6 and Nogo-deficient mice

4-8 weeks old C57BL/6 and Nogo-deficient female mice were first sedated with an intraperitoneal injection of 300 µl of ketamine and xylazine mixture (1:1). The mice were then dissected to open the thoracic cavity to expose the heart. A 23-gauge Surflo winged infusion set (Terumo Europe) was inserted into the left ventricle and a snip was performed at the right atrium. The animals were perfused with cold

Ringer solution (0.86% NaCl, 0.03% KCl and 0.033% $CaCl_2$ in deionized water) to wash out the blood. When all blood had been washed out, as observed by the clear solution flowing out of the snipped atrium, cold 4% paraformaldehyde (PF) (Sigma-Aldrich) in 0.1 M phosphate buffer (0.08 M Na_2HPO_4 and 0.02 M NaH_2PO_4; pH 7.3-7.4) was then used to fix the animals for at least 30 min. The Ringer solution and PF were either freshly prepared or prepared the day before.

When the whole animals were completely fixed, the brains and spinal cords were carefully retrieved and left to post-fix in 4% PF overnight. On the next day, the tissues were rinsed with PBS and soaked in 30% sucrose in 0.1 M phosphate buffer as a cryoprotective measure for 24 hr or until the tissues have sunken.

2.6 Interaction studies

2.6.1 GST pull-down assays

In vitro GST pull-down assays were employed to investigate the interaction of Nogo A with Caspr (section 4.1.3), with GST, GST-Nogo-35, -40 and -66 fusion proteins bound to glutathione sepharose beads acting as "baits". GST was used as a negative control for the experiments. 20 µg of these "bait" proteins were incubated with 1.5 mg of cell lysates (containing stably or transiently expressed "prey" proteins) overnight with rolling at 4°C. The lysates were first diluted 1:4 to obtain a final concentration of 0.25% Tx-100 present before the addition of glutathione sepharose beads. Total beads volume was topped up to 30 µl with glutathione sepharose beads whenever necessary.

Following this, the beads were pelleted at 2,500 g for 30 s and the supernatant removed. The beads were washed three times with 1 ml of ice-cold lysis buffer containing 0.25% Tx-100, and finally two washes with ice-cold lysis buffer without

Tx-100. Elution of proteins bound to the beads directly (the "bait") or indirectly (the "prey") was carried out with SDS sample buffer for 10 min at 70°C before SDS-PAGE and western blotting were performed to check for the presence of target proteins that interacted with and therefore pull-downed by the GST fusion proteins.

2.6.2 Co-immunoprecipitation (Co-IP)

3 µg of antibodies specific for target antigens were added to 1.5 mg of lysates (containing Tx-100 at a final concentration of 0.25%) and the mixture was rolled overnight at 4°C. 30 µl of protein A or G sepharose beads (GE Healthcare) was then incubated with the mixture the next day for 2 hr at 4°C. The former was used to bind and pull-down rabbit antibodies while the latter was for mouse antibodies.

After that, the beads were centrifuged at 2,500 g for 30 s to remove the lysates and excess antibodies. Non-specific binding of proteins was removed by washing the beads three times with ice-cold lysis buffer containing 0.25% Tx-100 and two times with ice-cold lysis buffer without Tx-100. Any proteins interacting with the target protein bound by the antibody would co-precipitate with the latter in a protein complex that was pull-downed by the beads. Finally, the bound proteins and antibodies were eluted with the addition of SDS sample buffer and the co-IP samples were subjected to SDS-PAGE followed by western blot analysis.

2.7 Localization studies

2.7.1 Immunocytochemistry (ICC)

Cells were plated onto 12 mm microscope cover glasses coated with 30 µg/ml of PLL, and fixed with 4% PF for 15 min at room temperature the next day. For NF-κB p65 subunit translocation upon H_2O_2 or TNFα treatment, cells were plated into 6-

wells (each containing 5 PLL-coated coverslips) at a cell density of 0.625 X 10^5. Cells were treated as described in section 2.8.1 and a coverslip was taken out for fixation at each time point. The coverslips were then washed once in PBS, twice in 100 mM NH_4Cl/PBS and once in PBS, for 2 min per wash with gentle shaking. After washing, cells were permeabilized with 0.05% saponin (in PBS) extracted from Quillaja bark (Sigma-Aldrich) or 0.2% Tx-100/PBS for 10 min at room temperature. Methanol fixation was also employed for specific antibodies, where cells were incubated on ice for 5 min with cold methanol. No further permeabilization was necessary and subsequent washing steps were carried out in PBS.

The cells were then incubated with primary antibodies diluted in blocking buffer (2% BSA and 5% FBS in PBS) for 1 hr at room temperature. This was followed by washing twice in PBS. A third wash in 0.05% saponin /PBS or PBS alone was performed for cells permeabilized with saponin or Tx-100 respectively. Secondary antibodies (1:150) conjugated to fluorescein isothiocyanate (FITC) or Texas Red (TxR) (Jackson Immunoresearch Laboratories Inc., Westgrove, Pennyslvania, USA) were incubated with the cells for another 1 hr at room temperature. In experiments where a blocking control was performed, 0.3 µg of diluted Ng1V2 antibody (the amount that was usually used for one coverslip) was first incubated with 6 µg of GST-Ng1V2 (twenty times the amount of antibody used) overnight at 4°C before the primary antibody incubation step. Finally, the cells were washed three times with PBS before the coverslips were mounted onto glass slides (Sail Brand, Jiangsu, China) with Vectashield mounting medium (Vector Laboratories Inc., Burlingame, California, USA) and sealed with nail polish. For staining of cells with Hoechst, Hoechst 33342 (Molecular Probes Inc., Eugene, Oregon, USA) was added in the ratio of 1:20,000 in the first wash. The cells were then viewed with a

Carl Zeiss LSM 510 confocal microscope (Carl Zeiss Inc., Thornwood, New York, USA).

The primary antibodies used for ICC were as listed below. The following antibodies required permeabilization with saponin: Ng1V2 rabbit polyclonal antibodies at a concentration of 1-2 mg/ml (1:500; "home-made"), AR2 rabbit polyclonal antibodies (1:500; a kind gift from Dr Luc Dupuis from Inserm U692, Strasbourg, France), anti-HA monoclonal antibody (1:100; 12CA5), and mouse monoclonal antibodies against Tuj (1:50; T8660; Sigma-Aldrich), 2', 3'-cyclic nucleotide 3'-phosphodiesterase (CNPase) (1:100; C6200X; USBiological, Swampscott, Massachusetts, USA) and glial fibrillary acidic protein (GFAP) (1:200; G3893; Sigma-Aldrich). Tx-100 was used for permeabilization for these antibodies: anti-glucose regulated protein 94 (GRP94) goat polyclonal antibodies (1:50; sc-1794) and anti-NF-κB p65 mouse monoclonal antibodies (1:50; sc-8008). Methanol fixation was employed in ICC experiments using anti-RTN3 rabbit polyclonal antibodies (1:125; AB72814; Abcam, Cambridge, UK).

2.7.2 Immunohistochemistry (IHC)

Fixed brain and spinal cord tissues as prepared in section 2.5.3 were embedded and frozen in Tissue-Tek Optimum Cutting Temperature (O.C.T.) compound (Sakura Finetek USA Inc., Torrance, California, USA). The frozen tissues were cryosectioned into 20 µm parasagittal sections with a Microm HM 525 cryostat (Microm Laborgeräte, Bad Schwalbach, Germany) and placed onto glass slides coated with 5% glycerol. The sections were then stored at -80°C.

To perform immunohistochemistry (IHC), frozen sections were thawed and further fixed in 4% PF for 30 min at room temperature. Similar to the ICC procedure,

the sections were washed one time with PBS, two times with 100 mM NH_4Cl/ PBS and one time with PBS with gentle shaking for 5 min per wash. Sections were then permeabilized with 0.2% Tx-100/PBS for 1 hr at room temperature, followed by an incubation with blocking buffer (4% BSA and 10% FBS in PBS) for another hr.

After three washes with PBS at 10 min each, primary antibodies diluted in the blocking buffer were placed onto the sections and incubation took place in a humidified chamber overnight at 4°C. For blocking controls in certain experiments, 0.7 µg of diluted Ng1V2 antibody (the amount used per section) was first incubated with 14 µg of GST-Ng1V2 (twenty times that of antibody used) for 4 hr or overnight at 4°C before incubating the primary antibody with the sections. On the next day after primary antibody incubation, the sections were washed trice with PBS for 10 min per wash before incubation with respective secondary antibodies conjugated to FITC or TxR for 1 hr at room temperature.

To stain the nuclei, the sections were placed in PBS containing Hoechst 33342 (diluted 1:20,000 in PBS) for 10 min with gentle shaking. This was followed by three washes of PBS at 10 min each. The mounting medium Vectashield was then dropped onto the sections, and these were eventually overlaid with coverslips. Viewing of the sections was then carried out using a Carl Zeiss LSM 510 confocal microscope.

The dilutions for Ng1V2 antibodies and those against Tuj, CNPase and GFAP used in IHC were the same as that for ICC studies. The "homemade" rabbit polyclonal antibodies against Caspr (at 0.2-0.5 mg/ml) were used in a dilution ratio of 1:150. Monoclonal antibodies against Caspr (1:150; 75-001) and K^+ channels (1:300; 75-008) were obtained from US Davis/ National Institutes of Health (NIH) NeuroMab Facility (Davis, California, USA).

2.8 Apoptosis assessment assays

2.8.1 Propidium iodide (PI) labelling/ flow cytometry

SH-SY5Y stable cell-lines were plated in triplicates at a cell density of 0.625 X 10^5 per 6-well. Fresh medium (without G418) was given to the cells after 40 hr of plating. The cells were treated with various drugs the following day and harvested at the required time points. For H_2O_2 treatment, cells were treated with 100 µM of stabilized H_2O_2 (Merck KGaA, Darmstadt, Germany) for 30 min before H_2O_2 was removed, the cells washed once and replenished with fresh medium. Serum withdrawal was performed by growing the cells in serum-free medium after washing them twice with the same serum-free medium. For the other treatments, cells were directly incubated in fresh medium containing the drugs. Staurosporine (A.G. Scientific Inc., San Diego, California, USA), etoposide (A.G. Scientific Inc.), tunicamycin (Sigma-Aldrich) and TNFα (Prospec-Tany TechnoGene Ltd, Rehovot, Israel) were given at a final concentration of 0.5 µM, 20 µM, 20 µg/ml and 10 ng/ml respectively.

In experiments where cells were treated with inhibitors prior to H_2O_2 treatment, 50 µM of phosphoinositol-3-kinase (PI3K) inhibitor LY294002 (A.G. Scientific Inc.) and 10 µM of MEK 1/2 inhibitor U0126 (A.G. Scientific Inc.) were preincubated with the cells for 1 hr and 30 min respectively.

At the time of harvest, cells were collected together with the medium and the wells washed with 1 ml of ice-cold PBS to collect any residual cells. Cells were pelleted at 4,100 g for 5 min at 4°C, washed with 1 ml of ice-cold 1% FBS/PBS and spun again at the same speed. The pellet was then resuspended in 100 µl of ice-cold 1% FBS/PBS, and immediately fixed with 1 ml of ice-cold 75% ethanol to prevent clumping of cells. Fixing of the cells was carried out at 4°C until flow cytometry was

to be performed. To stain the cells with propidum iodide (PI), they were first pelleted as stated above to remove the ethanol. The pellet was washed once with 1 ml of ice-cold 1% FBS/PBS before resuspension in 500 µl of ice-cold 1% FBS/PBS containing PI (Sigma-Aldrich) and RNase A (Sigma-Aldrich) at a final concentration of 10 µg/ml and 250 µg/ml respectively. The cells were incubated for 1 hr at 37°C. Flow cytometry was performed using a BD FACSCanto™ II flow cytometer (BD Biosciences) and data was analysed with BD FACSDiva™ Software v5.0.2. Cell cycle profile histograms were drawn using the ModFit v2.9 software. The percentage of cell death was measured as the percentage of cells in sub G1 phase.

2.8.2 Fluorimetric caspase activation assay

Cells were plated in triplicates onto 100 mm dishes at a cell density of 3.75 X 10^5 respectively, and treated as according to flow cytometry analysis (section 2.8.1). At the end of treatment, cells were harvested together with the medium and pelleted at 4,100 g for 5 min at 4°C. The pellet was washed once with 1 ml of ice-cold PBS before resuspension in 135 µl of Cell lysis buffer (BD Biosciences). The resuspension was kept on ice for 10 min before proceeding with the fluorimetric assay. The lysates were spun at 4,600 g for 5 min at 4°C and the supernatants transferred into new tubes.

40 µl of the supernatants were added into each 96-well containing 40 µl of 2X reaction buffer (0.188 mM HEPES (pH 7.4), 0.038 mM EDTA, 0.188 mM KCl, 0.028 mM $MgCl_2$, 6 mM DTT, 1 mM PMSF and 1X protease inhibitor cocktail) and 4 nmoles of caspase substrate. Caspase-3 substrate (Ac-DEVD-AFC) was from A.G. Scientific Inc., while caspase-9 substrate (Ac-LEHD-AFC) was from AnaSpec Inc. (Fremont, California, USA). The proteolytic reactions were carried out in the dark for 1 hr at 37°C before fluorescence was measured using a SpectraFluor Plus

spectrofluorometer (Tecan Group Ltd., Männedorf, Switzerland) at an excitation wavelength of 400 nm and emission wavelength of 505 nm. Cleavage of the substrates by active caspases present would relieve the fluorophore AFC thereby generating a fluorescence signal. The relative fluorescence units (RFU) were normalized by the amount of protein for each sample (RFU/ µg).

2.9 Data analysis

2.9.1 Confocal image analysis

Presented ICC or IHC pictures were typically obtained from collapsing a Z-stack of individual confocal images taken at different planes.

Measurements of micrographs, such as the distances between the paired staining of Caspr and K^+ channels at the node of Ranvier (section 4.1.5) was performed using a measurement feature in the AxioVision software.

2.9.2 Densitometric analysis

Densitometry was performed using the ImageJ v1.43f software (http://rsbweb.nih.gov/ij/) that was available in public domain and developed by NIH.

2.9.3 Statistical analysis

Experiments were typically carried out in triplicates and repeated at least three times. Data was analyzed with the parametric two-tail Student's *t* test available on the GraphPad QuickCalcs website (http://www.graphpad.com/quickcalcs/ttest1.cfm) and expressed as mean ± sd, with significance levels as P values indicated in each figure.

Chapter 3 Subcellular and tissue localization of Nogo-A

Nogo-A is the longest splice isoform generated from the Nogo locus and it is the most CNS-enriched form. In this chapter, Nogo-A's subcellular and tissue localization, particularly in the CNS, is described.

3.1 Generation of Nogo-A specific antibodies

In order to specifically detect Nogo-A in cells and tissues, antibodies specific for Nogo-A were generated. A high affinity and specific antibody permits the study of the endogenous Nogo-A, as well as overexpressed, untagged form of the protein. The latter is especially crucial when tagging the protein could possibly result in a loss or alteration of function, as observed for N-terminal tagged Nogo-B as described in chapter 5.

Nogo-A specific antibodies were raised in rabbits using a GST fusion antigen that comprised of aa 223-399 of the human Nogo-A polypeptide. The sequence of the antigen is boxed in blue in Fig 3.1A. This region, termed Ng1V2, is encoded by part of exon 3 of *Nogo* and is uniquely present in Nogo-A but not in the other major splice isoforms, Nogo-B and -C, as illustrated in the schematic diagram of in Fig 3.1B. The peptide, after fusion with GST (29 kDa), has an approximate molecular size of 50 kDa (Fig 3.1C).

To confirm that the polyclonal Ng1V2 antibodies produced would detect only Nogo-A and not the other splice isoforms, a western blot was carried out using lysates of SH-SY5Y cells transiently overexpressing myc tagged Nogo-A, -B and -C as shown in Fig 3.2A. The monoclonal myc tag antibody, 9E10, detected all the three isoforms, Nogo-A (~220 kDa), Nogo-B (~50 kDa) and Nogo-C (~25 kDa),

confirming that the proteins were indeed expressed. Expectedly, Ng1V2 antibodies could only pick up the 220 kDa Nogo-A band.

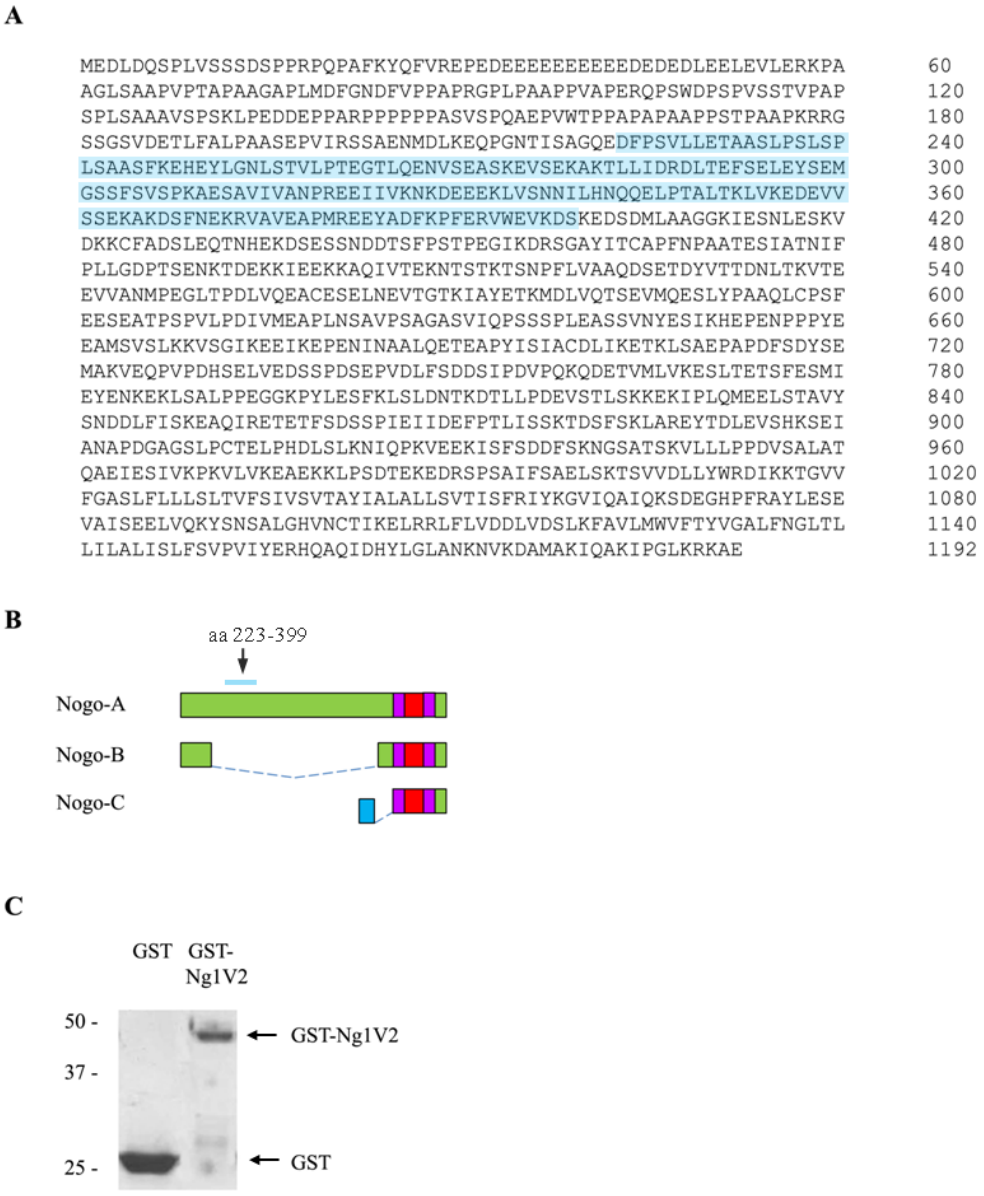

Fig 3.1 Amino acid sequence and protein size of the antigen used for the production of Ng1V2 rabbit polyclonal antibodies. ***(A)*** Amino acid sequence of human Nogo-A, with the Ng1V2 antigenic region demarcated by the blue box. ***(B)*** Schematic diagram of the Nogo isoforms, (Nogo-A, -B and -C). The Ng1V2 antigen region (aa 223-399) present solely in Nogo-A is indicated by the blue line. ***(C)*** The antigen, GST-Ng1V2, was resolved alongside with GST on a 9% SDS-PAGE gel and the gel was Coomassie Blue-stained to check for the protein's purity and size. Molecular size markers are indicated in kDa.

The antibodies were then checked for their specificity in detecting endogenous Nogo-A by ICC (Fig 3.2B). Immunostaining with Ng1V2 antibodies showed that Nogo-A in interphase cells exhibited mainly ER labelling, which co-localized exactly with GRP94, an ER lumenal marker (Fig 3.2B; merge picture in the upper panel). This suggested that majority of Nogo-A resided at the ER. Plasma membrane staining of Nogo-A (edges of the cells pointed out by the arrowheads in Fig 3.2B), where GRP94 staining seemed absent, was also noted. Blocking of the antibodies with the antigen, GST-Ng1V2, (Fig 3.2B, lower panel) abolished the ER staining of Nogo-A, confirming that the labelling by Ng1V2 antibodies was specific for Nogo-A.

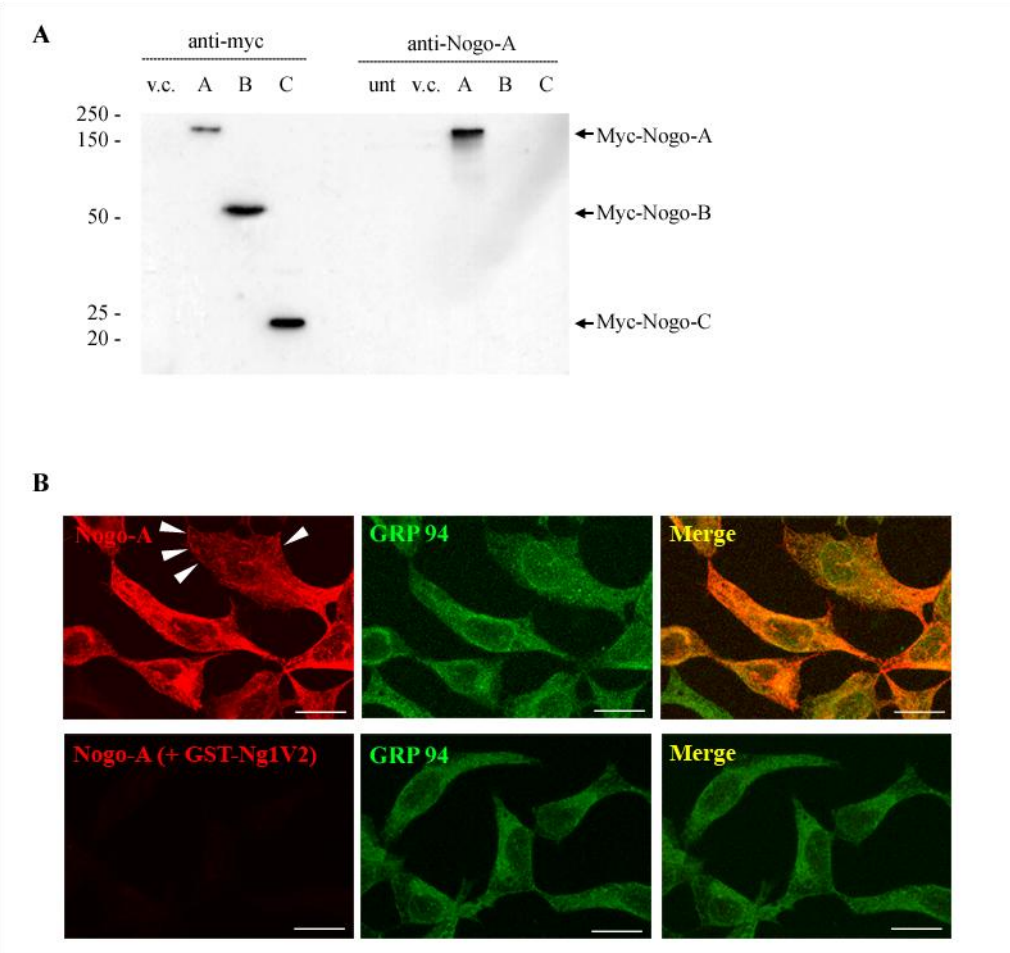

Fig 3.2 Nogo-A was specifically detected by Ng1V2 antibodies. ***(A)*** SH-SY5Y cells were transiently transfected with pDmyc as vector control (v.c.), myc-Nogo-A (A), myc-Nogo-B (B) and myc-Nogo-C (C) with Lipofectamine 2000 for 24 hr before the

cells were harvested. 20 µg of lysates were resolved on a 10% SDS-PAGE gel and subjected to western blotting with 9E10 mouse monoclonal (anti-myc) or Ng1V2 rabbit polyclonal (anti-Nogo-A) antibodies. Untransfected SH-SY5Y lysates (unt) were loaded as an additional negative control for blotting with Ng1V2 antibodies. ***(B) (Upper panel)*** SH-SY5Y Nogo-A (38) stable cells were fixed with 4% PF, permeabilized with 0.2% Tx-100/PBS and incubated with Ng1V2 *(red)* and anti-GRP94 *(green)* antibodies, followed by TxR- and FITC-conjugated secondary antibodies. Arrowheads indicate plasma membrane staining of Nogo-A. ***(Lower panel)*** Blocking of Ng1V2 antibodies was carried out by incubating the antibodies with its antigen, twenty times the amount of the antibody, overnight at 4°C before incubation with the cells. Bar = 20 µm.

3.2 Nogo-A is highly enriched in the CNS

To be better-equipped to elucidate the physiological roles of Nogo-A, it is important to first understand where the protein is expressed. For this purpose, a tissue survey using adult C57BL/6 mice was performed by western immunoblot analysis. As shown in Fig 3.3A, Nogo-A was highly enriched in the CNS, namely brain and spinal cord. Nogo-A was also found in low levels in organs like the heart and small intestine, and at almost undetectable levels in the other organs tested.

Specific cell type localization of Nogo-A within the adult CNS was further probed by performing IHC using cryosections of adult C57BL/6 mouse brain and spinal cord (Fig 3.3B). Nogo-A was found to be widely expressed in the brain, with observed staining in the cortex, cerebellum, deep cerebellar nuclei and the hippocampus (all regions including dentate gyrus (DG), CA3 and CA1). Expression of Nogo-A was seen in both white and grey matter regions of the spinal cord, and could be found in cells that resemble both oligodendrocytes as well as neurons (see section 3.3 below). Nogo-A staining in Fig 3.3B was confirmed to be specific as the staining was abolished on cryosections probed with Ng1V2 antibodies that were previously blocked by its antigen, GST-Ng1V2 (data not shown).

In order to check if Nogo-A's expression level in the brain is developmentally regulated, rats from various late stages of brain development, from E18 to 6 months

old, were sacrificed and the respective brain lysates probed. Nogo-A was expressed in the developing rat brain at E18, and the expression levels were fairly sustained well into adulthood (Fig 3.4).

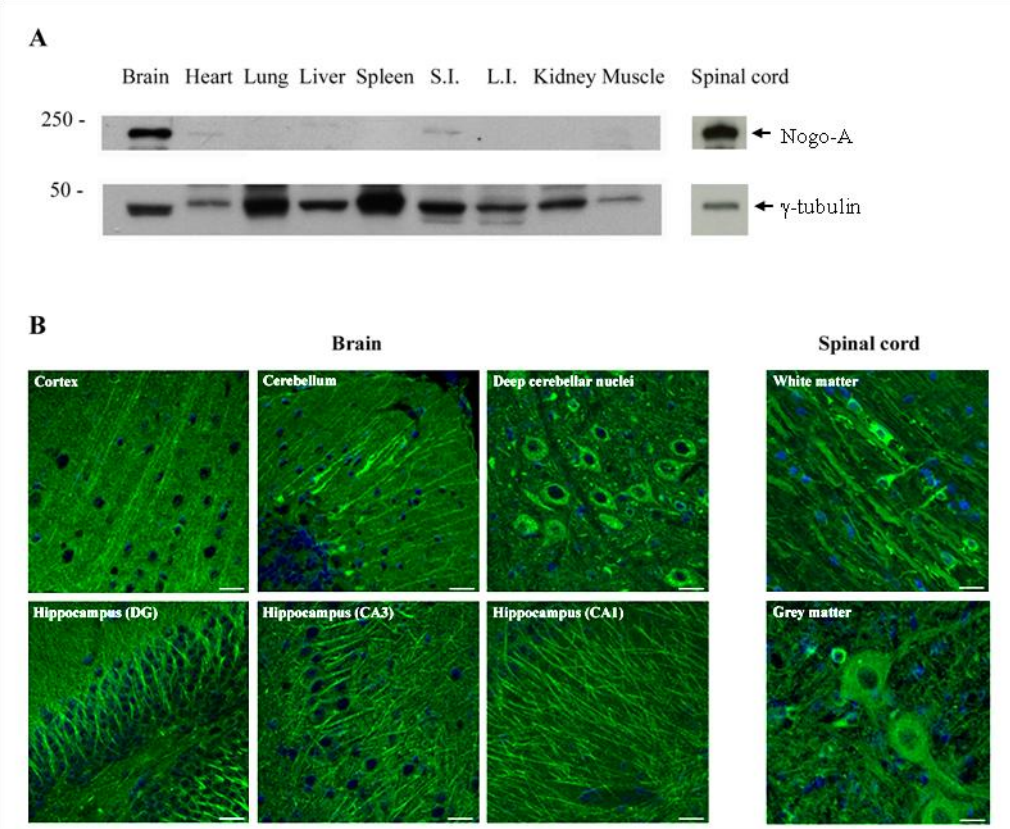

Fig 3.3 Nogo-A was highly enriched in the brain and spinal cord. ***(A)*** 100 µg of adult C57BL/6 tissue lysates were resolved on 8% SDS-PAGE gels and subjected to western blotting with Ng1V2 antibodies. γ-tubulin was probed as a loading control. S.I. and L.I. denoted small intestine and large intestine respectively. Note that the western blot on the right showing spinal cord was carried out on a separate membrane. ***(B)*** Adult C57BL/6 mouse brain and spinal cord parasagittal sections (20 µm thick) were immunostained with Ng1V2 antibodies *(green)*, followed by secondary antibodies conjugated with FITC. Hoechst 33342 was used to stain the nuclei (*blue*). Bar = 20 µm.

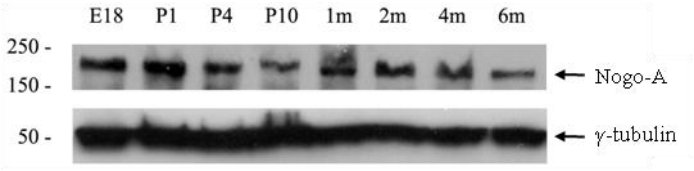

Fig 3.4 Expression of Nogo-A during brain development. 80 µg of rat brain lysates obtained from different developmental stages (Embryonic day (E) 18, postnatal days

(P) 1, 4 and 10, and postnatal months (m) 1, 2, 4 and 6) were resolved on an 8% SDS-PAGE gel and western blotted with Ng1V2 antibodies for Nogo-A, using γ-tubulin as a loading control.

3.3 Nogo-A is significantly expressed in both neurons and oligodendrocytes but not astrocytes

Nogo-A was first reported to be present in oligodendrocytes where it acted as a myelin-associated neurite outgrowth inhibitor. The presence of Nogo-A in the other major brain cell types, neurons and astrocytes, is not clear. Lysates from primary cultures of these three different cell types obtained from C57BL/6 mice and Sprague Dawley rats (Fig 3.5) showed that Nogo-A was indeed present in a significant amount in rat oligodendrocytes. Comparatively, astrocytes from the same source seemed to have very low levels of Nogo-A. Interestingly, it was found to be expressed in mouse cortical neurons. Mouse astrocytes also showed very low levels of Nogo-A expression. In fact, the presence of the low intensity band for Nogo-A in both the mouse and rat astrocytes could readily be explained by a contamination of oligodendrocytes in the primary astrocyte cultures. As the amount of primary oligodendrocytes obtained from mice was consistently low and insufficient for robust western blot analysis, oligodendrocytes from rats were used.

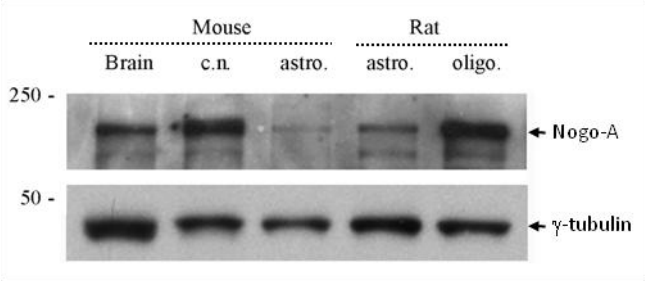

Fig 3.5 Nogo-A was expressed in primary cortical neurons and oligodendrocytes but not astrocytes. 20 μg of lysates from the indicated samples were resolved on an 8% SDS-PAGE gel and western blotted with Ng1V2 antibodies for Nogo-A, with γ-tubulin as a loading control. Mouse brain lysate was obtained from adult C57BL/6

mice while respective primary cultures were obtained as described in section 2.4.4 and 2.4.5. c.n. = cortical neurons. astro. = astrocytes. oligo. = oligodendrocytes.

Immunofluorescence microscopy analysis of primary cortical neuronal and mixed glial (containing both oligodendrocytes and astrocytes) cultures yielded results that were complementary to that of the immunoblots (Fig 3.6). Nogo-A (as observed from the immunostaining by Ng1V2 antibodies) co-localized with the neuronal marker Tuj, a neuron-specific class III β-tubulin, in the primary cortical neuronal culture in Fig 3.6A (upper panel). Nogo-A also co-localized with the oligodendrocytic marker, CNPase (indicated by arrows), but not GFAP (indicated by arrowheads), a marker for astrocytes (upper panels of Fig 3.6B and C respectively). To confirm that the immunofluorescence staining revealed by Ng1V2 antibodies was specific, controls were carried out by preincubating the antibodies with its antigen (GST-Ng1V2) prior to performing ICC. The specific Nogo-A staining of neurons and oligodendrocytes was effectively blocked in this manner (Fig 3.6A-C, lower panels). This reiterated the western blot results obtained earlier in Fig 3.5, and confirmed that Nogo-A was expressed at significantly high levels in neurons and oligodendrocytes while its expression in astrocytes, if any, was very low.

An investigation on the expression pattern of Nogo-A during the morphological differentiation of primary cortical neurons in culture was also performed. Primary cortical neurons were seeded and allowed to differentiate on PLL-coated dishes and their lysates were collected at various time intervals until DIV16. Note that cortical neurons at DIV0 were obtained straight after harvesting in suspension without plating them onto dishes. Fig 3.7 showed that the amount of Nogo-A was low at the point of harvest. However, Nogo-A was steadily expressed from DIV2 onwards until the late stages in culture, with a clear reduction at the end.

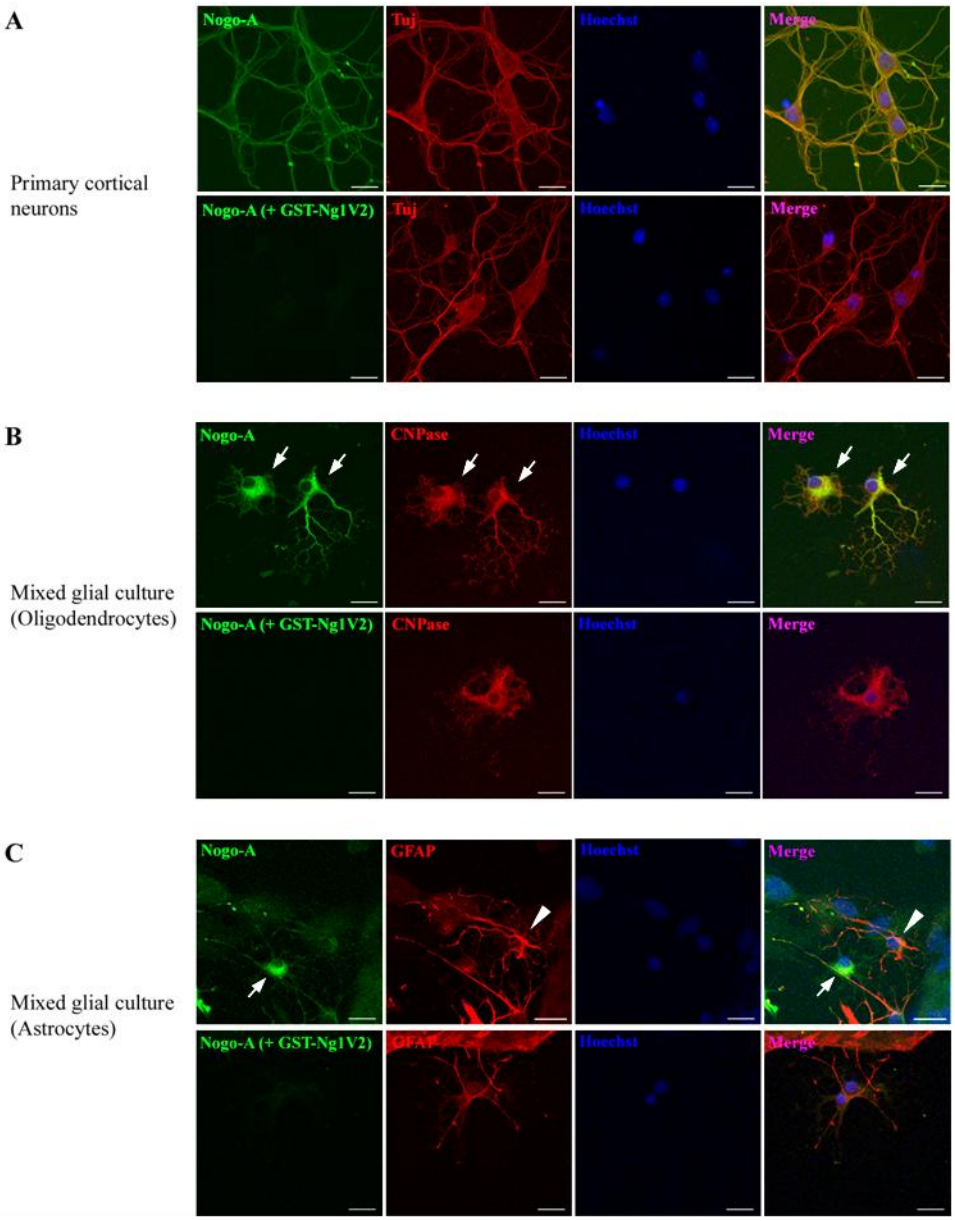

Fig 3.6 Nogo-A co-localized with cortical neurons and oligodendrocytes but not astrocytes in primary culture. Mouse primary cortical neurons (DIV7) ***(A; upper panel)*** and mixed glial culture ***(B, C; upper panels)*** were fixed with 4% PF, permeabilized with 0.05% saponin and incubated with Ng1V2 *(green)* and anti-Tuj ***(A)***, anti-CNPase ***(B)*** or anti-GFAP ***(C)*** *(red)* antibodies, followed by FITC- and TxR-conjugated secondary antibodies. Hoechst 33342 was used to stain the nuclei. Blocking of Ng1V2 antibodies ***(A-C; lower panels)*** was carried out by incubating Ng1V2 antibodies with its antigen, twenty times the amount of the antibody, overnight at 4°C before incubation with the cells. Arrows indicate oligodendrocytes. Arrowheads indicate astrocytes. Bar = 20 µm.

The decrease in Nogo-A observed at DIV16 was not due to a reduction in the number of cortical neurons present as a result of cell death. This is deduced from the fact that

the expression level of Tuj, which is a marker for neurons, was maintained at DIV16. The results suggested that Nogo-A may have a role during the differentiation of cortical neurons, with its levels downregulated at a late stage of neuronal maturation.

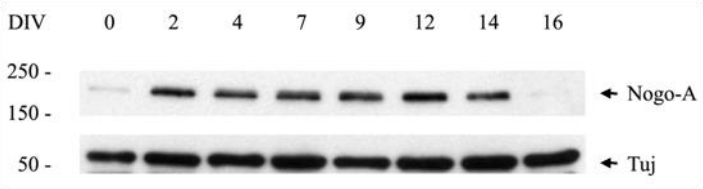

Fig 3.7 Nogo-A expression during cortical neuronal differentiation. 15 µg of cortical neuronal lysates obtained at DIV0-DIV16 were run on an 8% SDS-PAGE gel and western blotted with Ng1V2 antibodies for Nogo-A. Tuj was blotted to act as a loading control for neurons.

To illustrate that Nogo-A was indeed present in the two CNS cell types physiologically, and not an artefact as a result of manipulation of the primary cultures *in vitro*, spinal cord parasagittal cryosections were immunostained for Nogo-A and the individual neuronal (Tuj), oligodendrocytic (CNPase) and astrocytic (GFAP) markers. As shown in Fig 3.8A, for the white matter of the spinal cord, there were some degree of co-localization of Nogo-A and Tuj at the myelinated axons (upper panel; block arrows). The oligodendrocytes also showed staining of Nogo-A by the co-localization of Nogo-A and CNPase at the cell bodies (middle panel; arrows). As expected, no co-labelling of astrocytes was observed (lower panel; arrowheads). Hence, Nogo-A expression was confirmed to be localized only to the neurons and oligodendrocytes but not astrocytes.

Interestingly, when spinal cord sections were labelled for $K_{v1.2}$ (K^+) channels, which are selectively localized at the juxtaparanodes, it was observed that some of Nogo-A's expression was found located just beside the K^+ channels' staining at the side nearer to the node of Ranvier, as pointed out by the arrows (Fig 3.8B). This

suggested that Nogo-A may possibly be enriched at the paranodal region of the axon-glial junction. Further studies on this connection are reported in the next chapter.

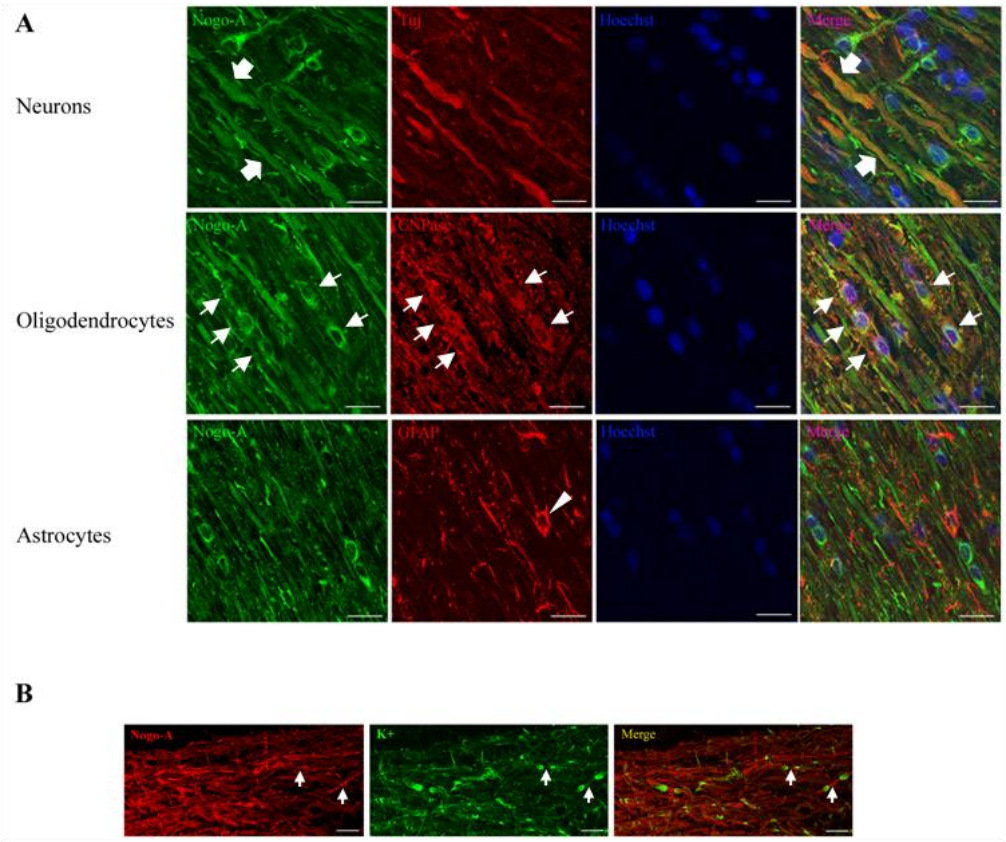

Fig 3.8 Nogo-A was present in the neurons, especially at the paranodes, and oligodendrocytes of the spinal cord. ***(A)*** Adult C57BL/6 mouse spinal cord parasagittal sections (20 µm thick) were immunostained with Ng1V2 *(green)* and anti-Tuj ***(upper panel)***, anti-CNPase ***(middle panel)*** or anti-GFAP ***(lower panel)*** *(red)* antibodies, followed by secondary antibodies conjugated with FITC and TxR. Hoechst 33342 was used to stain the nuclei. Block arrows indicate axons. Arrows indicate oligodendrocytes. Arrowhead indicates astrocyte. ***(B)*** Adult C57BL/6 mouse spinal cord parasagittal sections were incubated with Ng1V2 *(green)* and anti-K^+-channels *(red)* antibodies, followed by FITC- and TxR-conjugated secondary antibodies. Arrows indicate the paranodes. Bar = 20 µm.

3.4 Discussion – Localization of Nogo-A and the implicated functions

We have generated specific antibodies for Nogo-A. The antibodies could detect endogenous Nogo-A in cells (at the ER and plasma membrane) and in the adult CNS tissues (brain and spinal cord). In addition, we showed that Nogo-A expression

was present in the rat brain from E18 all the way to adulthood. Similar observations have been made by others (Meier *et. al.*, 2003).

Within the CNS, Nogo-A expression was present in both oligodendrocytes and neurons but strikingly absent in astrocytes. Nogo-A in adult CNS has been known to be associated with myelin to inhibit neuronal regeneration. Therefore, the neuronal expression of Nogo-A seems counterintuitive. With regards to this, Nogo-A on adult neurons may have other functions that were previously unsuspected. One of these functions could be neuroprotection, which will be looked into in chapter 5.

Most interestingly, Nogo-A was found to be enriched at the paranodes at the node of Ranvier. This observed staining in mouse closely resembled that observed in rat (Nie *et. al.*, 2003), and this further strengthened the notion that Nogo-A is enriched at the paranode. The role of Nogo-A enriched at this location will be further probed in the following chapter.

Chapter 4 Studies on the interacting proteins of Nogo-A

The Nogo-A specific antibodies that we have developed have allowed us to investigate the interaction between Nogo-A and two of its interacting partners. The two are namely the paranodal Caspr, and RTN3. These studies are described below.

4.1 Interaction of Nogo-A with Caspr, a paranodal marker

The observation that Nogo-A was enriched at the paranodes (Fig 3.8B) implied a possible function or activity of Nogo-A at the site. As Nogo-A at the paranodal region is most likely located at the oligodendroglial membrane, it is possible that there is a neuronal interacting partner for it at the axon-glia junction. The best-known receptor for Nogo-A, NgR, is not found to be enriched or even localized at the paranodes. As such, paranodal Nogo-A is unlikely to act by engaging NgR.

Caspr, a transmembrane protein which has an extracellular domain comprising of laminin-G-like domains and EGF repeats, is specifically localized at the paranodes on the neuronal membrane. Together with F3/contactin, Caspr has been shown to interact *in trans* with 155-kDa isoform of neurofascin (NF 155), which is on the oligodendroglial membrane, for the maintenance of the axoglial architecture at the paranodes (Charles *et. al.*, 2002). We, in collaboration with Dr Xiao Zhi Cheng's laboratory (Singapore General Hospital), have therefore investigated whether Caspr could function similarly by acting as Nogo-A's receptor at the paranodes and also Nogo-A's possible role at this location. While the work by Dr Xiao's group was performed in rats (Nie *et. al.*, 2003), we have focused our study in mice, as this model could draw benefit from comparative studies in the Nogo-deficient mouse model that we have eventually obtained.

4.1.1 Nogo-A co-localizes with Caspr at the paranodes

To determine if Caspr may be the neuronal receptor for paranodal Nogo-A, we first proceeded to confirm the localization of Caspr at the paranodes. An IHC staining of adult mouse spinal cord was carried out to double-label for Caspr and K^+ channels at paranodes and juxtaparanodes respectively (Fig 4.1A). As seen in the merge panel in the figure, the paired red staining of Caspr were juxtaposed next to each paired green staining of K^+ channels at the side proximal to the node. This confirms the paranodal localization of Caspr.

In order to check if Nogo-A and Caspr co-localized at paranodes, a similar IHC staining was performed with co-labelling of Nogo-A and Caspr. Fig 4.1B showed clear co-localization of these two proteins at the paranodes (arrows). Clear co-localization in all paranodal regions that were in view was not observed. This is probably due to the fact that it may not be topologically possible to see all of Nogo-A's signal, which was present in the inner- and outer-most layers of the myelin sheath wrapping around the axons, to coincide with that of Caspr in a spinal cord cryosection that was only 20 µm thick.

4.1.2 Nogo-A co-immunoprecipitates with Caspr

To assess if Caspr is indeed a binding partner for Nogo-A, a co-IP experiment was conducted to check for their possible interaction *in vitro* (Fig 4.2). CHO cells stably expressing Caspr and F3/contactin (CHO Caspr/F3) were used to transiently express Nogo-A for this purpose. The expression of F3/contactin in the above mentioned double-stable cell-line was essential for the proper transport of Caspr to the cell surface (Faivre-Sarrailh *et. al.*, 2000). It was also advantageous to use stable cell-lines for co-IP experiments, as it was easier to singly transfect the cells to obtain cells

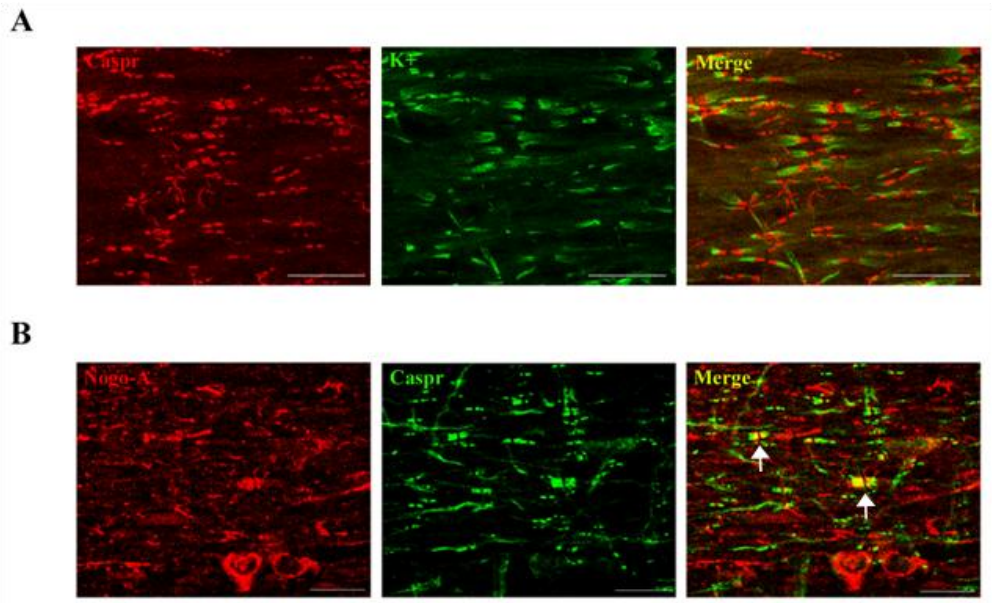

Fig 4.1 Nogo-A co-localized with Caspr at the paranodes. ***(A)*** Adult C57BL/6 mouse spinal cord parasagittal sections (20 µm thick) were immunostained with anti-Caspr *(red)* and anti-K^+ channels *(green)* antibodies overnight, followed by secondary antibodies conjugated with TxR and FITC respectively. ***(B)*** Adult C57BL/6 mouse spinal cord parasagittal sections (20 µm thick) were immunostained with Ng1V2 *(red)* and anti-Caspr *(green)* antibodies overnight, followed by secondary antibodies conjugated with TxR and FITC respectively. Arrows in the merge panel point to clear cases of Nogo-A-Caspr co-localization, which appears yellow. Bar = 20 µm.

expressing both of the proteins of interest. In comparison, we have noticed that the efficiency of having both proteins expressed in the same cells was much lower when the two were introduced together by transient transfection.

The results showed that Ng1V2 antibodies could co-IP Caspr, suggesting that Nogo-A and Caspr could interact with each other when co-expressed in cells. The reciprocal co-IP experiment, using our "home-made" Caspr antibodies (refer to Fig 4.3 for the antigenic region and the antigen's molecular weight), was attempted, but we did not have much success in co-precipitating Nogo-A (data not shown). One possible reason for this is that the antibodies we have generated against Caspr did not IP well. Another could be that the Caspr antibodies were blocking the interaction site/s between the two proteins. However, that Nogo-A and Caspr could be co-IP by

the Ng1V2 antibodies is indicative of a possible interaction between the two proteins *in vivo*.

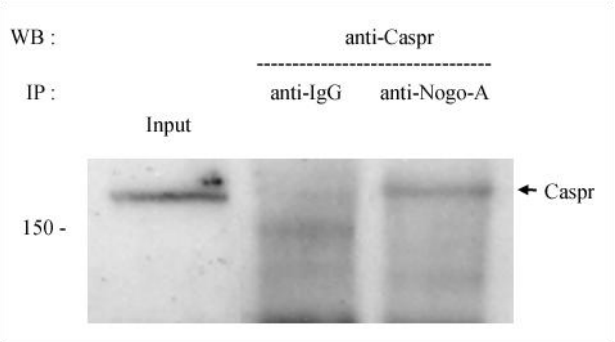

Fig 4.2 Nogo-A co-IP Caspr. CHO Caspr/F3 stably expressing cells were transiently transfected with untagged Nogo-A construct using Lipofectamine 2000 for 48 hr. 1.5 mg of the lysates were then incubated with rabbit IgG (anti-IgG) as negative control or Ng1V2 (anti-Nogo-A) antibodies overnight before addition of protein A sepharose beads for 2 hr. The samples were resolved on an 8% SDS-PAGE gel and western-blotted with anti-Caspr antibodies. Input was 1/15 of the amount used for co-IP.

4.1.3 Nogo-66, in its entirety, is essential for Nogo-A's interaction with Caspr

Caspr shares 50% similarity with another paralogue, Caspr 2. We asked if Nogo-A could interact with Caspr 2 as well. We have therefore also generated antibodies against Caspr 2 (see chapter 2).The amino acid sequence alignment of the two Caspr homologues, and the antigenic regions (boxed in blue) used for generating the two antibodies, are depicted in Fig 4.3A. The Caspr and Caspr 2 fragments were fused to GST and their respective sizes were approximately 37 and 34 kDa (Fig 4.3B).

For Nogo-A (on oligodendrocyte) and Caspr (on neuron) to interact *in trans*, the site on Nogo-A that may potentially interact with Caspr would likely be the Nogo-66 domain which is postulated to face the extracellular region. To investigate this, an *in vitro* GST pull-down assay was performed using GST tagged Nogo-66 to check for any interaction with Caspr, employing the CHO Caspr/F3 stable cell-line which we obtained from our collaborator (see chapter 2.4.3). Fig 4.4A showed that GST-Nogo-

A

```
Caspr   (human)    1     MMHL-RLFC---ILLAAVSGA--EGWGYYG----CDEELVGPLYARSLGASSYYSLLTAPRFARLH---GISGWSPRIGD  67
Caspr 2 (human)    1     MQAAPRAGCGAALLLWIVSSCLCRAWTAPSTSQKCDEPLVSGLPHVAFSSSSSISGSYSPGYAKINKRGGAGGWSPSDSD  80

Caspr   (human)    68    PNPWLQIDLMKKHRIRAVATQGSFNSWDWVTRYMLLYGDRVDSWTPFYQRGHNSTFFGNVNESAVVRHDLHFHFTARYIR  147
Caspr 2 (human)    81    HYQWLQVDFGNRKQISAIATQGRYSSSDWVTQYRMLYSDTGRNWKPYHQDGNIWAFPGNINSDGVVRHELQHPIIARYVR  160

Caspr   (human)    148   IVPLAWNPRGKIGLRLGLYGCPYKADILYFDGDDAISYRFPRGVSRSLWDVFAFSFKTEEKDGLLLHAEGAQGDYVTLEL  227
Caspr 2 (human)    161   IVPLDWNGEGRIGLRIEVYGCSYWADVINFDGHVVLPYRFRNKKMKTLKDVIALNFKTSESEGVILHGEGQQGDYITLEL  240

Caspr   (human)    228   EGAHLLLHMSLGSSPIQPRPGHTTVSAGGVLNDQHWHYVRVDRFGRDVNFTLDGYVQRFILNGDFERLNLDTEMFIGGLV  307
Caspr 2 (human)    241   KKAKLVLSLNLGSNQLGPIYGHTSVMTGSLLDDHHWHSVVIERQGRSINLTLDRSMQHFRTNGEFDYLDLDYEITFGGIP  320

Caspr   (human)    308   GAARKNLAYRHNFRGCIENVIFNRVNIADLAVRRHSRITFEGKVAFRCLDPVPHPINFGGPHNFVQVPGFPRRGRLAVSF  387
Caspr 2 (human)    321   FSGKPSSSSRKNFKGCMESINYNGVNITDLARRKKLEPSNVGNLSFSCVEPYTVPVFFNAT-SYLEVPGRLNQDLFSVSF  399

Caspr   (human)    388   RFRTWDLTGLLLFSRLGDGLGHVELTLSEGQVNVSI--AQSGRKKLQFAAGYRLNDGFWHEVNFVAQENHAVISIDDVEG  465
Caspr 2 (human)    400   QFRTWNPNGLLVFSHFADNLGNVEIDLTESKVGVHINITQTKMSQIDISSGSGLNDGQWHEVRFLAKENFAILTIDGDEA  479

Caspr   (human)    466   AEVRVSYPLLIRTGTSYFFGGCPKPASRWDCHSNQTAFHGCMELLKVDGQLVNLTLVEGRRLGFYAEVLFDTCGITDRCS  545
Caspr 2 (human)    480   SAVRTNSPLQVKTGEKYFFGGFLNQMNNSSHSVLQPSFQGCMQLIQVDDQLVNLYEVAQRKPGSFANVSIDMCAIIDRCV  559

Caspr   (human)    546   PNMCEHDGRCYQSWDDFICYCELTGYKGETCHTPLYKESCEAYRLSGKTSGNFTIDPDGSGPLKPFVVYCDIRENRAWTV  625
Caspr 2 (human)    560   PNHCEHGGKCSQTWDSFKCTCDETGYSGATCHNSIYEPSCEAYKHLGQTSNYYWIDPDGSGPLGPLKVYCNMTEDKVWTI  639

Caspr   (human)    626   VRHDRLWTTRVTGSSMERPFLGAIQYWNASWEEVSALANASQHCEQWIEFSCYNSRLLNTAGGYPYSFWIGRNEEQHFYW  705
Caspr 2 (human)    640   VSHDLQMQTPVVGYNPEKYSVTQLVY-SASMDQISAITDSAEYCEQYVSYFCKMSRLLNTPDGSPYTWWVGKANEKHYYW  718

Caspr   (human)    706   GGSQPGIQRCACGLDRSCVDPALYCNCDADQPQWRTDKGLLTFVDHLPVTQVVIGDTNRSTSEAQFFLRPLRCYGDRNSW  785
Caspr 2 (human)    719   GGSGPGIQKCACGIERNCTDPKYYCNCDADYKQWRKDAGFLSYKDHLPVSQVVVGDTDRQGSEAKLSVGPLRCQGDRNYW  798

Caspr   (human)    786   NTISFHT-GAALRFPPIRANHSLDVSFYFRTSAPSGVFLENMGGPYCQWRRPYVRVELNTSRDVVFAFDVGNGDENLTVH  864
Caspr 2 (human)    799   NAASFPNPSSYLHFSTFQGETSADISFYFKTLTPWGVFLENMG------KEDFIKLELKSATEVSFSFDVGNGPVEIVVR  872

Caspr   (human)    865   SDDFEFNDDEWHLVRAEINVKQARLRVDHRPWVLRPMPLQTYIWMEYDQPLYVGSAELKRRPFVGCLRAMRLNGVTLNLE  944
Caspr 2 (human)    873   SPT-PLNDDQWHRVTAERNVKQASLQVDRLPQQIRKAPTEGHTRLELYSQLFVGGAG-GQQGFLGCIRSLRMNGVTLDLE  950

Caspr   (human)    945   GRANASEGTSPNCTGHCAHPRLPCFHGGRCVERYSYYTCDCDLTAFDGPYCNHDIGGFFEPGTWMRYNLQSALRSAAREF  1024
Caspr 2 (human)    951   ERAKVTSGFISGCSGHCTSYGTNCENGGKCLERYHGYSCDCSNTAYDGTFCNKDVGAFFEEGMWLRYNFQAPATNARDSS  1030

Caspr   (human)    1025  SHMLSRPVPGYEPGYIPGYDTPGYVPGYHGPGYRLPDYPRPGRPVPGYRGPVYNVTGEEVSFSFSTSSAPAVLLYVSSFV  1104
Caspr 2 (human)    1031  SRVDNAP------------DQQNSHP--------------------------DLAQEEIRFSFSTTKAPCILLYISSFT  1071

Caspr   (human)    1105  RDYMAVLIKDDGTLQLRYQLGTS--PYVYQLTTRPVTDGQPHSINITRVYRNLFIQVDYFPLTEQKFSLLVDSQLDSPKA  1182
Caspr 2 (human)    1072  TDFLAVLVKPTGSLQIRYNLGGTREPYNIDVDHRNMANGQPHSVNITRHEKTIFLKLDHYPSVSYHLPSSSDTLFNSPKS  1151

Caspr   (human)    1183  LYLGRVMETGVIDPEIQRYNTPGFSGCLSGVRFNNVAPLKTHFRTPRPMTAELAEALRVQGELSESNCGAMPRLVSEVPP  1262
Caspr 2 (human)    1152  LFLGKVIETGKIDQEIHKYNTPGFTGCLSRVQFNQIAPLKAALRQ-----TNASAHVHIQGELVESNCGASPLTLSPMSS  1226

Caspr   (human)    1263  ELDPWYLP------PDFPYYHDEGWV--------AILLGFLVAFLLLGLVGMLVLFYLQNHRYKGSYHTNEPKAAHEYHP  1328
Caspr 2 (human)    1227  ATDPWHLDHLDSASADFPYNPGQGQAIRNGVNRNSAIIGGVIAVVIFTILCTLVFLIRYMFRHKGTYHTNEAKGA-----  1301

Caspr   (human)    1329  GSKPPLPTSGPAQVPTPTAAPNQAPASAPAPAPTPAPAPGPRDQNLPQILEESRSE---  1384
Caspr 2 (human)    1302  ----------------------ESAESADAAIMN-------NDPNFTETIDESKKEWLI  1331
```

B

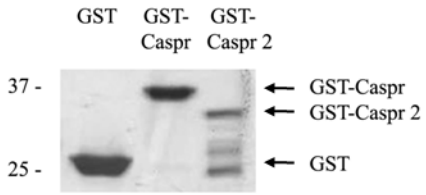

Fig 4.3 Antigenic regions for Caspr and Caspr 2 antibodies. ***(A)*** Alignment of human Caspr and Caspr 2 using COBALT Multiple Alignment Tool from NCBI website (www.ncbi.nlm.nih.gov). Antigenic regions used for generation of the two antibodies are boxed in blue. ***(B)*** 2 µg of GST, GST-Caspr and GST-Caspr 2 were resolved on a 9% SDS-PAGE gel which was stained by Coomassie Blue to check for protein purity and size.

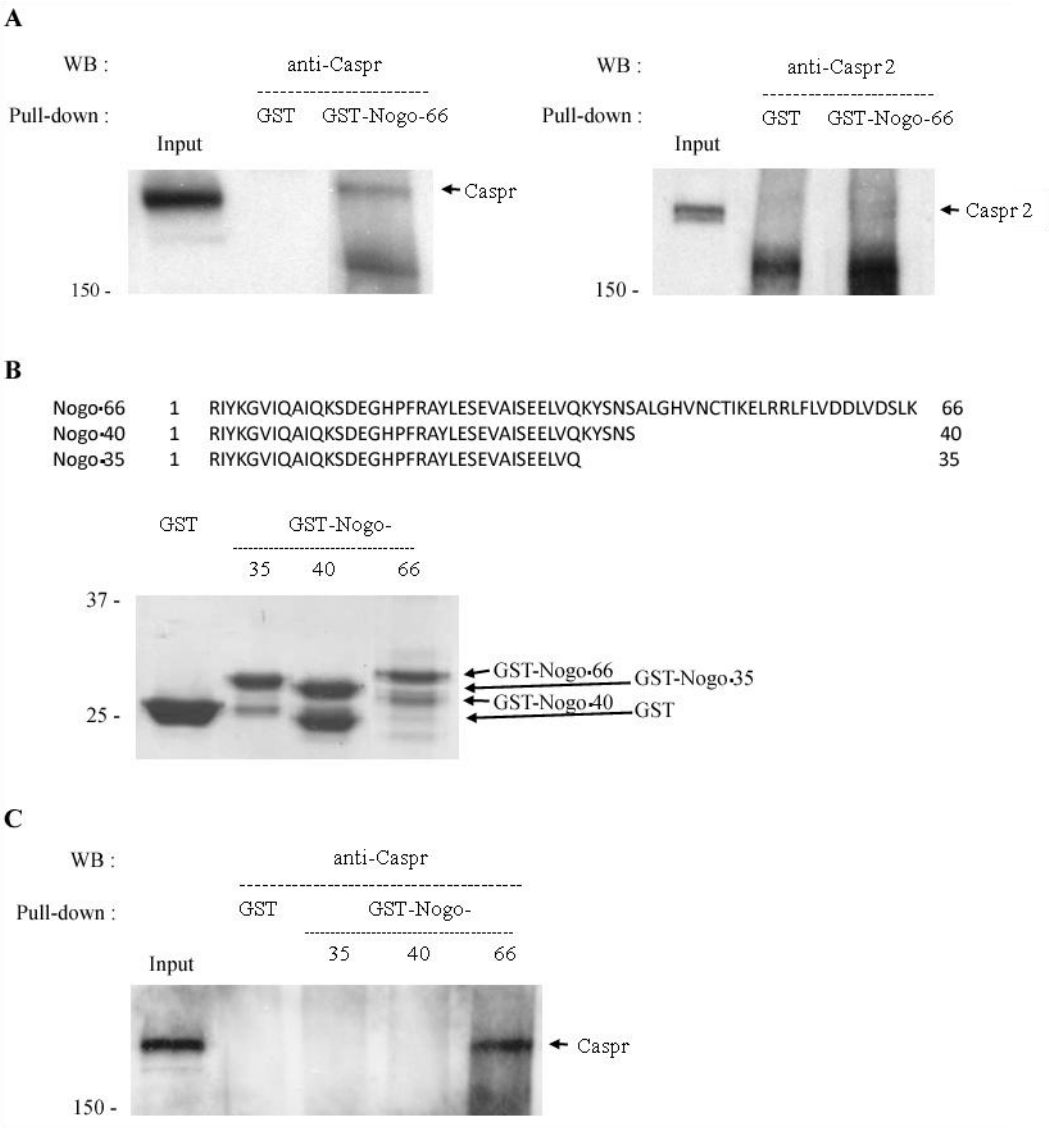

Fig 4.4 The entire Nogo-66 was required to pull-down Caspr. ***(A)*** 1.5 mg of lysates from CHO Caspr/F3 cells *(left)* or HEK293 cells transiently expressing Caspr 2 *(right)* were incubated with 20 µg of GST as negative control or GST-Nogo-66 bound to glutathione sepharose beads overnight. The beads collected were resolved on an 8% SDS-PAGE gel and western-blotted with anti-Caspr *(left)* or anti-Caspr 2 *(right)* antibodies. Input was 1/20 of the amount used for the GST pull-down assays. ***(B)*** Amino acid sequences *(top)* and GST fusion protein sizes by Coomassie Blue staining *(bottom)* of Nogo-35, -40 and -66. ***(C)*** 20 µg of GST-Nogo-35, -40 and -66 were incubated with 1.5 mg of CHO Caspr/F3 lysates and the samples were similarly checked as stated in ***(A)*** with anti-Caspr antibodies. GST proteins were used as negative control. Input was 1/30 of the amount used for the GST pull-down assays.

66 could pull-down Caspr (left) but not Caspr 2 (right), illustrating that the Nogo-66 domain was essential and sufficient for Nogo-A to however, that the pull-down assay for Caspr 2 was performed using lysates of HEK293 cells transiently transfected with

an untagged Caspr 2 construct. There remains, of course, the possibility that coexpression of Caspr 2 with F3 is required for its interaction with Nogo-66.

Is the entire Nogo-66 domain required for the interaction with Caspr? To answer this, two truncation products of the Nogo-66 domain, Nogo-35 and -40, were generated tagged to GST. Their amino acid sequences are listed in Fig 4.4B alongside that of Nogo-66, together with their protein sizes in the gel image shown below the sequences. Although Nogo-35 is shorter than Nogo-40 in terms of the number of amino acids, the size of its GST fusion protein is actually larger than that of GST-Nogo-40, probably because of differences in molecular shape. As above, GST pull-down assays were performed using these GST fusion proteins. Interestingly, only GST-Nogo-66 but not the other two shorter forms, GST-Nogo-35 and -40, could pull-down Caspr (Fig 4.4C). This suggested that the entire Nogo-66 domain was likely required for the interaction between Nogo-A and Caspr.

4.1.4 Expression of Nogo-A and Caspr during development

Nogo-A has been shown earlier in section 3.2 (Fig 3.4) to be expressed in the brain from E18 to adulthood. To understand if Nogo-A and Caspr could function together during any stage of brain development, a check on Caspr's expression during this same period was performed.

As seen in Fig 4.5, Caspr expression was barely detectable during embryonic stage (E18) up to P4 where the protein levels began to be upregulated, and maintained during adulthood. This implied that Nogo-A could possibly interact with Caspr only from P4 onwards. A Nogo-A-Caspr interaction may therefore have a postnatal function, rather than one during embryonic development.

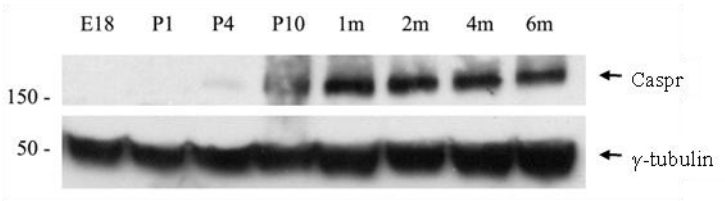

Fig 4.5 Expression of Caspr during brain development. 80 µg of rat brain lysates obtained from different developmental stages (Embryonic day (E) 18, postnatal days (P) 1, 4 and 10, and postnatal months (m) 1, 2, 4 and 6) were resolved on an 8% SDS-PAGE gel and western blotted with anti-Caspr antibodies, using γ-tubulin as a loading control.

4.1.5 Nogo-A is not essential for the architecture organization at the node of Ranvier

The presence of Nogo-A at axo-glial junctions at the paranodes and its interaction with Caspr suggests a possible function for Nogo-A in the formation, or stabilization, of the architecture organization at the axo-glial junctions at the node of Ranvier. That Nogo-A is important for the formation of axo-glial junctions seems unlikely judging from the results obtained in the previous section. Nevertheless, Nogo-A may still be important in the second function. Specific segregation of proteins in the different domains at the node of Ranvier, such as Na^+ channels at the node, Caspr at the paranode, and K^+ channels and Caspr 2 at the juxtaparanode, requires tight regulation. It is possible that Nogo-A may somehow be involved in this.

To investigate if Nogo-A plays an important role in this regard, wild type C57BL/6 and Nogo-deficient mice were examined for any differences in the placement of Caspr and K^+ channels at the paranodes and juxtaparanodes respectively. Spinal cord cryosections were double-labelled for Caspr and K^+ channels (Fig 4.6A) and the distance between pairs of staining for each of the markers at each node of Ranvier was measured. Nogo-A expression was confirmed to be absent in the Nogo-deficient mouse spinal cord as evident by the lack of Nogo-A staining as compared to the wild type one (extreme right panel). As shown in Fig

4.6B, there were no significant differences in the distances of the two markers measured between wild type and Nogo-deficient mice. For Caspr, the distance between the pair of paranodal staining was at a 95% confidence interval of 0.84 ± 0.06 µm for wild type mouse, while that of Nogo-deficient mouse was 0.82 ± 0.06 µm. At the same confidence level, the distance between the paired juxtaparanodal labelling for K^+ channels at each node of Ranvier for wild type mouse was 4.38 ± 0.29 µm, while for Nogo-deficient mouse, the distance was 4.56 ± 0.25 µm. The absence of Nogo-A in mice therefore did not significantly affect the spatial organization of Caspr and K^+ channels at the node of Ranvier. Hence, Nogo-A may

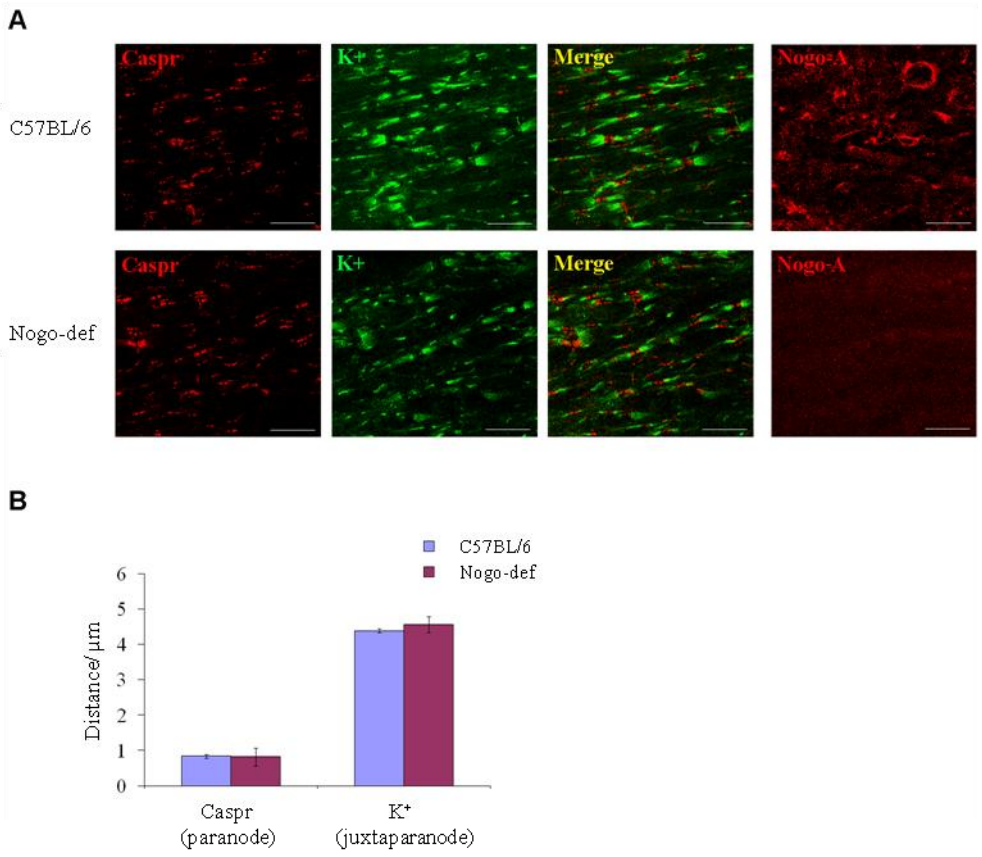

Fig 4.6 Nogo-A did not affect the architecture organization at the node of Ranvier. ***(A)*** Adult C57BL/6 and Nogo-deficient mouse spinal cord parasagittal sections (20 µm thick) were immunostained with anti-Caspr *(red)* and anti-K^+ channels *(green)* antibodies overnight, followed by secondary antibodies conjugated with TxR and FITC respectively. Note that for the extreme right panel, a separate section was used to label with Ng1V2 antibodies *(red)* for checking of Nogo-A

expression. Bar = 20 µm. ***(B)*** The distances between each paired staining of Caspr or K^+ channels in the immunolabelled sections were measured using the AxioVision software and presented in the graph (mean ± sd, n = 3).

not have an essential role to play in establishing and maintaining the architecture organization at the axo-glial junctions at the node of Ranvier.

4.2 Interaction of Nogo-A with RTN3, a fellow member of the Reticulon family

RTN3 is another reticulon family member which is found to be highly enriched in the brain, although its expression is present in other tissues as well. An earlier report had suggested an interaction between RTN3 and Nogo-B (Qi *et. al.*, 2003), at least *in vitro*. Since Nogo-A, like RTN3, is also expressed in neurons, their interaction may have a more physiological meaning than that between Nogo-B and RTN3. We therefore proceeded to investigate the possible interaction between Nogo-A and RTN3.

4.2.1 Nogo-A co-localizes with RTN3 at ER

As Nogo-A and RTN3 belong to the same Reticulon family, the domain structure of RTN3 is rather similar to that of Nogo-A. The RHD domain contains a 66-aa hydrophilic loop sandwiched between TM1 and TM2, and it also harbors a dilysine motif at the C terminus (Fig 4.7A).

To confirm the localization, or co-localization of the two RTNs, ICC analysis was carried out by simultaneous staining of Nogo-A and RTN3 using a SH-SY5Y cell line stably expressing Nogo-A and transiently transfected with a HA tagged RTN3 expression construct. Fig 4.7B confirmed that the two proteins co-localized extensively at the ER.

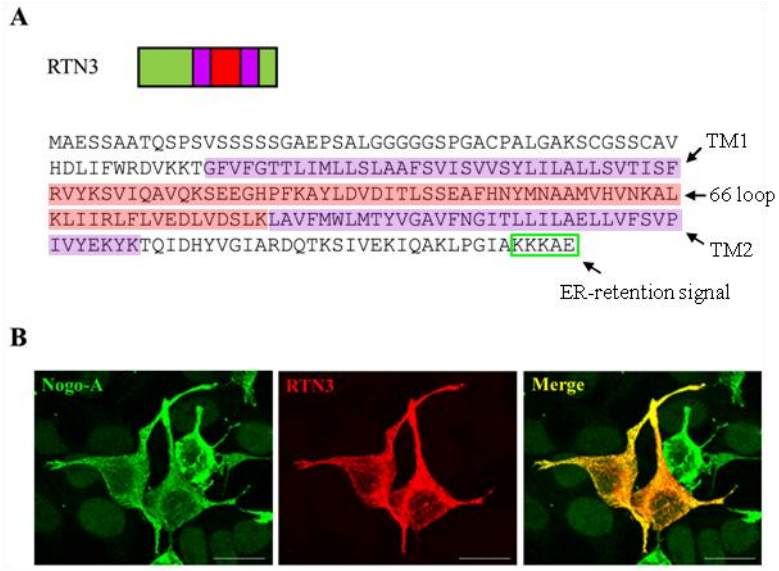

Fig 4.7 Nogo-A co-localized with RTN3 at the ER. ***(A)*** Sequence and domain structure of RTN3. TM domain 1 (TM1) and 2 (TM2) are indicated by the purple boxes and the 66 loop is boxed in red. The ER-retention signal is outline in the green box. ***(B)*** SH-SY5Y Nogo-A (38) stable cells transiently transfected with HA-RTN3 were fixed with 4% PF, permeabilized with 0.05% saponin and incubated with Ng1V2 *(green)* and anti-HA *(red)* antibodies, followed by FITC- and TxR-conjugated secondary antibodies. Bar = 20 µm.

4.2.2 Nogo-A co-immunoprecipitates with RTN3

To ask if Nogo-A could interact with RTN3, CHO cells stably expressing Nogo-A (CHO Nogo-A) were transiently transfected with myc tagged RTN3, and co-IP assays were performed. Myc-RTN1 and 2 were also transiently expressed in this stable cell-line, and co-IP between Nogo-A and these two reticulons were concurrently carried out.

As shown in Fig 4.8A, Ng1V2 antibodies could co-IP all three fellow reticulons, RTN1, 2 and 3, but to different extents. Nogo-A was able to interact with RTN3 much better than RTN1 and 2, as evident by the denser RTN3 band co-immunoprecipitated. A greater proportion of RTN3 was pull-downed by the same amount of Ng1V2 antibodies given that the starting amount of RTN1, 2 or 3 present in the lysates was about the same, judging from intensities of the input lanes. In fact,

the interaction between Nogo-A and RTN1 or 2 could be negligible, with Nogo-A immunoprecipitating less than 1% of RTN1 or RTN2 present in the lysates. This observation was corroborated by the reciprocal co-IP where 9E10 myc monoclonal antibodies pulling down myc-RTN3 co-immunoprecipitated significantly more Nogo-A than RTN1 and 2 (Fig 4.8B). Hence, Nogo-A appears to interact with RTN3 with unusually high affinity compared to the other two reticulon family members, RTN1 and RTN2.

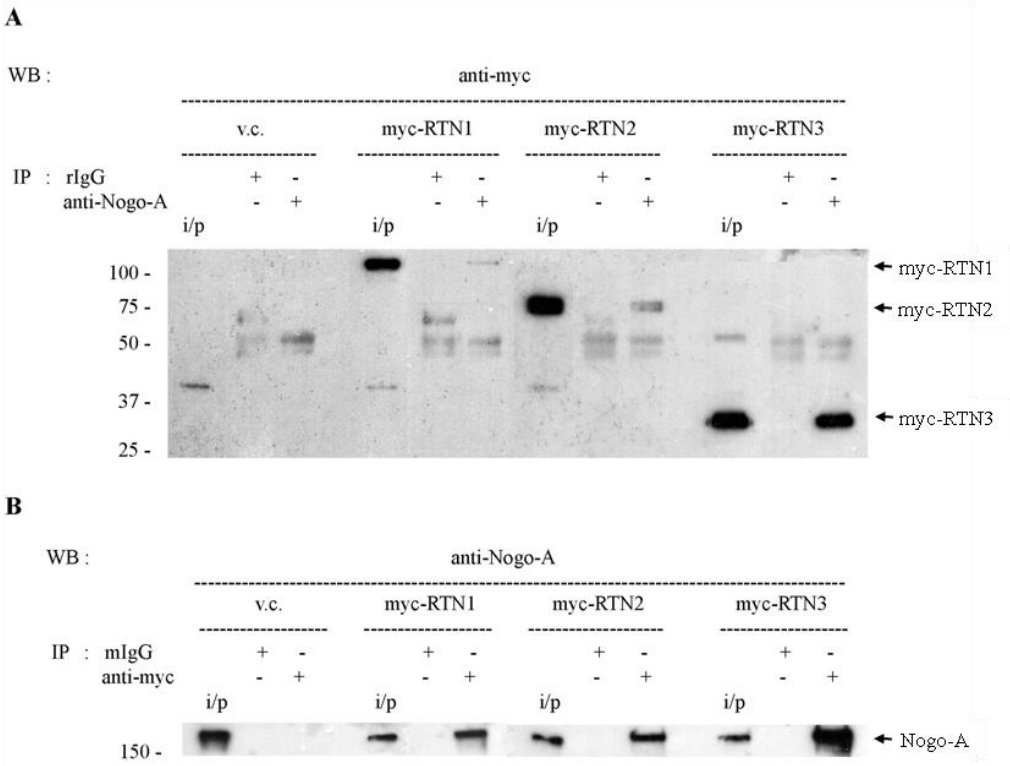

Fig 4.8 Nogo-A co-IP RTN3 to a better extent than with RTN1 and 2. ***(A)*** 1.5 mg of lysates from CHO Nogo-A stable cell-line transiently expressing myc-RTN1, 2 and 3 were incubated with rabbit IgG (rIgG) as a negative control or Ng1V2 (anti-Nogo-A) antibodies overnight before incubation with protein A sepharose beads for 2 hr. Vector control (v.c.) was CHO Nogo-A cells transiently transfected with pDmyc. A 10% SDS-PAGE gel was run and western blotting using 9E10 antibodies (anti-myc) was performed. Input was 1/100 of the amount used for co-IP. ***(B)*** Using the same lysates as stated in (A), a similar experimental set-up as described in (A) was performed, except that the co-IP was performed using mouse IgG (mIgG) as a negative control or 9E10 (anti-myc) antibodies. The samples were resolved on an 8% SDS-PAGE gel and western blotting using Ng1V2 antibodies (anti-Nogo-A) was carried out. Input was 1/50 of the amount used for co-IP.

4.2.3 The region from TM1 to TM2 of Nogo-A is necessary for its interaction with RTN3

After confirming that Nogo-A was able to interact with RTN3 specifically by reciprocal co-IP analyses, it was of interest to determine the region on Nogo-A which was necessary for its interaction with RTN3. In order to delineate the domains that were important, several truncation expression constructs were generated to check if their interactions with RTN3 were impaired. For this purpose, HEK293 cells were transfected to generate a stable cell-line expressing full-length HA tagged RTN3 (HEK293 HA-RTN3). HEK293 cells were used as these cells were well known for their high transfection efficiency. In addition, this provided a cell system that is different from the CHO cells employed in section 4.2.2 above (which were used to confirm Nogo-A and RTN3 interaction), thereby allowing us to find out if Nogo-A and RTN3 could interact with each other in more than one type of cellular environment.

HEK293 HA-RTN3 cells were transiently transfected with myc tagged truncated Nogo-A constructs (as illustrated in Fig 4.9A) and their lysates were used to perform reciprocal co-IP assays, with HA-RTN3 immunoprecipitating myc-truncated Nogo-A (Fig 4.9B) and vice versa (Fig 4.9C). As seen in the co-IP result presented in Fig 4.9B, HA-RTN3 was able to immunoprecipitate full-length Nogo-A (A fl), -B (B fl) and truncated Nogo-A without the cytoplasmic domain (A(-cyto)) to a similar extent. However, the absence of TM1 (A(-TM1)) in Nogo-A caused a reduction in the amount of HA-RTN3 immunoprecipitated. It was interesting to note that, in contrast, the truncation of TM2 (A(-TM2)) did not affect Nogo-A's interaction with RTN3 as much. This was inferred from the amount of input and proportion of RTN3

immunoprecipitated. Removal of the whole RHD (A(-TMS)) led to a complete loss of interaction between Nogo-A and RTN3.

The reciprocal co-IP results in Fig 4.9C showed similar findings as Fig 4.9B for all the Nogo-A truncation proteins, except for that of A(-cyto). For A(-cyto), there

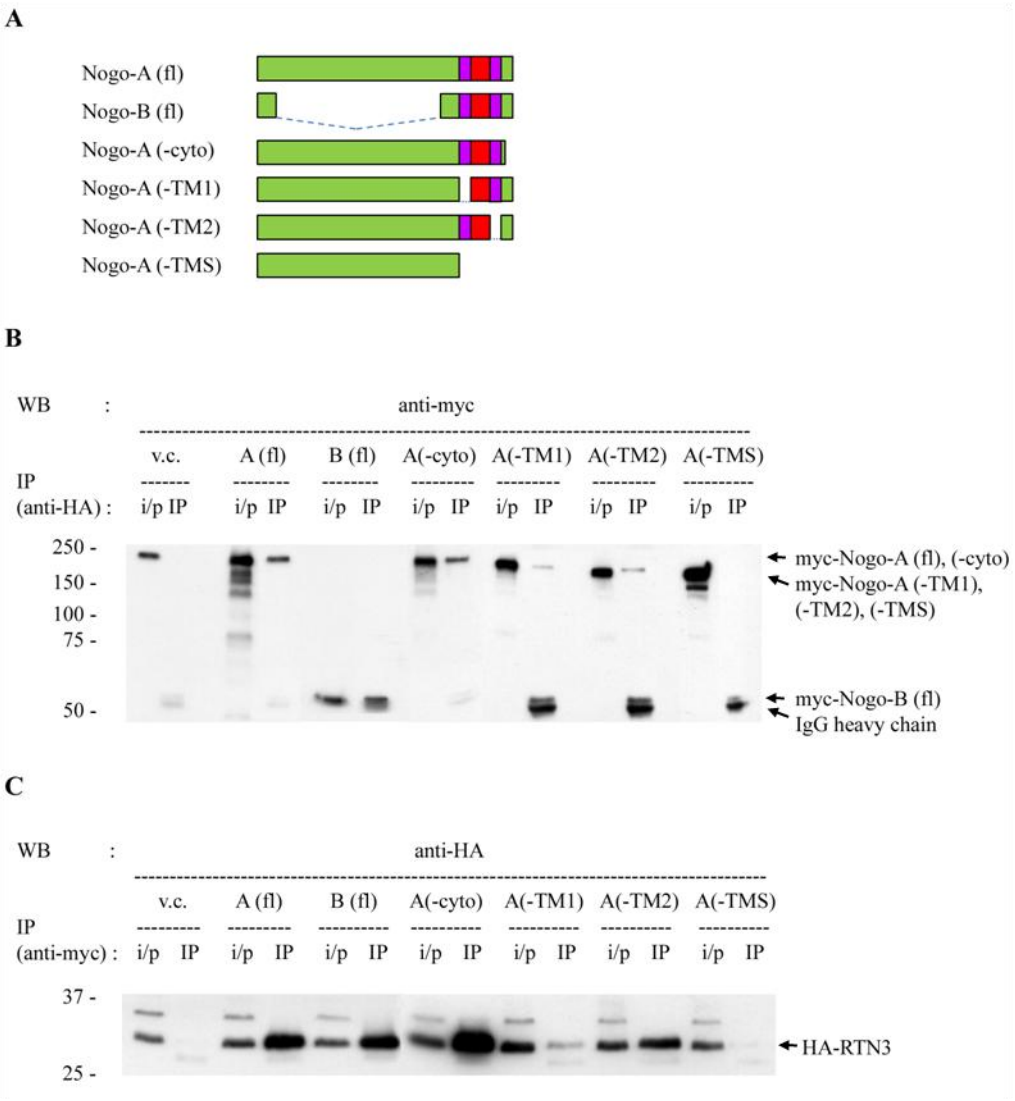

Fig 4.9 The region from TM1 to TM2 of Nogo-A was necessary for its interaction with RTN3. ***(A)*** Schematic diagram of the Nogo-A truncated proteins generated. ***(B)*** 1.5 mg of lysates from HEK293 HA-RTN3 cells transiently expressing myc-truncated Nogo-A proteins were incubated with anti-HA antibodies (anti-HA) for co-IP. Vector control (v.c.) was HEK293 pDHA stable cells transiently transfected with full-length myc-Nogo-A. The samples were run on an 8% SDS-PAGE gel and western blotting was carried out with 9E10 antibodies (anti-myc). Input was 1/20-50 of the amount used for co-IP. ***(B)*** Using the same lysates as stated in (A), a similar experimental set-up as described in (A) was performed, except that the co-IP was performed using

9E10 (anti-myc) antibodies. Vector control (v.c.) was HEK293 HA-RTN3 cells transiently transfected with pDmyc. A 10% SDS-PAGE gel was run and western blotting using anti-HA antibodies (anti-HA) was performed. Input was 1/50 of the amount used for co-IP.

was instead an increase in the amount of HA-RTN3 immunoprecipitated. This anomaly could not be explained.

The results obtained therefore suggested that the region on Nogo-A from TM1 to TM2, including the Nogo-66 domain, was necessary for the interaction between Nogo-A and RTN3, with TM1 playing a more important role in the interaction with RTN3 than TM2. The role of Nogo-66 domain in this interaction could not be excluded.

4.2.4 Both TM domains and possibly the N-terminus of RTN3 is involved in its interaction with Nogo-A

The findings from the previous section have delineated the domains on Nogo-A which played a part in the binding with RTN3. Will the similar domains on RTN3 be enough for its interaction with Nogo-A, or other parts of RTN3 may also be involved as well? To this end, truncation constructs of RTN3 were generated and as described earlier, the truncated proteins (depicted in Fig 4.10A) were transiently expressed and checked for their binding with full-length Nogo-A using HEK293 cells with stable expression of Nogo-A (HEK293 Nogo-A).

In Fig 4.10B, where Ng1V2 antibodies immunoprecipitated Nogo-A and co-IP of truncated RTN3 was investigated, the lack of the N-terminus (3 (-N)), TM1 (3 (-TM1)) and TM2 (3 (-TM2)) resulted in a decrease in the amount of the truncated RTN3 protein immunoprecipitated by Nogo-A. The removal of both TM domains (3

(-TMS)) caused a complete loss of interaction with Nogo-A. We arrived at the same conclusion from the reciprocal co-IP experiment as shown in Fig 4.10C.

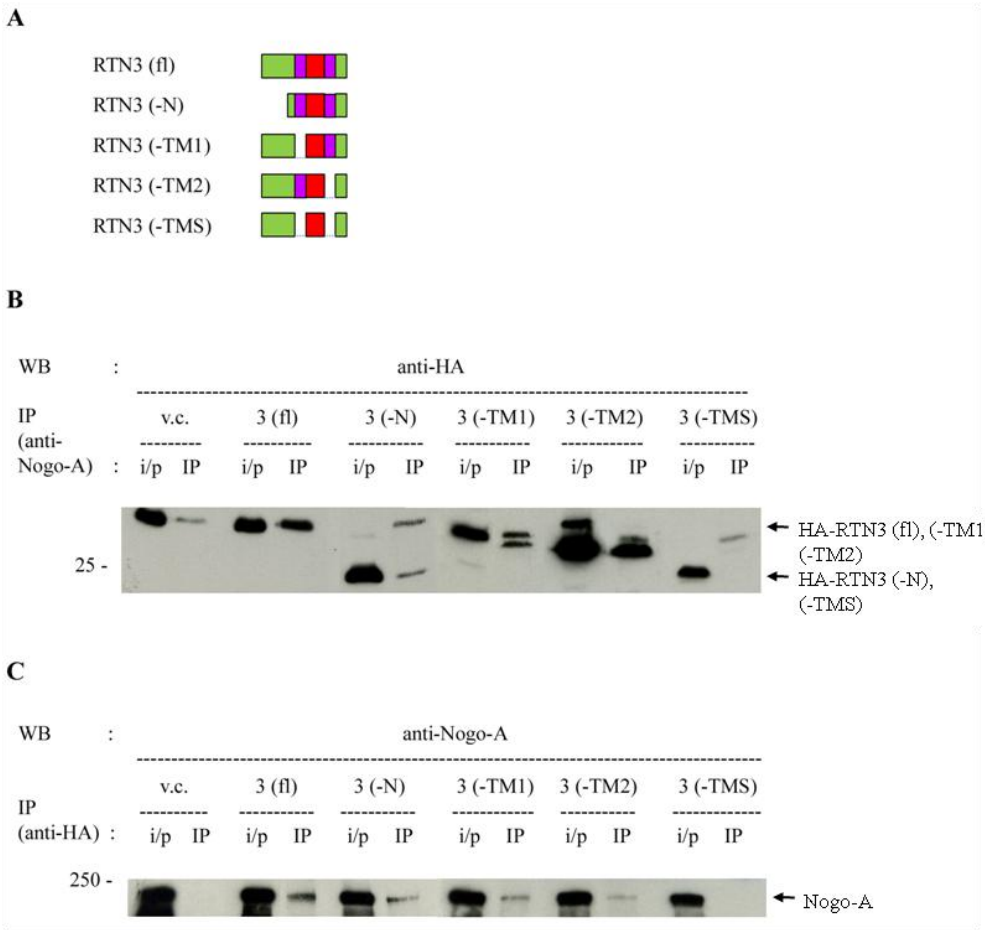

Fig 4.10 Both TM domains were essential for RTN3's interaction with Nogo-A. ***(A)*** Schematic diagram of RTN3 truncation proteins used. ***(B)*** HEK293 Nogo-A cells were transiently transfected with HA-truncated RTN3 constructs and 1.5 mg of these lysates were incubated with Ng1V2 antibodies (anti-Nogo-A) for co-IP. Vector control (v.c.) was HEK293 pCIneo stable cells transiently transfected with full-length HA-RTN3. The samples were run on a 12% SDS-PAGE gel and western blotting was carried out with anti-HA antibodies (anti-HA). Input was 1/13.33-100 of the amount used for co-IP. ***(B)*** Using the same lysates as stated in (A), a similar experimental set-up as described in (A) was performed, except that the co-IP was performed using anti-HA (anti-HA) antibodies. Vector control (v.c.) was HEK293 pDHA cells transiently transfected with full-length Nogo-A. An 8% SDS-PAGE gel was run and western blotting using Ng1V2 antibodies (anti-Nogo-A) was performed. Input was 1/40 of the amount used for co-IP.

Taken as a whole, the results suggested that both the TM domains worked in conjunction in the interaction of RTN3 with Nogo-A, since removal of one of the TM

domains only led to a reduction in interaction while removing both regions caused RTN3 to totally be unable to interact with Nogo-A. It could also be possible that the TM domains were necessary for RTN3 to be localized at the ER so as to be in close proximity with Nogo-A for their interaction to occur. Interestingly, the N-terminus may also play a supplementary role in RTN3's binding to Nogo-A.

4.3 Discussion – Nogo-A's interaction with Caspr and RTN3

The function of Nogo-A at the paranodes, first highlighted at the end of chapter 3, was further studied in this chapter. Nogo-A was found to co-localize and interact with the paranodal Caspr. The interaction between the two proteins appeared to involve, and require the entire Nogo-66 domain of Nogo-A. An investigation on the expression of Caspr during brain development revealed a postnatal expression time for Caspr. This implies that any functional interaction between Nogo-A and Caspr likely occurs in postnatal stages, and not during embryonic development. This notion is also supported by the fact that neither Caspr nor Nogo knockout mice are embryonic lethal or have severe developmental defects.

As Caspr has been implicated to play an important role in the molecular organization at the node of Ranvier, we hypothesized that Nogo-A could also be involved in a similar function. However, a detailed investigation on the architectural organization at the node of Ranvier in Nogo-deficient mice showed no significant changes to the different domains at the node of Ranvier. We examined closely the spatial localization of Caspr and K^+ channels and found no significant differences between these in Nogo-deficient mice compared to wild type. At the moment, the physiological significance of the interaction between Nogo-A and Caspr remains unclear.

We also studied the interaction between Nogo-A and fellow members of the reticulon family. Co-IP experiments revealed that Nogo-A had an unusually high affinity for RTN3 compared to RTN1 and RTN2. From the molecular dissection analysis, their interactions required at least one of the two TM domains. Loss of both TM domains led to a complete loss of interaction between the two RTNs. The possible implications of the interaction between Nogo-A and RTN3, particularly in neurons will be discussed further in chapter 7.

Chapter 5 Nogo-A and other isoforms are protective against a variety of apoptotic insults

In the previous chapters, we have presented data indicating the presence of Nogo-A in neurons, and its interaction with Caspr and RTN3. All these results appear to have little, if anything, to do with Nogo-A's classical function as a myelin-associated inhibitor. We have pondered on the possible physiological (as opposed to pathological) roles of Nogo-A in neurons. In particular, we ask what the cell autonomous function of the Nogo-A expressed in neurons may be. Interestingly, other workers in the laboratory have observed that Nogo-A levels are upregulated in neuronal cell bodies (but not obvious in oligodendrocytes) after spinal cord injury or brain ischemia induced by middle cerebral artery occlusion. Similar observations of Nogo-A upregulation in some CNS injuries have also been made by others (Eslamboli *et. al.*, 2006; Marklund *et. al.*, 2006; Meier *et. al.*, 2003; Wang *et. al.*, 2002c; Wang *et. al.*, 2006).

We reason that this Nogo-A upregulation is a result of transcription profile changes of neurons at the site of injury, largely by those spared from immediate demise resulting from the injuries. If so, Nogo-A's elevated expression could simply be a result of co-elevation together with other injury response genes, and this elevation has no real purpose, but could instead result in an inhibition of regeneration at a later stage. Alternatively, Nogo-A may have a hitherto unappreciated role in neuronal survival, and its elevation could be part of a protective mechanism against neuronal death. Investigations on this possible protective role of Nogo-A is detailed in this chapter.

5.1 Generation of SH-SY5Y cell-lines stably and moderately overexpressing Nogo-A, -B, -C and RTN3

To facilitate investigations on the cell autonomous function(s) of Nogo-A, SH-SY5Y cell-lines stably expressing Nogo-A (SH-SY5Y Nogo-A) were generated. This neuroblastoma cell-line was chosen because it is a popular cell culture model for various "neuronal" processes such as neuritogenesis, neurotransmitter secretion, as well as neuronal cell death. Additionally, it has low Nogo-A levels. This is potentially advantageous as any effects on survival of the cells could be clearly observed upon manipulation of Nogo-A levels. For comparison, SH-SY5Y vector control (transfected with empty vector), Nogo-B, Nogo-C and RTN3 stably expressing cells were also created. Nogo-B and -C stables serve to check Nogo-A's specificity in protection, if any. RTN3 is included in the analysis to gauge if any effect seen with Nogo-A could be extrapolated to the other members of the RTN family.

A stable clone harbouring the empty vector and two stable clones each for the other constructs were selected and used for subsequent investigations. Expression levels of the stably expressing proteins were shown in Fig 5.1A, using γ-tubulin as a loading control. Both the different clones of Nogo isoforms and RTN3 showed varying levels of moderate protein expression. However, high expression as determined by western blot does not necessary correlate to a high percentage of expressing cells. Hence, ICC was performed in addition to visually gauge the percentage of cells stably overexpressing the transgenes (Fig 5.1B). A good majority (>85%) of the cells of the two SH-SY5Y Nogo-A stable clones, 16 and 38, were expressing Nogo-A. The stable cell-lines for Nogo-B (11 and 35), Nogo-C (1 and 23) and RTN3 (11 and 20), however, showed lower percentages of cells stably expressing their respective transgenes.

As clonal differences were not significant, only results of a representative clone each for Nogo-C and RTN3, which were acting as controls, would be presented in the subsequent sections.

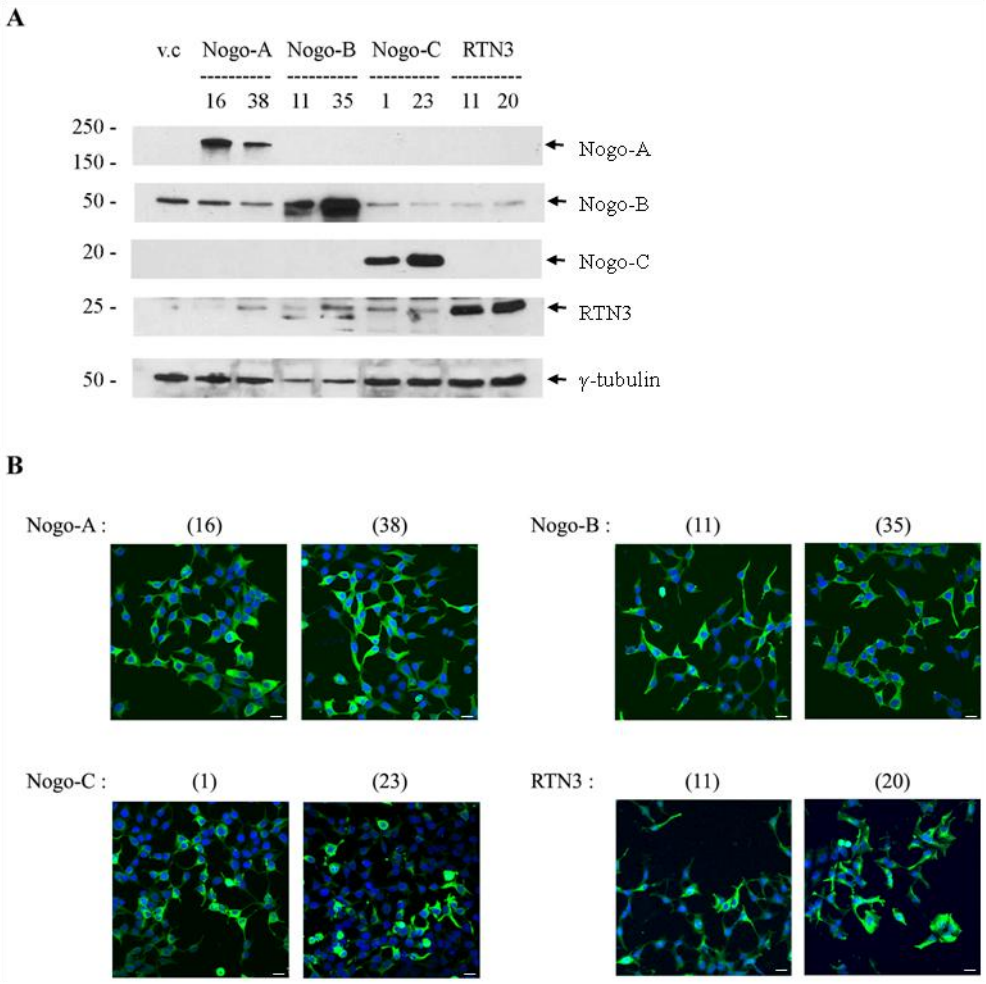

Fig 5.1 Stable protein expression profiles in SH-SY5Y stable cell-lines. ***(A)*** 20 µg of lysates from SH-SY5Y vector control (v.c.), Nogo-A (16, 38), -B (11, 35), -C (1, 23) and RTN3 (11, 20) stable cell-lines were resolved on a 10% SDS-PAGE gel. Western-blotting was first performed with AR2 rabbit polyclonal antibodies to detect Nogo-A, -B and -C proteins. The membrane was subsequently probed with anti-RTN3 or anti-γ-tubulin antibodies. ***(B)*** SH-SY5Y Nogo-A (16, 38), -B (11, 35) and -C (1, 23) cells were fixed with 4% PF and permeabilized with 0.05% saponin/PBS. They were then incubated with AR2 antibodies, followed by FITC-conjugated secondary antibodies. For RTN3 stable cells (11, 20), they were fixed in ice-cold methanol before incubation with anti-RTN3 antibodies followed by secondary antibodies conjugated with FITC. Hoechst 33342 was used to stain the nuclei. Bar = 20 µm.

5.2 All three major Nogo isoforms and RTN3 protect against serum withdrawal-induced cell death

Serum withdrawal denies SH-SY5Y cells of essential growth factors and is known to cause cell death by apoptosis (Macleod *et. al.*, 2001). To find out if Nogo-A, -B, -C and RTN3 could modulate this apoptotic insult, the cells, together with the vector control cells, were subjected to serum deprivation (0% FBS) for 48 hr before PI staining and flow cytometry analysis.

Fig 5.2A showed the cell cycle profiles of these cell-lines after 48 hr of serum withdrawal. Proportion of cells dying by apoptosis is represented by the percentage of the sub G1 population, and was depicted in the graph and table in Fig 5.2B and C respectively. Vector control cells (v.c.) displayed a 95% confidence interval of 14.47 ± 1.51% for sub G1 population with a corresponding decrease in G1 population as seen from its cell cycle profile in Fig 5.2A, as compared to 4.6 ± 0.23% for its sub G1 population at 0 hr. Comparatively, the sub G1 populations for all Nogo isoforms (Nogo-A 7.17-7.63%; Nogo-B 7.37-9.1%; Nogo-C 7.87%) and RTN3 (7.57%) expressing cells were significantly lower than vector control cells after serum deprivation (Fig 5.2B), and did not show as much an increase in their sub G1 population as compared to their respective untreated cells at 0 hr (Fig 5.2C). Interestingly, as judged from the DNA content profile, Nogo-C expressing cells seemed to behave in a different manner from those expressing Nogo-A, -B and RTN3, with an increase in S phase-arrested cells instead of the typical G1 arrest exhibited by the other three RTNs (Fig 5.2A).

In any case, all Nogo isoforms and RTN3 appear to exert a significant degree of protection in SH-SY5Y cells from cell death induced by serum withdrawal/removal of growth factors.

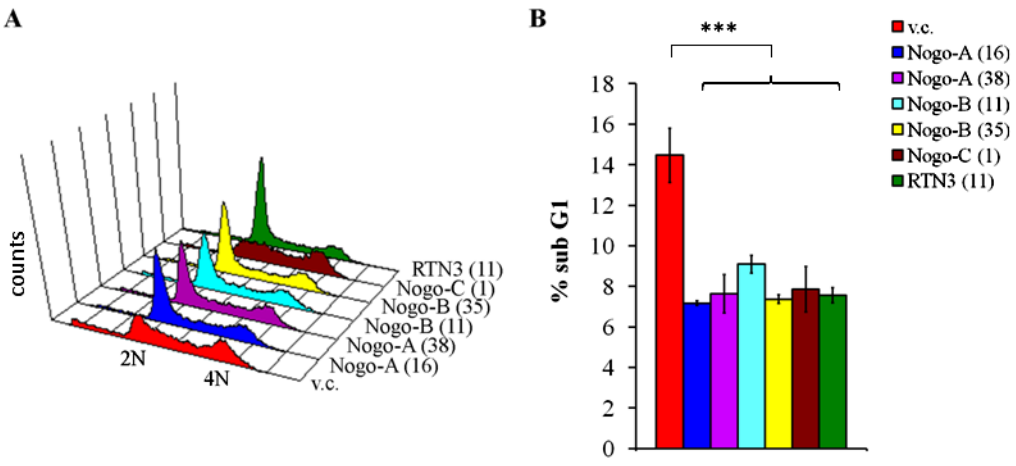

C

	% sub G1	
Cell-lines	0 hr	48 hr
v.c.	4.60 ± 0.23	14.47 ± 1.51
Nogo-A (16)	4.27 ± 0.73	7.17 ± 0.13
Nogo-A (38)	5.27 ± 0.35	7.63 ± 1.08
Nogo-B (11)	8.10 ± 0.71	9.1 ± 0.49
Nogo-B (35)	9.80 ± 0.63	7.37 ± 0.24
Nogo-C (1)	3.60 ± 0.11	7.87 ± 1.27
RTN3 (11)	8.53 ± 0.24	7.57 ± 0.43

Fig 5.2 All Nogo isoforms and RTN3 protected SH-SY5Y against serum withdrawal-induced cell death. SH-SY5Y vector control (v.c.), Nogo-A (16, 38), -B (11, 35), -C (1) and RTN3 (11) cells were serum deprived for 48 hr before the cells were stained with PI and analysed by flow cytometry using FACS Canto II. Data is representative of three independent experiments. ***(A)*** Cell cycle profiling of the stable cell-lines after 48 hr of serum withdrawal using ModFit v2.9. ***(B)*** % of sub G1 population in the serum-deprived stable cell-lines at 48 hr (mean ± sd, n = 3). *** $P < 0.01$ compared with v.c. ***(C)*** The 95% confidence interval of sub G1 population of the stables when untreated at 0 hr and after 48 hr of serum withdrawal.

5.3 All three major Nogo isoforms and RTN3 protect against staurosporine-induced cell death

Another classical inducer of apoptosis, staurosporine, was tested for its ability to cause cell death in these stable cell-lines. Staurosporine is a general protein kinase inhibitor, which acts by binding to the kinases and competitively prevents ATP from binding. It causes cells to arrest at G2 phase and initiates apoptotic cell death. Staurosporine therefore presents a mechanistically different mode of apoptosis

induction compared to serum withdrawal, and an arguably harsher one. Cells were treated with 0.5 µM of the drug for 48 hr and then analysed for cell death.

As shown in Fig 5.3, all the cell-lines stably expressing the Nogo isoforms and RTN3 have significantly reduced cell death induced by staurosporine, as compared to vector control cells. Staurosporine induced half of the population of vector control cells to die, achieving a 95% confidence interval of 45.03 ± 1.96% for its sub G1 population. Comparatively, the Nogo isoforms and RTN3 were able to reduce cell death in SH-SY5Y by almost half. SH-SY5Y Nogo-A, -B, -C and RTN3 lines exhibited sub G1 populations of only 14.7-17.5%, 14.4-15.93%, 12.27% and 19.07% respectively.

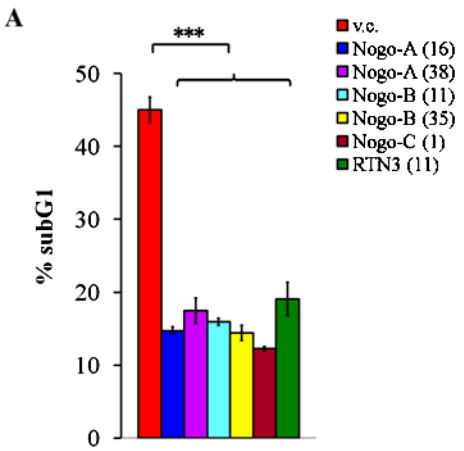

B

Cell-lines	% sub G1	
	0 hr	48 hr
v.c.	4.97 ± 1.25	45.03 ± 1.96
Nogo-A (16)	3.90 ± 0.11	14.70 ± 0.58
Nogo-A (38)	5.70 ± 0.88	17.50 ± 1.96
Nogo-B (11)	7.37 ± 0.68	15.93 ± 0.58
Nogo-B (35)	8.20 ± 0.30	14.40 ± 1.20
Nogo-C (1)	3.40 ± 0.23	12.27 ± 0.28
RTN3 (11)	6.37 ± 0.13	19.07 ± 2.58

Fig 5.3 All Nogo isoforms and RTN3 protected SH-SY5Y against staurosporine-induced cell death. SH-SY5Y vector control (v.c.), Nogo-A (16, 38), -B (11, 35), -C (1) and RTN3 (11) cells were treated with 0.5 µM of staurosporine for 48 hr before the cells were analysed by flow cytometry. Data is representative of three independent experiments. ***(A)*** % of sub G1 population in staurosporine-treated stable cell-lines at 48 hr (mean ± sd, n = 3). *** $P < 0.01$ compared with v.c. ***(B)*** The 95% confidence interval of sub G1 population of the stables when untreated at 0 hr and after 48 hr of staurosporine treatment.

5.4 Nogo-A, -B and RTN3, but not Nogo-C, protect against etoposide-induced cell death

To check if the Nogo isoforms and RTN3 could similarly protect against cell death caused by DNA damage, the cells were treated with the common anticancer drug etoposide. Etoposide inhibits the enzyme topoisomerase II, thereby preventing rewinding of the DNA double helix strands and ultimately results in un-repairable breaks in DNA.

The cell-lines were treated with 20 µM of etoposide for 72 hr before significant cell death was observed (Fig 5.4). The sub G1 population for vector control cells was, at a 95% confidence interval, 55.47 ± 3.3%. Similar to staurosporine treatment, Nogo-A, -B and RTN3 expression were able to protect the cells against etoposide-induced cell death by half or even more, with the cells displaying a sub G1 population of only 15.5-15.83%, 17.7-22.37% and 26.03% respectively. A G1/S cell

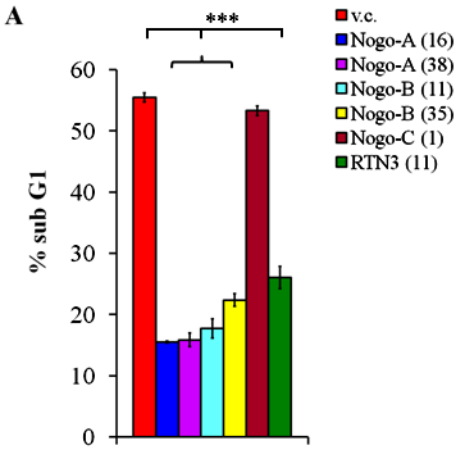

B

Cell-lines	% sub G1	
	0 hr	72 hr
v.c.	5.63 ± 0.53	55.47 ± 3.30
Nogo-A (16)	4.93 ± 0.77	15.50 ± 0.85
Nogo-A (38)	7.10 ± 0.30	15.83 ± 1.05
Nogo-B (11)	10.50 ± 0.79	17.70 ± 1.28
Nogo-B (35)	12.13 ± 0.75	22.37 ± 0.86
Nogo-C (1)	5.27 ± 0.17	53.30 ± 0.20
RTN3 (20)	16.63 ± 0.36	26.03 ± 0.73

Fig 5.4 Nogo-A, -B and RTN3 protected SH-SY5Y against etoposide-induced cell death, but not Nogo-C. SH-SY5Y vector control (v.c.), Nogo-A (16, 38), -B (11, 35), -C (1) and RTN3 (11) cells were treated with 20 µM of etoposide for 72 hr before flow cytometry analysis was carried out. Data is representative of three independent experiments. ***(A)*** % of sub G1 population in etoposide-treated stable cell-lines at 72 hr (mean ± sd, n = 3). *** $P < 0.01$ compared with v.c. ***(B)*** The 95% confidence interval

of sub G1 population of the stables when untreated at 0 hr and after 72 hr of etoposide treatment.

cycle phase arrest was observed in these cells while no such arrest was seen in the vector control cells. Comparatively, Nogo-A seemed to be able to provide the best protection. Nogo-C, however, was unable to provide the same protection as the other RTNs, with its cells dying almost as much as the vector control cells (~53.3%).

5.5 Nogo-A, -B and RTN3, but not Nogo-C, enhance cell death induced by tunicamycin

Yet a different kind of cell death-inducing mechanism, this time via the induction of ER stress, was investigated in terms of the RTNs' protective ability. The drug tunicamycin acts by inhibiting N-linked glycosylation of proteins and causes proteins to accumulate in ER. This activates the unfolded protein response (UPR) in cells, and the prolonged ER stress eventually leads to apoptosis.

Cells were subjected to tunicamycin treatment at a concentration of 20 μg/ml for 72 hr before they were analysed by flow cytometry. As shown in Fig 5.5, vector control cells were actually not dying as yet at the 72 hr time point, with a sub G1 population of 6.23% that was comparable to that at 0 hr, which was 5.63%. Interestingly, Nogo-A, -B and RTN3 stable cell-lines were dying more than that of vector control cells. They displayed 12.77-23.27%, 15.83-16.03% and 19.87% sub G1 population respectively. SH-SY5Y Nogo-C, on the other hand, behaved like the vector control cells, with no increase in the sub G1 population at 72 hr when compared to 0 hr (5.27%).

It is noteworthy that ER stress induced by tunicyamycin resulted in cell death that was not protected by Nogo-A, -B and RTN3. Contrasting to the protection they

render against the other types of cell death induction described in the preceding sections, these reticulons actually enhanced tunicamycin-induced death.

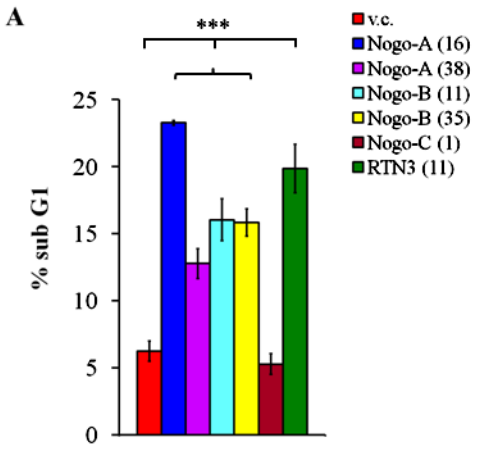

B

Cell-lines	% sub G1 0 hr	% sub G1 72 hr
v.c.	5.63 ± 0.53	6 23 ± 0.85
Nogo-A (16)	4.93 ± 0.77	23.27 ± 0.17
Nogo-A (38)	7.10 ± 0.30	12.77 ± 1.25
Nogo-B (11)	10.50 ± 0.79	16.03 ± 1.79
Nogo-B (35)	12.13 ± 0.75	15.83 ± 1.13
Nogo-C (1)	5.27 ± 0.17	5 27 ± 0.88
RTN3 (20)	16.63 ± 0.36	19.87 ± 2.06

Fig 5.5 Nogo-A, -B and RTN3 enhanced SH-SY5Y cell death by tunicamycin while Nogo-C had no effect. SH-SY5Y vector control (v.c.), Nogo-A (16, 38), -B (11, 35), -C (1) and RTN3 (11) cells were treated with 20 µg/ml of tunicamycin for 72 hr before cell death analysis was performed. Data is representative of three independent experiments. ***(A)*** % of sub G1 population in tunicamycin-treated stable cell-lines at 72 hr (mean ± sd, n = 3). *** $P < 0.01$ compared with v.c. ***(B)*** The 95% confidence interval of sub G1 population of the stables when untreated at 0 hr and after 72 hr of tunicamycin treatment.

5.6 Only Nogo-A and -B could protect against H_2O_2-induced cell death

Oxidative stress has been touted to be a crucial factor in the causation of many neurodegenerative diseases and also in the pathogenesis of cerebral ischemia and reperfusion injury. Reactive oxygen species (ROS) such as H_2O_2, superoxide (O_2^-), hydroxyl radical (OH^-) and peroxynitrate ($ONOO^-$) generated as a result of oxidative stress could cause perturbations to the membranes and proteins directly and also activate intracellular signalling pathways, eventually leading to neuronal cell death (Fatokun *et. al.*, 2008).

To study if Nogo could also protect against oxidative stress, the stable cell-lines were treated with stabilized H_2O_2, which is commonly used to simulate oxidative stress in diseases and injuries. Cells were treated with 100 µM of H_2O_2 for

30 min and washed once to remove any traces of H_2O_2. The cells were then harvested for flow cytometry analysis after 48 hr, counting from point of H_2O_2 addition. As displayed in Fig 5.6, vector control, Nogo-C and RTN3 stable cell-lines all showed a similar percentage of sub G1 population (13.23-14.4%) after 48 hr of H_2O_2 treatment, with concomitant decrease in G1 population. However, there was only a slight increase in sub G1 population in Nogo-A (3.7%) and -B (5.5-6.97%) stable cell-lines as compared to their respective sub G1 population at 0 hr.

These results suggested that Nogo-A and -B could rather specifically protect SH-SY5Y cells from H_2O_2-induced cell death, while Nogo-C and RTN3 were unable to provide the same protection. Interestingly, this indicates that the N-terminus of Nogo (which is the difference between Nogo-A/B and Nogo-C) is crucial for the protection against oxidative stress by H_2O_2. This also means that the N-terminus of Nogo-B, which is common in both Nogo-A and -B, is probably sufficient for the protection rendered by Nogo-A and -B.

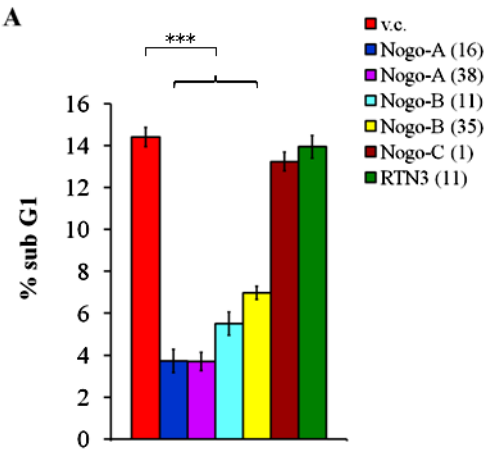

B

Cell-lines	% sub G1	
	0 hr	48 hr
v.c.	1.60 ± 0.30	14.40 ± 0.52
Nogo-A (16)	2.10 ± 0.23	3.73 ± 0.63
Nogo-A (38)	2.20 ± 0.11	3.70 ± 0.49
Nogo-B (11)	4.83 ± 0.51	5.50 ± 0.63
Nogo-B (35)	5.63 ± 0.07	6.97 ± 0.35
Nogo-C (1)	3.83 ± 0.26	13.23 ± 0.51
RTN3 (11)	5.30 ± 0.52	13.93 ± 0.62

Fig 5.6 Nogo-A and -B specifically protected SH-SY5Y against H_2O_2-induced cell death. SH-SY5Y vector control (v.c.), Nogo-A (16, 38), -B (11, 35), -C (1) and RTN3 (11) cells were treated with 100 µM H_2O_2 for 30 min before H_2O_2 was washed off and the cells grown in complete RPMI medium until 48 hr from the start of addition of H_2O_2. Analysis of cell death was performed using flow cytometry. Data is representative of three independent experiments. ***(A)*** % of sub G1 population in the H_2O_2-treated stable cell-lines at the 48 hr time point (mean ± sd, n = 3). *** $P < 0.01$

compared with v.c. ***(B)*** The 95% confidence interval of sub G1 population of the stables when untreated at 0 hr and after 48 hr of H_2O_2 treatment.

5.7 Discussion – Nogo-A's role in neuroprotection

SH-SY5Y cells with stable and moderate overexpression of Nogo-A, -B, -C and RTN3 were subjected to various treatments that induced apoptosis by different ways. All the Nogo isoforms and RTN3 were able to protect the cells against serum withdrawal and staurosporine. Interestingly, all except Nogo-C were able to provide protection against etoposide. The reverse was seen with tunicamycin, where all except Nogo-C enhanced cell death induced by the drug. Interestingly, only Nogo-A and -B were able to prevent cells from dying when subjected to oxidative stress induced by H_2O_2.

The differing observations obtained with the various treatments suggest that the mechanisms by which the Nogo isoforms and RTN3 confer protection against cell death could be fairly complex. Investigations on the possible mechanisms involved in protection against the death insults will be elaborated in the next chapter. Nevertheless, the protective ability of Nogo-A against a wide range of apoptotic insults (except tunicamycin) is clearly illustrated. This has strong implications on the notion of Nogo-A playing a neuroprotective role during CNS injury.

Chapter 6 Possible mechanisms involved in Nogo-A's protection against H_2O_2-induced cell death

Of all the protective effects and profiles reported in the previous chapter, Nogo-A and -B's rather specific ability to attenuate apoptosis induction by H_2O_2 has particular pathophysiological relevance. Not only is Nogo-A expressed in CNS neurons, but oxidative stress-induced neuronal death in either acute (injury) or chronic (neurodegenerative diseases) manners occurs in the CNS *in vivo*. We therefore chose to attempt to investigate the underlying mechanism of Nogo-A's protective effect against H_2O_2.

6.1 Protection against H_2O_2 requires N-terminus of Nogo-A/B

As shown in the previous chapter, Nogo-A and -B, but not -C, were able to prevent SH-SY5Y cells from dying by H_2O_2 treatment. This suggested that the the N-terminal region common to both Nogo-A and -B is the crucial determinant for the protective effect.

To ascertain that this is indeed the case, three other SH-SY5Y stable cell-lines expressing Nogo-B tagged/truncation were created: (1) SH-SY5Y HA-Nogo-B, where a HA tag was fused to the N-terminus of full-length Nogo-B, (2) SH-SY5Y Nogo-B (1-200), which contained only the first 200 aa of Nogo-B and with the RHD domain deleted completely, and (3) SH-SY5Y Nogo-B (N-TM1), which contained the N-terminus portion of Nogo-B up until the first TM domain. A schematic diagram of these constructs is depicted in Fig 6.1A. The stable protein expression levels in these cells were shown in Fig 6.1B (bottom).

To investigate if these proteins had any differing effects on survival against H_2O_2, the stable cell-lines were treated the same way with H_2O_2 as before. As seen in

Fig 6.1B (top), HA-Nogo-B (3) exhibited an increase in sub G1 population in a way that resembled vector control cells. The former had 18.43% while the latter 16.5%. Untagged Nogo-B (11) stable clone, like before, better survived the H_2O_2 treatment (% sub G1 = 7.1%). This suggested that N-terminus fusion with the HA tag had attenuated Nogo-B's protection against H_2O_2. One possible explanation for this observation could be that a structural change of the N-terminal portion is effected by the HA epitope fusion. Interestingly, the other new Nogo-B truncation construct expressing stable cell-lines, Nogo-B (1-200) and (N-TM1), were not only not protected from H_2O_2 treatment, but showed a significantly higher increase in sub G1 population of 20.8% and 24.67% respectively.

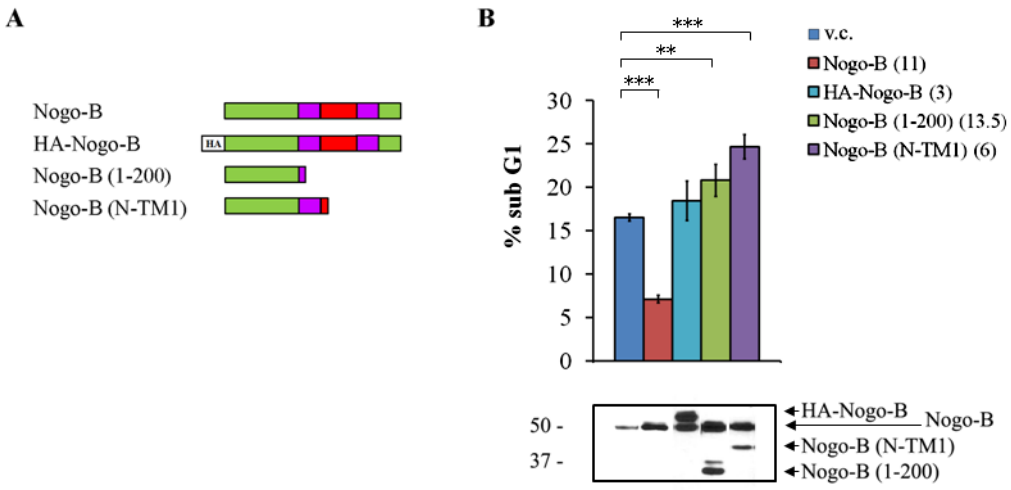

Fig 6.1 The N terminus of Nogo-B was involved in protection against H_2O_2-induced cell death. ***(A)*** Domain stucture of the different Nogo-B proteins expressed in the various Nogo-B stable cell-lines. ***(B) (Top)*** SH-SY5Y vector control (v.c.), Nogo-B (11), HA-Nogo-B (3), Nogo-B (1-200) (13.5) and Nogo-B (N-TM1) (6) cells were treated with 100 µM H_2O_2 for 30 min before H_2O_2 was washed off and the cells grown in complete RPMI medium until 48 hr from the start of addition of H_2O_2. Analysis of cell death was performed using flow cytometry. % of sub G1 population in the H_2O_2-treated stable cell-lines at 48 hr was as shown in the graph (mean ± sd, n = 3). ** $P < 0.05$ compared with v.c. *** $P < 0.01$ compared with v.c. Data is representative of three independent experiments. ***(Bottom)*** Expression levels of the various types of Nogo-B proteins in the stable cell-lines, probed with anti-Nogo goat polyclonal antibodies.

The results suggested that the common N-terminus of Nogo-A/B may be important for Nogo-A/B's protective function against H_2O_2. However, this protection was exhibited only in a proper context in conjunction with the RHD domain.

6.2 Protection by Nogo-A does not involve classical survival pathways

6.2.1 Intrinsic differences in classical survival markers in the stable cell-lines

We next attempted to understand the underlying mechanism by which Nogo-A could protect against cell death induced by H_2O_2. As many neuroprotective agents act by inducing cellular survival pathways, we investigated if RTNs' expression in the stable cells has resulted in any intrinsic changes to the expression and activity of classical pro-survival molecules such as Akt and Erk. GSK3α/β was examined as well since it could be phosphorylated by Akt and has an influence on survival. From Fig 6.2, it was observed that there were no significant differences in the levels of total as well as phosphorylated Akt, Erk1/2 and GSK3α/β between vector control and RTN-expressing stable cell-lines.

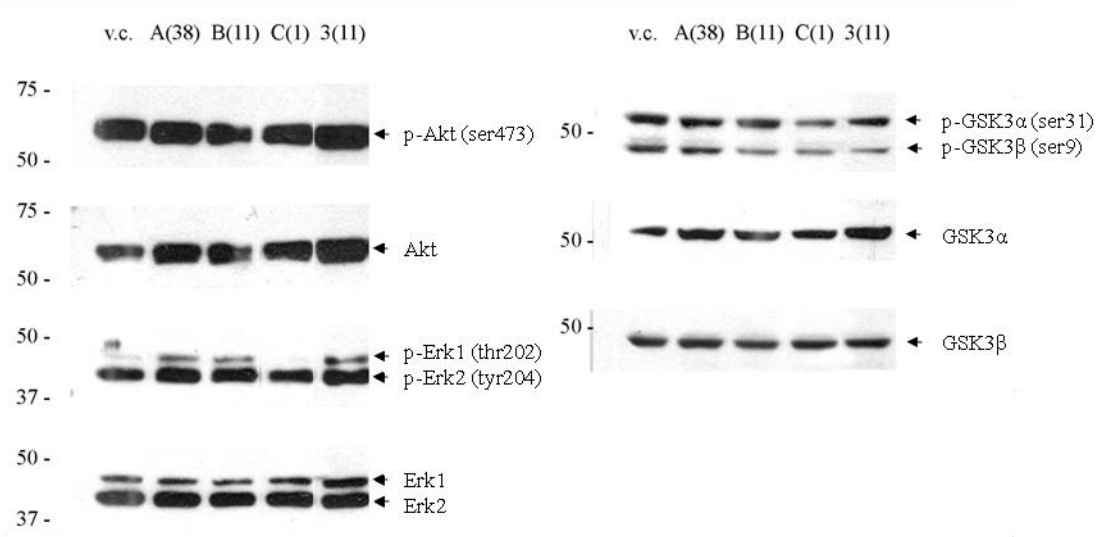

Fig 6.2 Total and phosphorylated protein levels of Akt, Erk and GSK3α/β were unaltered by RTNs' expression. 50 µg of lysates obtained from SH-SY5Y vector

control (v.c.), Nogo-A (A(38)), -B (B(11)), -C (C(1)) and RTN3 (3(11)) were resolved on 10% SDS-PAGE gels and western blotted with antibodies against total and phosphorylated Akt, Erk1/2 and GSK3α/β.

6.2.2 Activation of Akt and Erk upon H_2O_2 treatment

Although no intrinsic differences were found for the basal levels of total and phosphorylated Akt and Erk in the stable cell-lines, it may still be possible that Nogo-A affects the activation of Akt and Erk by H_2O_2 thereby resulting in the survival effect observed.

To investigate this possibility, vector control and SH-SY5Y Nogo-A (38) cells were stimulated with 100 μM of H_2O_2 from 0 to 8 hr and their lysates harvested at various time points to check for Akt and Erk phosphorylation. The results were shown in Fig 6.3. Phosphorylation levels of Akt increased within 15 min and subsided after 30 min for both cell types. Phosphorylated Akt continued to decrease to a minimal level after 8 hr for vector control cells, but returned to sustained basal levels in Nogo-A stable cells. Similarly, Erk phosphorylation peaked at 15 min, was reduced by 30 min and was maintained at a low level in vector control cells. As for Nogo-A cells, significant folds of increase in Erk phosphorylation was not observed, but there was a drastic reduction during 30 min to 1 hr. The levels of phospho-Erk returned to baseline by 2 hr.

The ability of Akt phosphorylation to be longer sustained in Nogo-A expressing stable cells but not vector control cells suggested that it could confer some pro-survival effect. However, the better sustained Akt phosphorylation at later time points could also simply indicate normal cell growth after the cells have survived H_2O_2 treatment via other unrelated mechanisms.

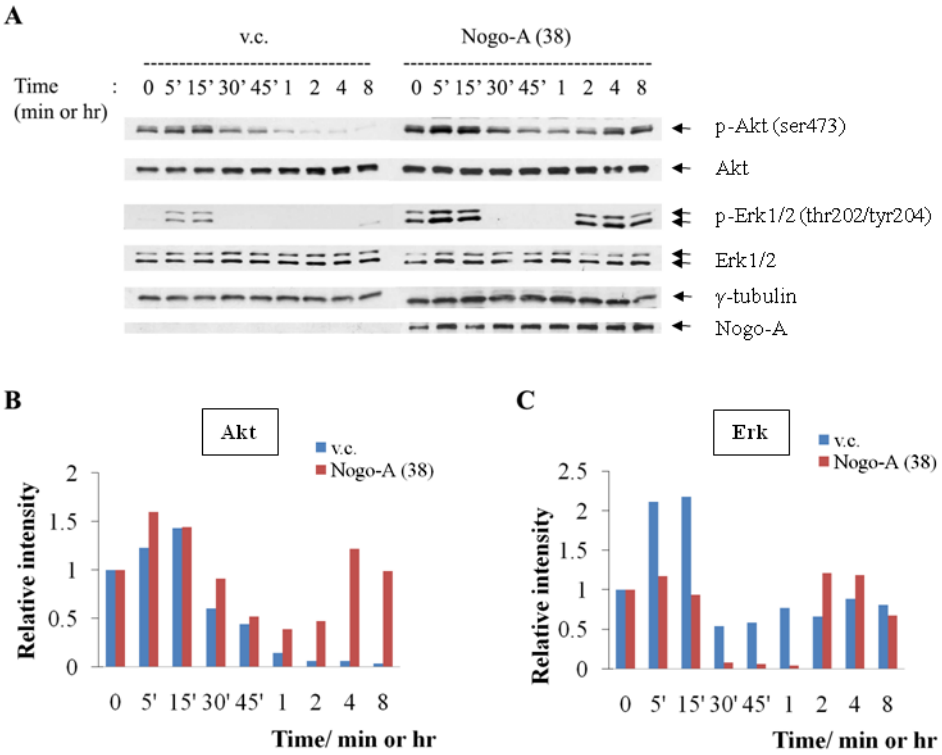

Fig 6.3 Akt and Erk activation upon H_2O_2 treatment. ***(A)*** 50 µg of treated lysates obtained from SH-SY5Y vector control (v.c.) and Nogo-A (38) were resolved on 8% SDS-PAGE gels and western blotted with antibodies against total and phosphorylated Akt, Erk1/2, γ-tubulin and Nogo-A. ***(B and C)*** Densitometric measurements of (A) and data presented as phosphorylated/total Akt (B) or Erk (C) with respect to 0 hr.

6.2.3 Inhibition of Akt and Erk do not influence Nogo-A's protective ability

To further confirm if Akt and Erk play any roles in Nogo-A's protection, cells were pretreated with inhibitors of these two kinases. The inhibitors, LY294002 (LY) and U0126, act on the upstream regulators of Akt and Erk, namely PI3K and MEK1/2, respectively. Cells were pre-treated with 50 µM of LY for 1 hr or 10 µM of U0126 for 30 min before H_2O_2 treatment. Two types of inhibitor treatment regiment were carried out. One was a short-term inhibition, where the inhibitor was removed together with H_2O_2 after the 30 min H_2O_2 treatment. This aimed to answer if activation of Akt or Erk induced by H_2O_2 was important for protection by Nogo-A. The second type was a long-term inhibition, where cells were incubated with the inhibitor until harvest time. This would answer if the presence of Akt and Erk at the 8

hr time point as mentioned in the preceding section could explain the pro-survival effect of Nogo-A.

Results of Akt inhibition was shown in Fig 6.4. Phosphorylation of Akt at both ser473 and thr308 were efficiently blocked by LY, while Erk phosphorylation was unaffected (Fig 6.4A). As seen in Fig 6.4B, short-term inhibition of Akt actually made the vector cells more susceptible to H_2O_2-induced death. However, no significant changes were observed for Nogo-A stable cells. Long-term inhibition of Akt (Fig 6.4C) caused G2 arrest in vector control cells, thereby preventing them from dying, while no significant differences were seen for Nogo-A cells. Notably, G2 arrest was more prominent in vector cells than Nogo-A ones. Another point to note was that incubation with LY alone without H_2O_2 for 48 hr increased cell death in both cells.

Erk inhibition did not cause Nogo-A to lose its protective effect as well. The Erk inhibitor, U0126, could completely abolish Erk1/2 phosphorylation while not affecting phosphorylation of Akt at ser473 (Fig 6.5A). Similar to Akt inhibition, inhibition of Erk in a short-term manner induced more vector control cells to die (Fig 6.5B). This meant that Erk activation by H_2O_2 did have some protective role in these cells. Nogo-A stable cells did not show significant changes in cell death. Long-term Erk inhibition also resulted in G2 arrest in both cells, with the arrest more obvious in vector control cells than the Nogo-A expressing ones. This inadvertently led to a reduction of death in vector cells. As with LY, addition of U0126 alone for 48 hr in the absence of H_2O_2 was itself promoting cell death in the two cell-lines.

In summary, the inhibitor studies indicated that both Akt and Erk did not seem to be involved in any significant manner in Nogo-A's protection against H_2O_2.

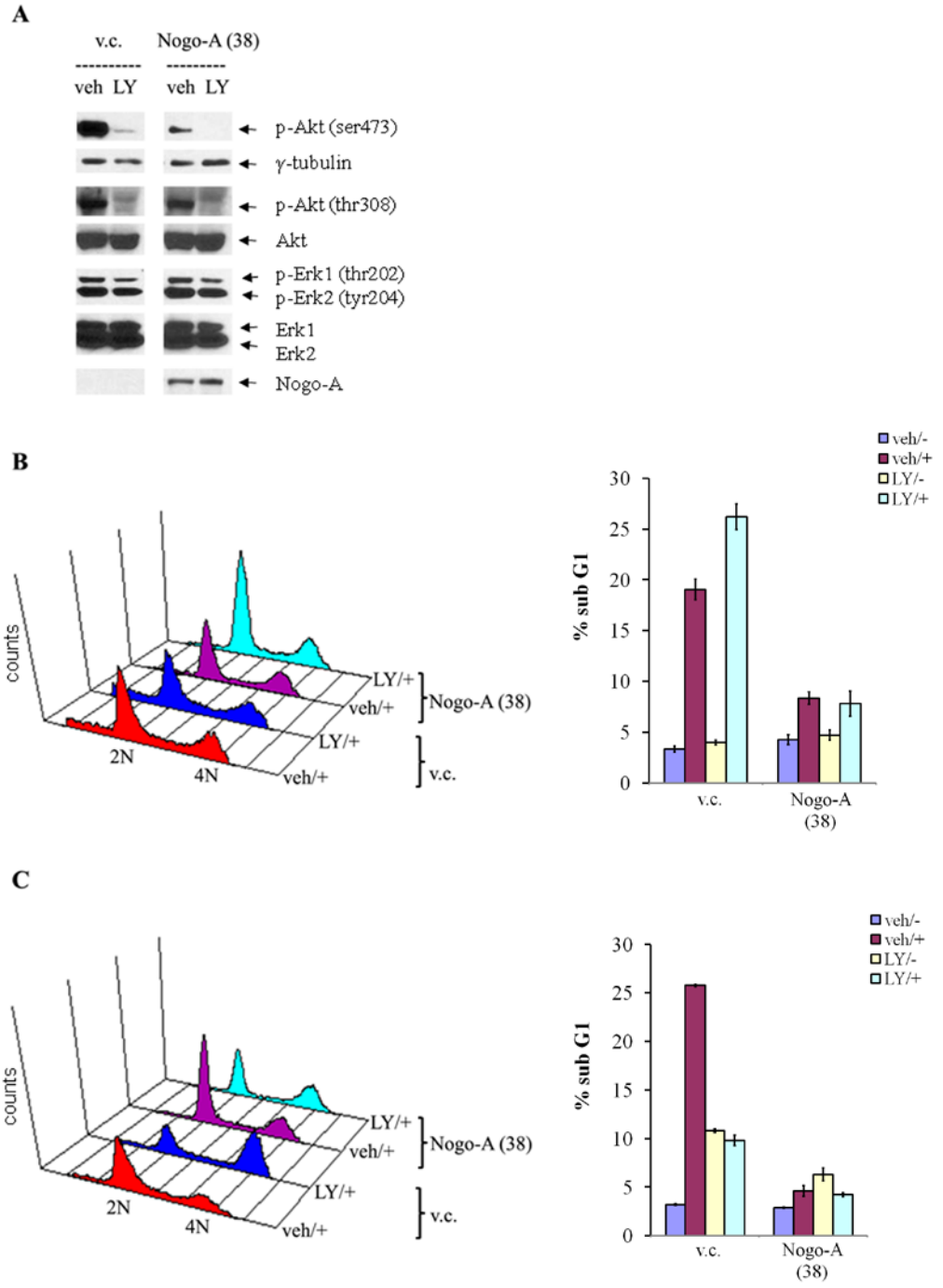

Fig 6.4 Inhibition of Akt did not enhance cell death in Nogo-A stable cells. ***(A)*** 50 µg of lysates from SH-SY5Y vector control (v.c.) and Nogo-A (38) pretreated with vehicle (veh) and LY294002 (LY) were resolved on a 8% SDS-PAGE gel and western blotted with antibodies against total and phosphorylated Akt, Erk1/2, γ-tubulin and Nogo-A. Note that p-Akt (ser473) and (thr308) blotting were on separate membranes. ***(B and C)*** Short-term (B) and long-term (C) inhibition of Akt. The histograms (left) were drawn using ModFit v2.9. Sub G1 populations of treated cells (right) were graphed as mean ± sd (n = 3).

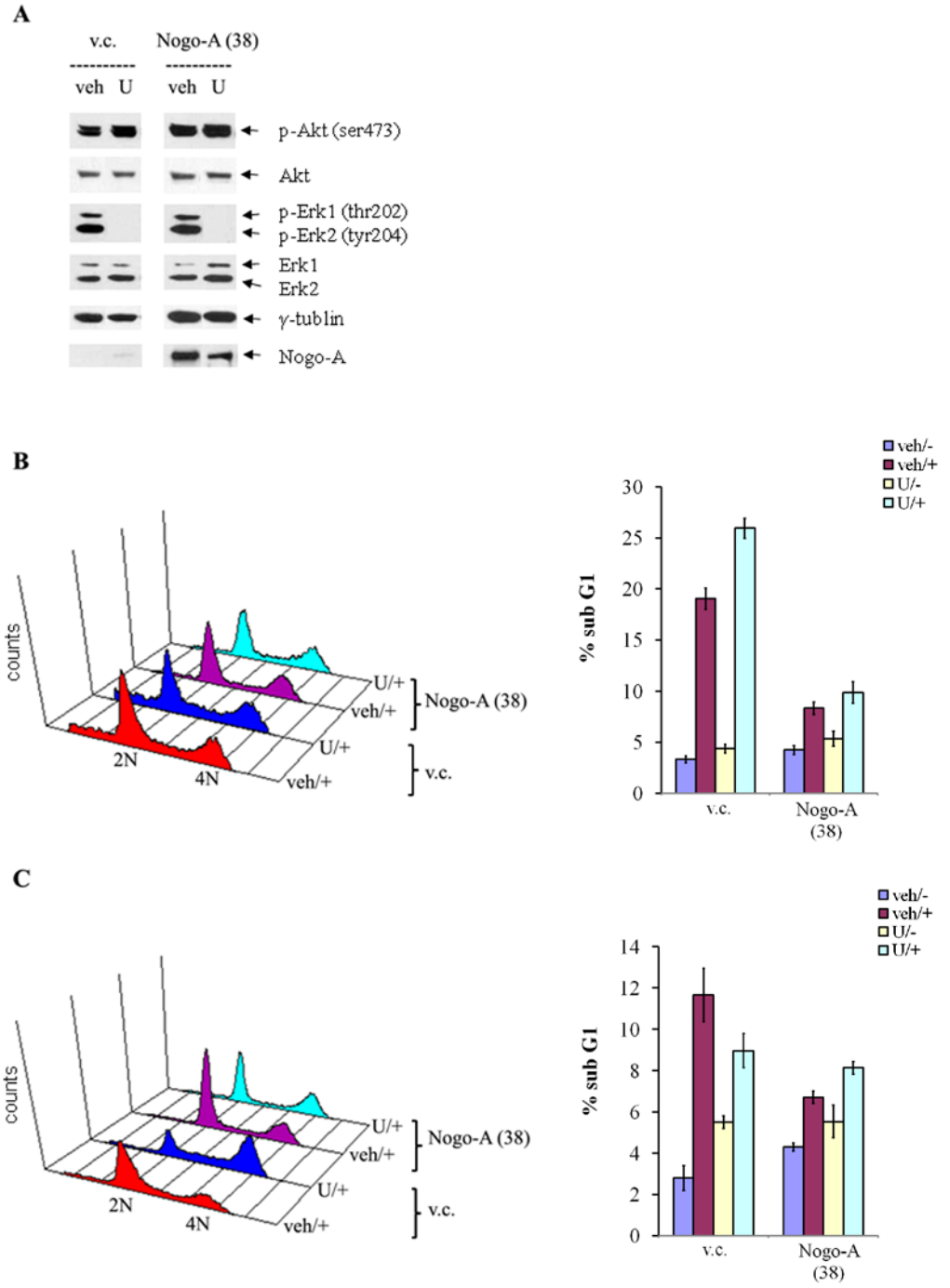

Fig 6.5 Inhibition of Erk did not enhance cell death in Nogo-A stable cells. ***(A)*** 50 µg of lysates from SH-SY5Y vector control (v.c.) and Nogo-A (38) pretreated with vehicle (veh) and U0126 (U) were resolved on a 8% SDS-PAGE gel and western blotted with antibodies against total and phosphorylated Akt, Erk1/2, γ-tubulin and Nogo-A. ***(B and C)*** Short-term (B) and long-term (C) inhibition of Erk. The histograms (left) were drawn using ModFit v2.9. Sub G1 populations of treated cells (right) were graphed as mean ± sd (n = 3).

6.3 Involvement of the mitochondria-associated intrinsic apoptotic pathway in Nogo-A's protective effect

The mitochondria are the key organelles that mediate the intrinsic apoptotic pathway. Oxidative stress has been reported to induce apoptosis in neuronal cells through the mitochondrial pathway, where ROS-induced cytochrome c release from the mitochondria, and the subsequent caspase-3 activation eventually led to apoptosis (Annunziato *et. al.*, 2003).

Investigations were carried out to understand if this compartment plays any role in modulating the protection by Nogo-A against cell death. Involvement of the extrinsic apoptotic pathway was not explored due to the fact that the caspases functioning in this pathway, caspases-8 and -10, were reported to be absent in SH-SY5Y cells (Eggert *et. al.*, 2001).

6.3.1 Changes in the levels of mitochondrial death-associated proteins with Nogo isoforms and RTN3 expression

Many proteins have been implicated in the intrinsic apoptosis pathway, and the Bcl-2 family of proteins features prominently in this regard. Members of this family have well-documented roles in apoptosis at the mitochondria, either enhancing (pro-apoptotic) or preventing (anti-apoptotic) cell death.

To find out if overexpression of Nogo isoforms and RTN3 have altered the basal expression status of these proteins and thereby influencing cell survival, the expression levels of the Bcl-2 family proteins were examined by western blot in the stable cell-lines (Fig 6.6). Levels of the anti-apoptotic Bcl-2 and Bcl-xL proteins were not significantly different between the vector control cells and those overexpressing Nogo-A, -B, -C and RTN3. Interestingly, the levels of total and activated pro-

apoptotic Bax were upregulated to a significant extent in cells stably expressing Nogo-A, -B and RTN3. Nogo-C stable cells, however, had an expression level similar to the vector control cells. The levels of another known pro-apoptotic protein, Bid, was also examined. Truncated Bid (tBid), the cleaved product of full-length Bid, is known to translocate to the mitochondrion to induce apoptosis. Bid seemed to be cleaved to a moderately lower extent in all Nogo isoform and RTN3 stable cells compared to the vector control cells.

In addition, another pro-apoptotic factor, the apoptosis inducing factor (AIF), which is released from the mitochondrion to induce cell death, was investigated. The Nogo isoform and RTN3 expressing cells appeared to have moderately lower AIF levels compared to vector control ones (Fig 6.6).

As Bax activation is a general determining step in the induction of apoptosis via the intrinsic pathway, the increased levels of activated and total Bax in Nogo-A, -B and RTN3 expressing cells suggested that these cells should have intrinsically higher levels of cell death. Indeed, the levels of activated caspase-3 in these cells were higher than vector control and Nogo-C ones (Fig 6.7), with RTN3 cells having the highest level, followed by the Nogo-B and the Nogo-A cells. Notably, the activated caspase-3 levels correlated with the higher basal sub G1 population in untreated Nogo-B and RTN3 cells, as shown in chapter 5.

As the Nogo isoform and RTN3 expressing cells are in general more resistant to apoptotic insults, their elevated basal levels of activated Bax and caspase-3, may, at the first glance, appear counterintuitive. However, as we shall discuss later, this may suggest a case of preconditioning that could help explain why these cells are more resistant to apoptotic insults.

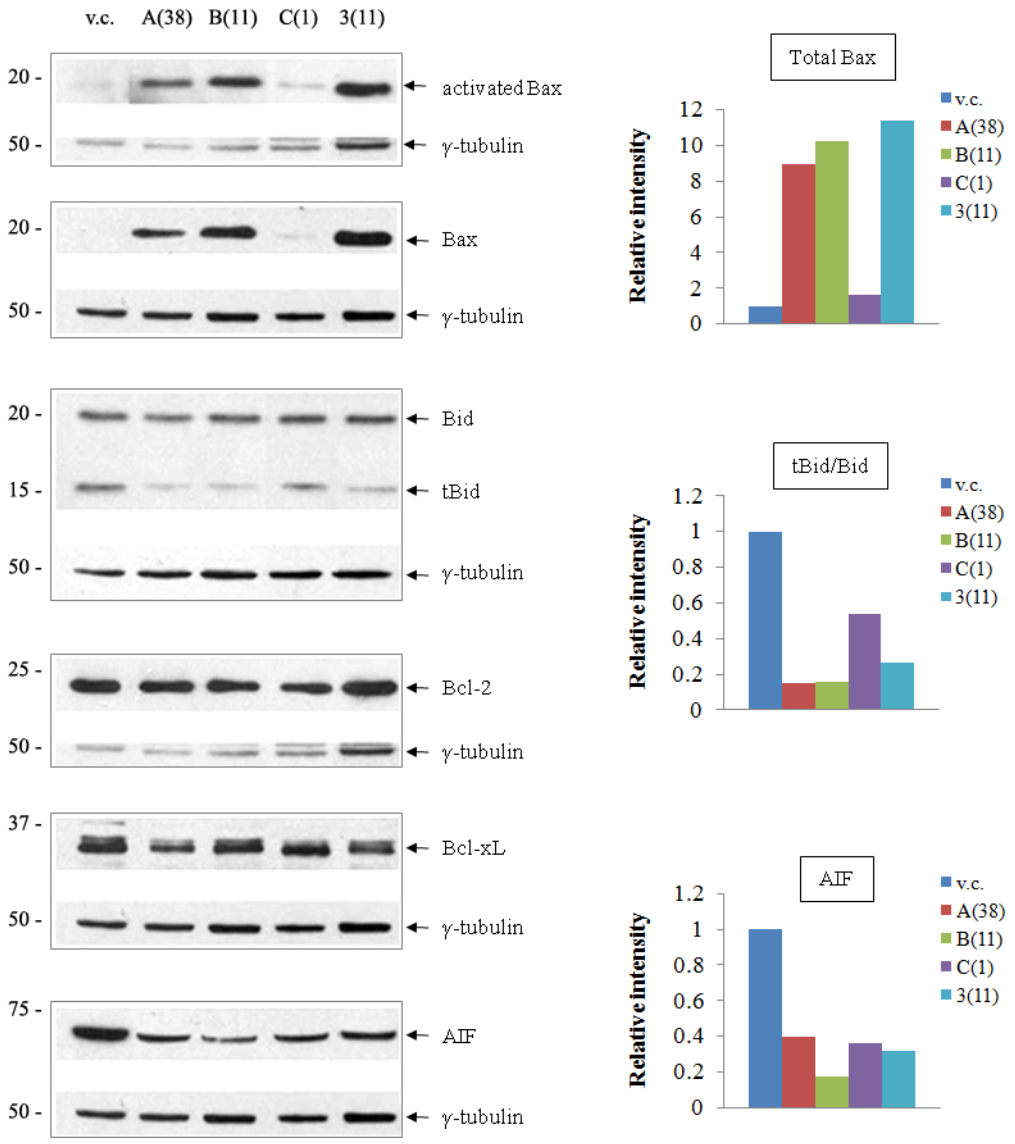

Fig 6.6 Expression levels of Bcl-2 family proteins and AIF in SH-SY5Y stable cell-lines. 50 µg of lysates from SH-SY5Y vector control (v.c.), Nogo-A (A(38)), -B (B(11)), -C (C(1)) and RTN3 (3(11)) were resolved on 12-15% SDS-PAGE gels and western blotted with antibodies against the proteins indicated. (Left) Western blot results of the probed proteins in the stable cell-lines. (Right) Densitometric results of total Bax and AIF normalized against γ-tubulin, and truncated Bid normalized against total Bid.

6.3.2 Nogo-A and -B expression reduce H_2O_2-induced activation of caspase-3 and -9

In order to check if the intrinsic apoptosis pathway plays a role in H_2O_2 induction of cell death, the mode and kinetics of activation of caspases-3 and -9 were

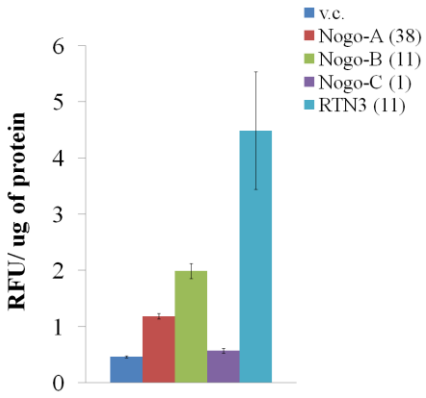

Fig 6.7 Intrinsic caspase-3 activation in SH-SY5Y stable cell-lines. Lysates of SH-SY5Y vector control (v.c.), Nogo-A (A(38)), -B (B(11)), -C (C(1)) and RTN3 (3(11)) were subjected to caspase-3 activation assay. The fluorescence signal generated due to the cleavage of caspase-3 substrate by activated caspase-3 in the lysates was measured and plotted as relative fluorescence units (RFU) per µg of protein.

investigated in the stable cell-lines. Caspase-9 is the initiator caspase responsible for the apoptosis triggered by the intrinsic pathway through cytochrome c release, while caspase-3 is downstream of caspase-9 and the major executioner caspase for caspase-dependent apoptotic cell death.

Cells were assayed for activated caspase-3 and -9 after being treated with H_2O_2 for 24 hr. In line with cell death assessed by sub G1 measurements, caspase-3 (Fig 6.8A) and -9 (Fig 6.8B) were shown to be activated faster and at significantly higher levels in vector control, Nogo-C and RTN3 cells when compared to Nogo-A and -B cells. Activation of caspases upon H_2O_2 treatment also confirmed that the cell death induced by H_2O_2 in the former three cell-lines was by apoptosis. The results, taken together, suggested that Nogo-A and -B may somehow act to inhibit the intrinsic apoptosis pathway, thereby attenuating the activation of caspase-9 and downstream caspase-3, and eventually protecting against apoptosis.

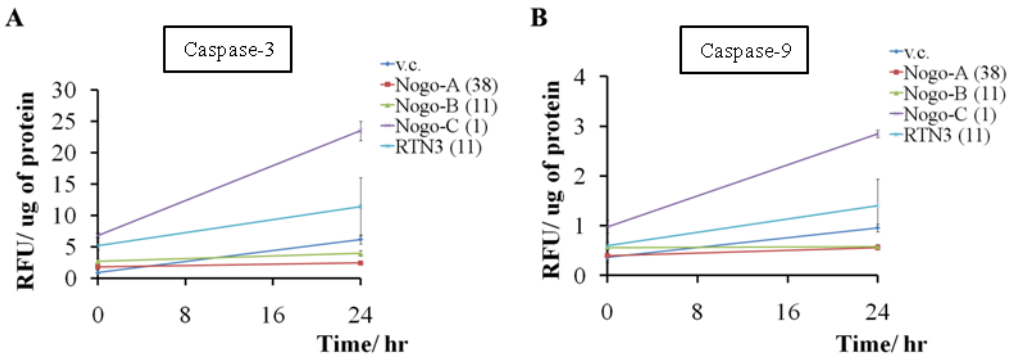

Fig 6.8 Activation of caspase-3 and -9 in SH-SY5Y stable cell-lines upon H_2O_2 treatment. Lysates of SH-SY5Y vector control (v.c.), Nogo-A (38), -B (11), -C (1) and RTN3 (11) treated with H_2O_2 were collected at 0 and 24 hr, and subjected to caspase-3 ***(A)*** and -9 ***(B)*** activation assays. The fluorescence signal generated due to the cleavage of caspase-3 and -9 substrates by respective activated caspases in the lysates was measured and plotted as relative fluorescence units (RFU) per µg of protein.

6.4 The role of the unfolded protein response (UPR) or ER stress response in Nogo-A's protective function

The ER can also induce cell death upon ER stress by activation of the UPR or ER overload response (EOR). To check if stable expression of the RTNs in SH-SY5Y activates the UPR pathway in the cells, lysates were checked for any upregulation of marker proteins of UPR such as GRP78 and GRP94. Both proteins are chaperones which are upregulated upon UPR induction to cope with the increased amount of unfolded proteins accumulating in ER. As shown in Fig 6.9A, there were no significant differences between the four cell-lines in their intrinsic basal levels of GRP78 and GRP94.

Despite an absence of a clearly elevated adaptive response to ER stress, it is still possible that Nogo-A could affect UPR activation in a manner that enhances survival of cells. To check this possibility, vector control and SH-SY5Y Nogo-A (38) cells were treated with H_2O_2 and checked for the extent and kinetics of UPR activation through immunoblot analysis for GRP78, GRP94, and the phosphorylation

of eIF2α at ser51 by protein kinase R-like ER kinase (PERK). As shown in Fig 6.9B, no significant induction of UPR was observed in either of the cells upon H_2O_2 treatment. The levels of phosphorylated eIF2α, GRP78 and GRP94 were not significantly elevated throughout the whole period investigated, even up to 48 hr for the two chaperones. Hence, it is unlikely that any UPR-based preconditioning or differential activation of UPR caused by Nogo-A expression could explain the protective effect of Nogo-A.

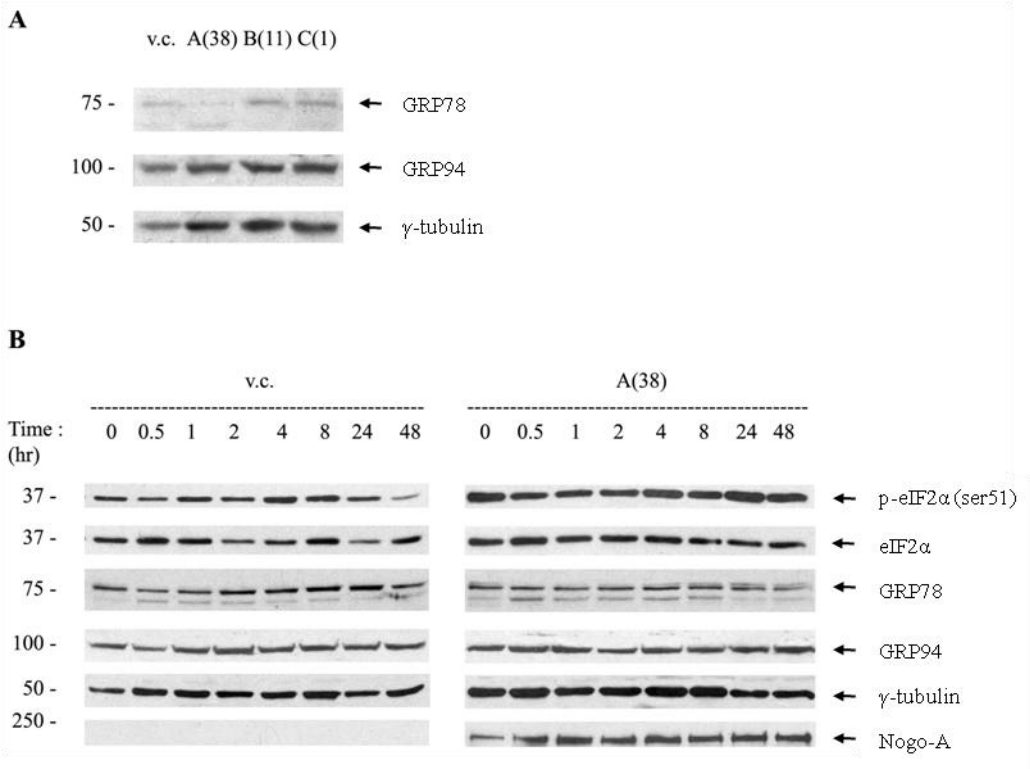

Fig 6.9 Activation of UPR in SH-SY5Y stable cell-lines. ***(A)*** 50 µg of lysates from untreated SH-SY5Y vector control (v.c.), Nogo-A (A(38)), -B (B(11)) and -C (C(1)) were resolved on 10% SDS-PAGE gels and western blotted with antibodies against the proteins indicated. ***(B)*** SH-SY5Y vector control (v.c.) and Nogo-A (A(38)) were treated with H_2O_2 before the lysates were obtained at the specified timepoints and then similarly processed as (A).

6.5 Investigations on changes in nuclear factor κB (NF-κB)

The role of nuclear factor κB (NF-κB) in apoptosis in response to H_2O_2 has been fairly controversial. It has been reported by different groups to be both cell death-inducing, or protective against cell death in SH-SY5Y cells. Nogo-B overexpression has been reported by others to induce activation of NF-kB (Kuang *et. al.*, 2006). This makes activation of the latter a possible mechanism underlying Nogo-A's protective effect. Hence, we sought to investigate if NF-κB plays any roles in Nogo-A's protection against H_2O_2. The predominant forms of NF-κB signalling network component in neurons, as well as SH-SY5Y cells, are p65/RelA and p50. We have therefore focused our investigations on p65/RelA.

6.5.1 Intrinsic differences of NF-κB p65 subunit in the stable cells

Activation of NF-kB pathway results in a translocation of the p65 subunit into the nucleus. Firstly, an assessment of the basal levels of p65 in the total, cytosolic and nuclear fractions was carried out (Fig 6.10). Poly (ADP-ribose) polymerase (PARP) and Cu-Zn superoxide dismutase (SOD) were probed to check for the purity of the nuclear and cytosolic fractions respectively. Total p65 expressed in all cells were similar (Fig 6.10A). However, there seemed to be an increase in p65 levels in the nuclear fractions of the reticulon expressing cells as compared to vector control cells, while no differences were observed in the cytosolic fractions.

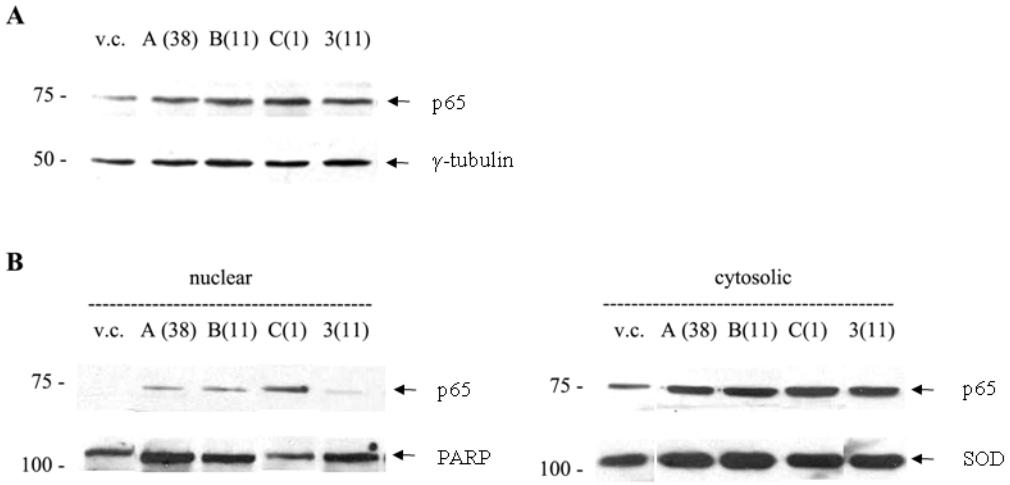

Fig 6.10 Expression levels of NF-κB p65 subunit in SH-SY5Y stable cell-lines. Total lysates (50 µg) ***(A)***, nuclear and cytosolic fractions (20 µg) ***(B)*** of SH-SY5Y vector control (v.c.), Nogo-A (A(38)), -B (B(11)), -C (C(1)) and RTN3 (3(11)) were resolved on 8% SDS-PAGE gels and western blotted with antibodies against the proteins as indicated.

6.5.2 NF-κB p65 nuclear translocation in SH-SY5Y cells induced by TNFα is affected by Nogo isoforms and RTN3 expression

NF-κB p65 subunit translocation and activation has been shown to be effectively induced by the cytokine tumor necrosis factor α (TNFα). To check if p65 translocation and nuclear accumulation in SH-SY5Y is affected by Nogo isoforms and RTN3, TNFα was used to stimulate the cell-lines and p65 translocation was examined by ICC.

As shown in Fig 6.11A, nuclear staining of p65 after 1 hr of TNFα stimulation was much more obvious in Nogo-A, -B and RTN3 stable cells than vector control or Nogo-C cells. In fact, translocation of p65 could be observed much earlier in Nogo-A, -B and RTN3 cells, with some nuclear staining already obvious after 30 min (data not shown). p65's nuclear staining peaked at about 2 hr before the basal pattern of distribution was resumed by 4 hr. There also seemed to be a sustained presence of p65 in the nucleus for some Nogo-A, -B and RTN3 cells at the later time-point.

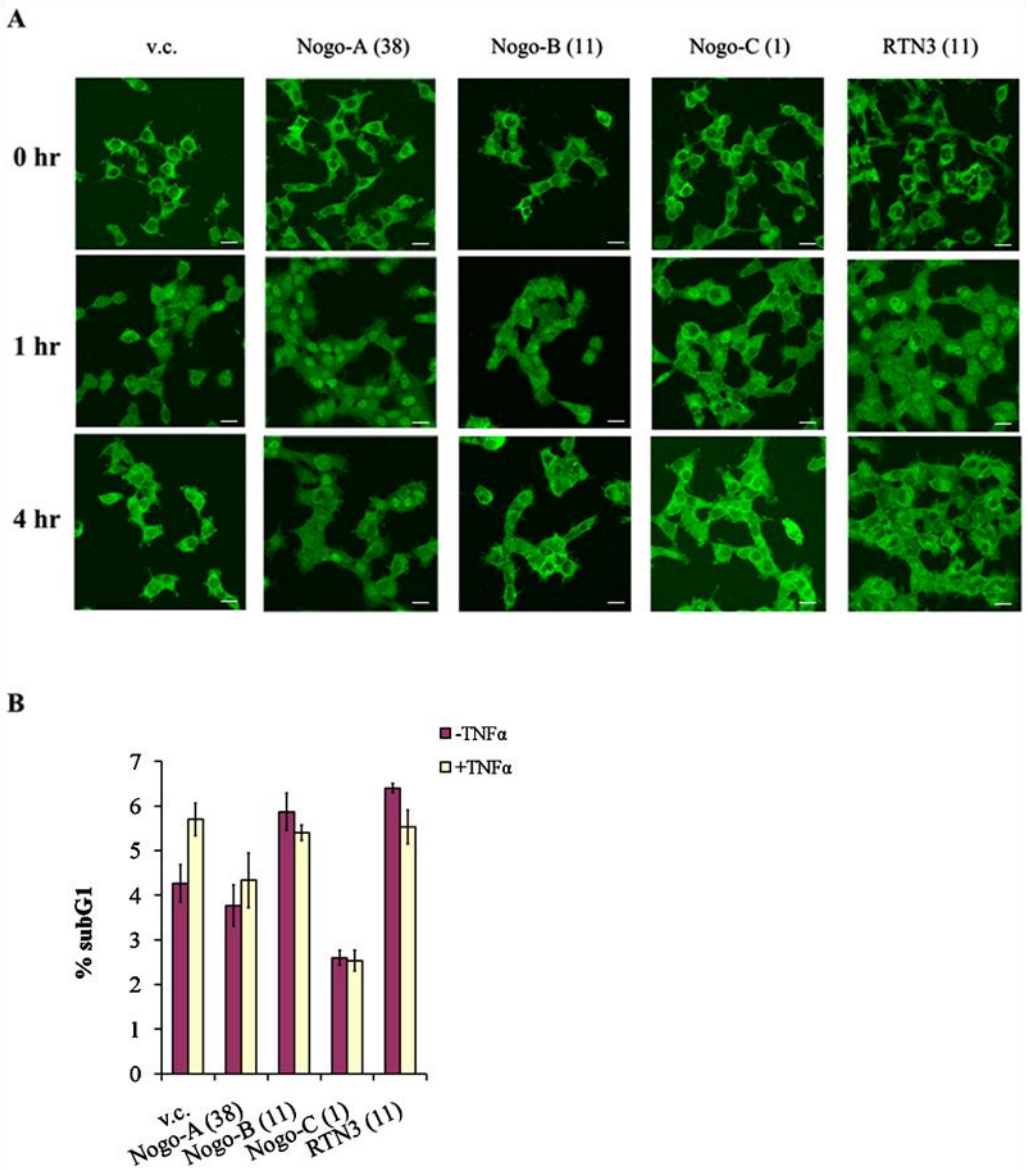

Fig 6.11 TNFα-induced NF-κB p65 subunit translocation in stable cell-lines did not lead to cell death. ***(A)*** SH-SY5Y vector control (v.c.), Nogo-A (38), -B (11), -C (1) and RTN3 (11) cells were treated with TNFα and fixed at 0, 1 and 4 hr with 4% PF and permeabilized with 0.2% Tx-100/PBS. They were then incubated with anti-NF-kB p65 antibodies, followed by FITC-conjugated secondary antibodies. Bar = 20 µm. ***(B)*** Flow cytometry analysis of stable cells left untreated (-TNFα) or treated with TNFα (+TNFα) for 24 hr. % of sub G1 population was as shown in the graph (mean ± sd, n = 3).

To examine if the observed p65 translocation induced by TNFα would affect cell survival, TNFα-treated cells were subjected to flow cytometry analysis (Fig 6.11B). No significant differences in their sub G1 population were observed after 24 hr of treatment with TNFα.

6.5.3 Translocation of NF-κB p65 subunit upon stimulation with H_2O_2

We next investigated whether the extent of H_2O_2-induced p65 cytoplasmic-nuclear translocation in the SH-SY5Y cell lines were different. Cells were treated with H_2O_2 and checked for p65 translocation by ICC. Interestingly, there was no observable nuclear accumulation of p65 in vector control cells at all. However, a good percentage of Nogo-A, -B and RTN3 stable cells exhibited p65 staining in the nucleus, beginning at about 90 min and obvious at about 3 hr (Fig 6.12). On the other hand, Nogo-C cells behaved like vector control cells and did not show any nuclear accumulation of p65.

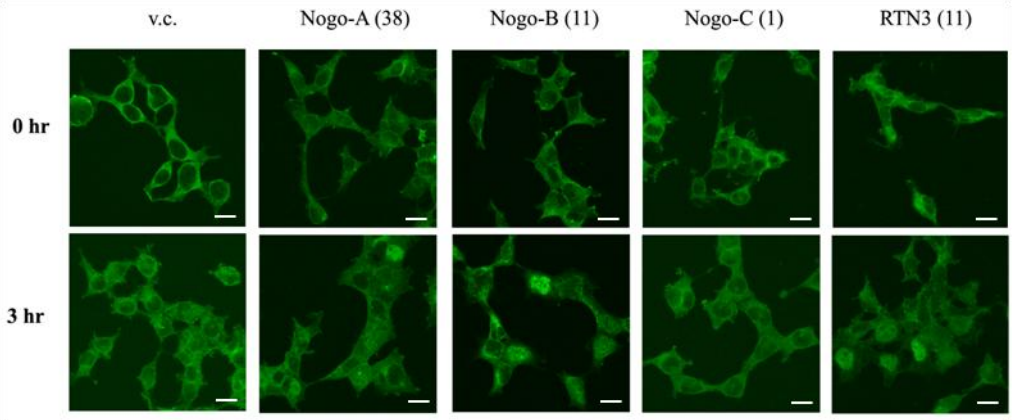

Fig 6.12 NF-κB p65 subunit translocation in stable cell-lines upon H_2O_2 treatment. SH-SY5Y vector control (v.c.), Nogo-A (38), -B (11), -C (1) and RTN3 (11) cells were treated with H_2O_2 for 3 hr before fixation with 4% PF and permeabilized with 0.2% Tx-100/PBS. They were then incubated with anti- NF-kB p65 antibodies, followed by FITC-conjugated secondary antibodies. Bar = 20 μm.

These observations, taken as a whole, implied that Nogo/RTN3 expression could enhance nuclear translocation of p65 and NF-κB activation upon induction by both TNFα and H_2O_2. As p65 is a mediator of canonical NF-κB signalling that could activate the transcription of pro-survival genes, this may partly explain why Nogo-A is protective.

6.6 Discussion – mechanisms involved in Nogo-A's protection against H_2O_2-induced cell death

From the data presented above, the N-terminus common to Nogo-A and -B was important in protecting SH-SY5Y cells against H_2O_2-induced cell death. However, this domain alone (aa 1-200) or a Nogo-B protein truncated after TM1 (N-TM1) had no protective effect. This implied that the RHD played a supportive role for the N-terminus in preventing H_2O_2-induced cell death. It is unclear in this regard whether the RHD simply provides membrane anchorage and topological orientation for the protective function of the N-terminal region to be manifested, or the RHD domain itself has a direct accessory role. More insights await the identification of molecules that interact with these domains.

Activation of classical pro-survival Akt and Erk signalling pathways were found not to be involved in Nogo-A's protection against H_2O_2. There were also no upregulation of anti-apoptotic proteins such as Bcl-2 and Bcl-xL in the stable cell-lines. However, two pro-apoptotic molecules, truncated Bid and AIF, were found to be downregulated in all stable cell-lines. This might provide a partial explanation for an intrinsically enhanced resistance to apoptosis. Interestingly, there were significantly higher levels of total and activated Bax in Nogo-A,-B and RTN3 stable cells, but not in Nogo-C cells. Bax activation levels correlated with the basal amounts of activated caspase-3 in untreated cells. The sub G1 population in untreated Nogo-B and RTN3 cells were also higher than the rest. As shall be elaborated in chapter 7, the elevated basal levels of activated Bax and caspase-3 may reflect a preconditioned state that these cells are in. This may, in turn, allow the cells more tolerance against apoptotic insults.

Activation of caspase-3 and -9 upon treatment with H_2O_2, which implied that apoptosis was mediated by the intrinsic pathway, was found to occur in vector control, Nogo-C and RTN3 stable cells but not in Nogo-A and -B stable cells. This finding suggested that Nogo-A and -B may effect their protection by somehow attenuating the intrinsic apoptotic pathway.

A clear adaptive response to ER stress induced by overexpression of RTNs was not observed in the cells. This mildly contrasted the report of others (Kuang *et. al.*, 2006; Wan *et. al.*, 2007) that reticulon expression may induce significant amount of ER stress. One reason for this could be because of the moderate level of transgene expression in our stable cells. Although clear elevation of the protective GRP78 and GRP94 were not observed, Nogo-A expressing cells may still be in some way preconditioned or primed. One evidence for this is that ER stress induced by tunicamycin heightened their death over vector control cells.

Nogo-A, -B and RTN3 cell-lines exhibited moderately higher levels of NF-κB p65 subunit in the nucleus. H_2O_2 induction of p65 translocation occurred in Nogo-A, -B and RTN3 stable cells, but not in Nogo-C. Notably, Nogo-A, -B and RTN3 were able to activate p65 translocation faster and cause more complete nuclear translocation during TNFα stimulation and H_2O_2 treatment than Nogo-C. The nuclear translocation of p65 was also sustained longer in these three cells. More efficient activation of NF-κB-mediated transcription of pro-survival genes may therefore play a part in the protective activity of Nogo-A, -B and RTN3.

Although these investigations did not provide an exclusive explanation as to how Nogo-A protected SH-SY5Y against H_2O_2, some hints to the possible mechanisms were obtained. These are further discussed in the next chapter.

Chapter 7 Discussions and Conclusions

7.1 Localization of Nogo-A in CNS

Our Nogo-A specific antibodies generated were able to detect ER and plasma membrane staining of endogenous Nogo-A within cells, and demonstrate its enrichment in adult CNS tissues. As Nogo is first identified from myelin extracts, it is assumed to be perhaps an exclusively myelin-associated protein. Contrary to what one may assume, Nogo-A expression appears to be rather widespread, and not limited to the myelin or white matter tracts. It was detected in the cerebral cortex, cerebellum, hippocampus and spinal cord, where it also labelled neuronal cell bodies.

Expression of Nogo-A was also shown to be present in the developing rat brain from embryonic stage (E18) to adulthood. Although we did not check the developmental stages before E18, where neurogenesis began, we did show that differentiating cortical neurons in culture expressed Nogo-A. Nogo-A was indeed observed to be present during neurogenesis in chick early embryos (O'Neill *et. al.*, 2004). Together with others' results, this suggests either a role for Nogo-A in the differentiation of neurons, or simply a bystander, but not likely as an inhibitor of neurite outgrowth during this period.

Nogo-A was found to be localized in the oligodendrocytes and neurons, but not astrocytes. Liu *et. al.* (2002) had additionally showed Nogo-A's expression excluded from microglia. Indeed, the expression of Nogo-A in oligodendrocytes fitted its classically perceived role as a myelin-associated inhibitor of neuronal regeneration. The role of neuronal Nogo-A has been mystifying though, as it is counter intuitive that a neuron should express a molecule that would inhibit its regeneration. O'neill *et. al.* (2004) has showed that neuronal Nogo-A expression was downregulated upon

onset of myelination, and this could probably explained the ability of oligodendroglial Nogo-A to exert its neurite growth inhibitory function. Neuronal Nogo-A may function, as suggested, as an axonal guidance molecule during embryonic development, and a restrictor of aberrant neurite growth in the adult CNS (Yiu and He, 2006). An important point to note here is that Nogo-A acting *in trans* (ie. Nogo-A from oligodendrocyte membranes acting on neurons) is likely to be different from Nogo-A acting *in cis* (ie. Nogo-A on the neuronal membrane itself, performing a cell-autonomous activity).

In addition to Nogo-A expression in CNS, it is noteworthy that Nogo-A is also expressed, albeit at much lower levels, in the heart. The pathophysiological significance of Nogo-A in the heart was demonstrated by its upregulation in an animal model of heart failure, with a concomitant reduction in Nogo-B and Nogo-C levels. The changes in levels were normalized in a rescue model (Bullard *et. al.*, 2008). The N-terminus common to Nogo-A and -B could promote endothelial cell migration, while inhibiting that of vascular smooth muscle cells (Acevedo *et. al.*, 2004). In this connection, a role in regulating vascular remodelling has been implicated at least for Nogo-B (Acevedo *et. al.*, 2004).

7.2 Enrichment of Nogo-A at the paranode and its interaction with Caspr

Interestingly, Nogo-A was found to be enriched in the paranodal region of the node of Ranvier. We, in collaboration with others, have determined by electron microscopy that Nogo-A was present in the myelin sheath of oligodendrocytes rather than the neurons themselves (Nie *et al.*, 2003). We showed in chapter 4 that Nogo-A interacted with the paranodal protein Caspr. The Nogo-A domain which interacts with Caspr is essentially Nogo-66, the region postulated to be extracellularly oriented.

Interaction between Nogo-66 and Caspr was specific, as Nogo-66 was found not to bind to another paralogue, Caspr2. Shorter, truncated forms of Nogo-66, Nogo-35 and -40, were unable to pull-down Caspr in GST pull-down assays. The advent of Caspr expression in rat brain only after P4 meant that the Nogo-A-Caspr interaction may only have a functional role after this developmental stage.

Although interesting, the role of Nogo-A-Caspr interaction has remained unclear. Caspr has been widely known for its essential role in the formation and stabilization of the paranodal axoglial junction. It functions by forming a complex with the neuronal protein contactin/F3 on the axolemma and interacts with NF 155 on the oligodendroglial membrane (Charles *et. al.*, 2002). Caspr also interacts with the cytoskeletal adaptor protein 4.1B to effectively generate a membrane barrier at the paranodal junction, such that distinct subregions are formed at the node, paranode and juxtaparanode (Horresh *et. al.*, 2010). As such, the interaction of Nogo-A with Caspr was hypothesized to play a role related to this function of Caspr. Our collaborators (Nie *et al.*, 2003) had actually explored this possibility by using demyelinating EAE rat and *Shiverer* mouse models. They found that in these animal models, Nogo-A's clustering at the paranode was barely detectable. They also observed that the K^+ channels were not only localized at the juxtaparanodes but also colocalizing with Caspr at the paranodes. Hence, they postulated that the absence of Nogo-A at the paranode in these demyelinating animals may have caused the architecture at the node to be disorganized due to a lack of interaction between Nogo-A and Caspr. As demyelination leads to all glial molecules localizing at the axon-glial junction to be absent, including NF155 that is known for stabilising the axon-glial junctions and necessary for the organization of the architecture at the node, a conclusive answer of whether Nogo-A is essential in this function could not be deduced. With the

availability of our Nogo-deficient mice, we ventured to investigate this hypothesis by comparing these mice with wild type mice. Our results, however, implied that Nogo-A did not have an essential role in the architecture organization at the node of Ranvier. The spatial placement of Caspr and K^+ channels at the paranodes and juxtaparanodes respectively were unaffected in the spinal cord of Nogo-deficient mice. It is still possible that Nogo-A functions in supporting or organizing the structures at the paranodal junction, but in a redundant manner.

Interestingly, a recent report has demonstrated that Caspr was inhibitory to neurite outgrowth (Devanathan *et. al.*, 2010). Cerebellar neurons from $Caspr^{-/-}$ mice exhibited longer neurites than wild type ones. It was suggested that neuronal Caspr could bind to some extracellular ligands and activate intracellular signalling pathways that led to neurite outgrowth inhibition. Can Caspr be a novel inhibitory receptor for Nogo-A to elicit its inhibitory signals to the neurons? This hypothesis would need further validation.

7.3 Interaction of Nogo-A with RTN3

The earlier discovered RTNs have been known to interact and form dimers or complexes with one another (Senden *et. al.*, 1994). Interaction between Nogo-B and RTN3 has been reported (Qi *et. al.*, 2000). Nogo-B is more ubiquitous in its expression, with no enrichment in neurons, while RTN3 is brain-enriched. We hypothesized that a more physiological relevant RTN partner for RTN3 in the CNS neurons would be Nogo-A, and endeavoured to check the interaction between the two. Nogo-A could indeed be co-immunoprecipitated with RTN3 reciprocally. An interesting point to note from our findings was that Nogo-A was able to bind to RTN3 much better than to RTN1 or 2. Our molecular dissection showed that the interaction

between Nogo-A and RTN3 requires at least one of the TM domains. The absence of one TM domain caused a reduction in interaction. A complete abolishment of interaction was observed when one of the proteins had both TM domains removed. These results suggested that Nogo-A-RTN3 interaction occurred only in a membrane-associated context.

Several cellular roles have been postulated for RTN3. Binding of Nogo-A to RTN3 may have an effect on the latter's ability to carry out its functions. Shaping of the ER tubular structure required oligomerization of RTNs and complexing with DP1 (Voeltz *et. al.*, 2006). RTN3 has also been shown to regulate membrane trafficking between the ER and Golgi (Wakana *et. al.*, 2005). Nogo-A may interact with RTN3 to function in these aspects. In our experience, however, transient expression of Nogo-A at moderately high levels did not significantly affect the markers of organelles of the secretory pathway (data not shown).

Another possibly relevant function of Nogo-A-RTN3 interaction is CNS specific. RTN3 was known to interact with the APP processing β-secretase BACE1, thereby reducing its enzymatic activity and decreasing Aβ generation (He *et. al.*, 2004). Nogo-B and -C were also identified as potential binding partners of BACE1 and that they could similarly decrease Aβ generation (Murayama *et. al.*, 2006). The fact that BACE1 preferred binding to monomeric RTN3 suggested the importance of oligomerization of RTNs in this aspect (He *et. al.*, 2006). Preliminary results have shown that Nogo-A did not interact with BACE1 directly (data not shown). Hence, whether Nogo-A's binding to RTN3 would indirectly interfere with BACE1's cleavage of APP thereby affecting Aβ generation remains to be investigated. A role for RTN3 in the membrane transport of neurite outgrowth promoting molecules, synaptic adhesion-like molecules (SALMs), via their interaction was also suggested

recently (Chang *et. al.*, 2010). More work is required to properly delineate Nogo-A's influence on the said functions and activities of RTN3.

7.4 Neuroprotection by Nogo-A and the possible mechanisms involved

The upregulation of Nogo-A levels in neurons in models of CNS injury have prompted us to consider the possibility of Nogo-A having some neuroprotective activity. We have therefore explored the neuroprotective role of Nogo-A against various drugs/treatments that induce apoptosis in SH-SY5Y neuroblastoma cells. We found that protection by Nogo-A could be extended to a variety of apoptosis-inducing methods, including growth factor withdrawal, DNA damage, and oxidative stress, except for ER stress (see below).

The protection effect that we have seen could be classified into three types. The first is where all Nogo isoforms and RTN3 were protective, and these included cell death induced by serum withdrawal and staurosporine treatment. The second is where Nogo-A, -B and RTN3's effects were similar, but not Nogo-C. The difference could lie in the fact that Nogo-C has a shorter N-terminus (only 11 aa). The Nogo-A, -B and RTN3 expressing cells were protected against etoposide but exhibited enhanced cell death with tunicamycin treatment. The third type is the effect against H_2O_2, where only Nogo-A and -B were able to render protection to the cells. The different protection effects observed suggested that the mechanisms activated by Nogo-A and the other RTNs to enable protection may be rather complex to begin with.

The N-terminus of Nogo-A/B was found to play an essential part in protecting cells against H_2O_2, with supporting roles from the RHD domain. As shown, protection was abolished with Nogo-B truncated proteins containing only the N-terminus region (1-200) or truncated after TM1 (N-TM1). Although (1-200) was cytosolic, (N-TM1)

was apparently still ER-associated (data not shown). Therefore, the loss of protective effect by the above mutants may not be simply due to a loss of membrane attachment. It could, at least in part, result from the loss of efficient dimerization/ oligomerization.

To further uncover the mechanisms underlying the protective effect, we explored several possibilities. Firstly, whether classical Akt and Erk survival pathways were activated by Nogo-A was scrutinized. Inhibition of both Akt and Erk did not lead to an increase in cell death in Nogo-A expressing cells after H_2O_2 treatment. Therefore, these survival proteins were not essential for Nogo-A's protective function. A check on proteins acting in the intrinsic apoptotic pathway showed that the two anti-apoptotic proteins, Bcl-2 and Bcl-xL, were not intrinsically upregulated in Nogo-A cells. Truncated Bid and AIF were however shown to be downregulated in all the RTN expressing cells. Interestingly, total and activated Bax were present at significantly higher levels in Nogo-A, -B and RTN3 cells but not vector control or Nogo-C cells. Basal caspase-3 activity was also higher in these cells.

This apparent increase in basal activated Bax and caspase-3 activity may theoretically sensitize the cells to apoptotic insults. However, as we have seen, this is not the case, and the cells are actually more tolerant. Alternatively, the increased basal levels of Bax and caspase-3 could "precondition" the cells against a more severe insult by heightening the cells' survival response time and/or intensity. Although more evidence is required to firmly support this notion, we believe this may provide some explanation for the protective effect. In fact, the phenomenon of preconditioning in terms of neuronal death is widely known in experimental and pathophysiological contexts. Ischemic preconditioning, for example, refers to the observation that a mild and transient ischemic event could protect against neuronal demise induced by a more severe subsequent episode of ischemia. Ischemic preconditioning is equally applicable

to the heart. In a particularly interesting case of neuronal death preconditioning, lesioning of the peripheral branch of the dorsal root ganglion could protect the CNS branch of the neuron from subsequent lesioning (Fiblin, 2003).

It was also found that activation of caspase-3 and -9 were induced in H_2O_2-treated vector control, Nogo-C and RTN3 cells, which correlated with cell death, while Nogo-A and -B did not. This has strong implications for Nogo-A and -B to exert their protective functions by attenuating the activation of the intrinsic apoptotic pathway, thereby preventing subsequent caspase-dependent apoptosis.

Likewise, overexpression of RTNs has been proposed by others to induce ER stress by the activation of both UPR and EOR and hence apoptosis (Kuang *et. al.*, 2006**;** Wan *et. al.*, 2007). In our stable cells moderately overexpressing Nogo-A, -B, -C or RTN3, however, signs of any UPR induction were not obvious. There was no significant upregulation of the ER stress response molecular chaperones, GRP78 and GRP94. ER stress preconditioning has been suggested to have a protective function (Rutkowski *et. al.*, 2006), but prolonged ER stress would also lead to apoptosis. No significant induction of UPR was observed in either the vector control or Nogo-A expressing cells after being treated with H_2O_2. There was no obvious elevation in the levels of PERK-mediated phosphorylated eIF2α, GRP78 and GRP94, even up to a timepoint of 48 hr. This shows that H_2O_2 is unable to induce UPR in the SH-SY5Y stable cells. The results also suggest that any UPR-based preconditioning is unlikely to account for Nogo-A's protection. An interesting point to note is the fact that apoptosis induced by tunicamycin, a classical activator of ER stress, is exacerbated in Nogo-A, -B and RTN3 expressing cells. It is possible that expression of these constructs have enhanced the degree of ER stress by tunicamycin to the point such that the cells are tipped towards death rather than being preconditioned for survival.

As NF-κB plays an important role in neuronal survival, we sought to investigate its possible involvement in Nogo-A's protective function. All Nogo isoforms and RTN3 expressing cells seemed to have higher amount of the protein in the nucleus. It has been previously reported that Nogo-B overexpression could lead to an activation of NF-κB as a result of EOR induction (Kuang *et. al.*, 2006). Hence, we suspect that the increased NF-κB activation observed in the Nogo isoforms and RTN3 expressing cells is caused by an induction of EOR due to the stable expression of the RTNs. The expression of these proteins, with the exception of Nogo-C, also apparently enhanced p65 nuclear translocation induced by TNFα and H_2O_2. As the role of NF-κB in apoptosis has been controversial, the higher p65 levels in the nucleus could not conclusively indicate that the cells were protected via this mechanism. However, p65 translocation upon TNFα stimulation did not lead to apoptosis in SH-SY5Y.Taken together, our results suggested that enhanced p65 nuclear translocation may be part of the explanation for the protective effects seen. Our results were corroborated by a recent report which also implied that Nogo-A could have protective functions (Kilic *et. al.*, 2010). Nogo-$A^{-/-}$ mice exhibited decreased neuronal survival after focal cerebral ischemia. The authors suggested that Nogo-A maintained a low level of stress kinases p38/MAPK, SAPK/JNK1/2 and phosphatase-and-tensin homolog (PTEN) via RhoA activation, thereby promoting neuronal survival.

Our results have thus strengthened the notion of the role of Nogo-A in neuroprotection. Although our investigations could not pinpoint an exclusive mechanism to account for Nogo-A's protective activity, we think that elevated expression of Nogo-A in neurons likely affects several pro-survival pathways. These would include some form of preconditioning either through mitochondrial or ER-

stress associated factors, as well as sensitization of the cell to processes such as NF-κB translocation (Fig 7.1).

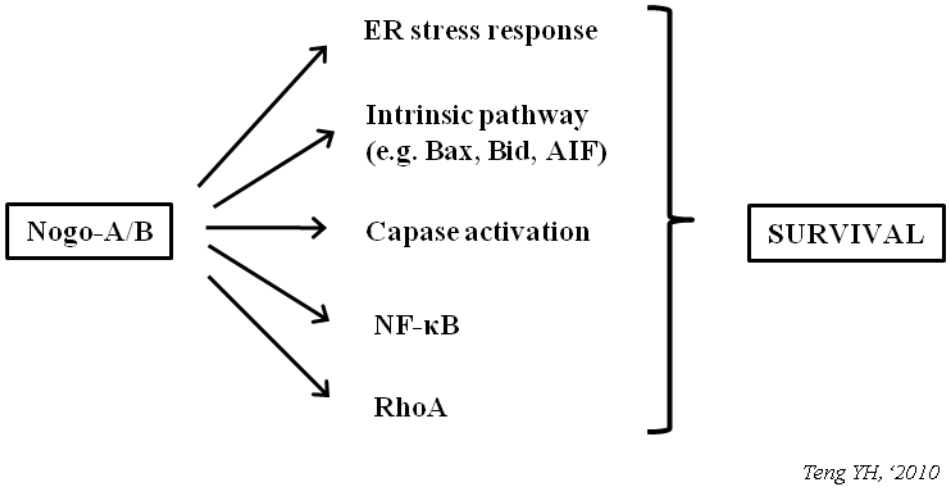

Fig 7.1 Possible mechanisms induced by Nogo-A and -B leading to survival. Several signalling pathways may be involved and work in concert in the protection against cell death rendered by Nogo-A and -B. These include induction and/or preconditioning of the ER stress response, inhibition of intrinsic apoptotic pathway, preconditioning by Bax and caspase-3, and activation of NF-κB. RhoA activation has also been shown to aid in survival conferred by Nogo-A (Kilic *et. al.*, 2010).

7.5 Concluding remarks

We have investigated Nogo-A in terms of cellular and tissue localization, interacting partners and its potential neuroprotective function. Much has been known about Nogo-A as an inhibitor of neurite outgrowth, but its cell autonomous function is basically unknown. Our investigations have therefore provided some insights on the other possible roles that Nogo-A may possess. Continuing the investigations of the mechanism underlying Nogo-A's neuroprotective activity would be an important pursuit in the immediate future. Our results may have also some important translational implications. They caution that any Nogo-directed interventions to enhance regeneration should aim to specifically disrupt Nogo-A's interactions that would transduce neurite growth inhibitory signals, but not its complete silencing or

deletion. The latter approach would likely deprive the neurons of Nogo-A's protective activity, and be contraindicative on the whole.

Chapter 8 Bibliography

Acevedo L., Yu J., Erdjument-Bromage H., Miao R.Q., Kim J.E., Fulton D., Tempst P., Strittmatter S.M. and Sessa W.C. (2004) A new role for Nogo as a regulator of vascular remodeling. Nat. Med., 10: 382-8.

Ahmed Z., Mazibrada G., Seabright R.J., Dent R.G., Berry M. and Logan A. (2006) TACE-induced cleavage of NgR and p75NTR in dorsal root ganglion cultures disinhibits outgrowth and promotes branching of neurites in the presence of inhibitory CNS myelin. FASEB J., 20: 1939-41.

Annunziato L., Amoroso S., Pannaccione A., Cataldi M., Pignataro G., D'Alessio A., Sirabella R., Secondo A., Sibaud L. and Di Renzo G.F. (2003) Apoptosis induced in neuronal cells by oxidative stress: role played by caspases and intracellular calcium ions. Toxicol. Lett., 139: 125-33.

Asher R.A., Morgenstern D.A., Moon L.D. and Fawcett J.W. (2001) Chondroitin sulphate proteoglycans: inhibitory components of the glial scar. Prog. Brain Res., 132: 611-9.

Atwal J.K., Pinkston-Gosse J., Syken J., Stawicki S., Wu Y., Shatz C. and Tessier-Lavigne M. (2008) PirB is a functional receptor for myelin inhibitors of axonal regeneration. Science, 322: 967-70.

Bandtlow C.E. (2003) Regeneration in the central nervous system. Exp. Gerontol., 38: 79-86.

Bandtlow C.E., Dlaska M., Pirker S., Czech T., Baumgartner C. and Sperk G. (2004) Increased expression of Nogo-A in hippocampal neurons of patients with temporal lobe epilepsy. Eur. J. Neurosci., 20: 195-206.

Barton W.A., Liu B.P., Tzvetkova D., Jeffrey P.D., Fournier A.E., Sah D., Cate R., Strittmatter S.M. and Nikolov D.B. (2003) Structure and axon outgrowth inhibitor binding of the Nogo-66 receptor and related proteins. EMBO J., 22: 3291-302.

Bléry M., Kubagawa H., Chen C.C., Vély F., Cooper M.D. and Vivier E. (1998) The paired Ig-like receptor PIR-B is an inhibitory receptor that recruits the protein-tyrosine phosphatase SHP-1. Proc. Natl. Acad. Sci. USA, 95: 2446-51.

Bourquin C., van der Haar M.E., Anz D., Sandholzer N., Neumaier I., Endres S., Skerra A., Schwab M.E. and Linington C. (2008) DNA vaccination efficiently induces antibodies to Nogo-A and does not exacerbate experimental autoimmune encephalomyelitis. Eur. J. Pharmacol., 588: 99-105.

Bradbury E.J., Moon L.D.F., Popat R.J., King V.R., Bennett G.S., Patel P.N., Fawcett J.W. and McMahon S.B. (2002) Chondroitinase ABC promotes functional recovery after spinal cord injury. Nature, 416: 636-640.

Bregman B.S., Kunkel-Bagden E., Schnell L., Dai H.N., Gao D. and Schwab M.E. (1995) Recovery from spinal cord injury mediated by antibodies to neurite growth inhibitors. Nature, 378: 498-501.

Budel S., Padukkavidana T., Liu B.P., Feng Z., Hu F., Johnson S., Lauren J., Park J.H., McGee A.W., Liao J., Stillman A., Kim J.E., Yang B.Z., Sodi S., Gelernter J., Zhao H., Hisama F., Arnsten A.F. and Strittmatter S.M. (2008) Genetic variants of Nogo-66 receptor with possible association to schizophrenia block myelin inhibition of axon growth. J. Neurosci., 28: 13161-72.

Buffo A., Zagrebelsky M., Huber A.B., Skerra A., Schwab M.E., Strata P. and Rossi F. (2000) Application of neutralizing antibodies against NI-35/250 myelin-associated neurite growth inhibitory proteins to the adult rat cerebellum induces sprouting of uninjured purkinje cell axons. J. Neurosci., 20: 2275-86.

Bullard T.A., Protack T.L., Aguilar F., Bagwe S., Massey H.T. and Blaxall B.C. (2008) Identification of Nogo as a novel indicator of heart failure. Physiol. Genomics., 32: 182-9.

Caelers A., Monge A., Michael J., Schwab M.E. and Bodmer D. (2009) Nogo in the Mammalian cochlea. Otol. Neurotol., 30: 668-75.

Cafferty W.B., Duffy P., Huebner E. and Strittmatter S.M. (2010) MAG and OMgp synergize with Nogo-A to restrict axonal growth and neurological recovery after spinal cord trauma. J. Neurosci., 30: 6825-37.

Cai D., Shen Y., De Bellard M., Tang S. and Filbin M.T. (1999) Prior exposure to neurotrophins blocks inhibition of axonal regeneration by MAG and myelin via a cAMP-dependent mechanism. Neuron, 22: 89-101.

Caroni P. and Schwab M,E. (1988a) Two membrane protein fractions from rat central myelin with inhibitory properties for neurite growth and fibroblast spreading. J. Cell Biol., 106: 1281-8.

Caroni P. and Schwab M.E. (1988b) Antibody against myelin-associated inhibitor of neurite growth neutralizes nonpermissive substrate properties of CNS white matter. Neuron, 1: 85-96.

Chang K., Seabold G.K., Wang C.Y. and Wenthold R.J. (2010) Reticulon 3 is an interacting partner of the SALM family of adhesion molecules. J. Neurosci. Res., 88: 266-74.

Charles P., Tait S., Faivre-Sarrailh C., Barbin G., Gunn-Moore F., Denisenko-Nehrbass N., Guennoc A.M., Girault J.A., Brophy P.J. and Lubetzki C. (2002) Neurofascin is a glial receptor for the paranodin/Caspr-contactin axonal complex at the axoglial junction. Curr. Biol., 12: 217-20.

Chauvet N., Prieto M. and Alonso G. (1998) Tanycytes present in the adult rat mediobasal hypothalamus support the regeneration of monoaminergic axons. Exp. Neurol., 151**:** 1-13.

Chen M.S., Huber A.B., van der Haar M.E., Frank M., Schnell L., Spillmann A.A., Christ F. and Schwab M.E. (2000) Nogo-A is a myelin-associated neurite outgrowth inhibitor and an antigen for monoclonal antibody IN-1. Nature, 403: 434-9.

Chen Y., Tang X., Cao X., Chen H. and Zhang X. (2006) Human Nogo-C overexpression induces HEK293 cell apoptosis via a mechanism that involves JNK-c-Jun pathway. Biochem. Biophys. Res. Commun., 348: 923-8.

Chen Y.C., Lu D.D., Cao X.R. and Zhang X.R. (2005) RTN4-C gene expression in hepatocellular carcinoma and its influence on SMMC7721 cell growth and apoptosis. Yi Chuan Xue Bao, 32: 891-7.

Chen W., Gu N., Duan S., Sun Y., Zheng Y., Li C., Pan Y., Xu Y., Feng G. and He L.. (2004) No association between the genetic polymorphisms within RTN4 and schizophrenia in the Chinese population. Neurosci. Lett., 365: 23-7.

Cole S.L. and Vassar R. (2007) The Alzheimer's disease beta-secretase enzyme, BACE1. Mol. Neurodegener., 2: 22.

Covault J., Lee J., Jensen K. and Kranzler H. (2004) Nogo 3'-untranslated region CAA insertion: failure to replicate association with schizophrenia and demonstration of marked population difference in frequency of the insertion. Brain Res. Mol. Brain Res., 120: 197-200.

Crutcher K.A. (1989) Tissue sections from the mature rat brain and spinal cord as substrates for neurite outgrowth in vitro: extensive growth on gray matter but little growth on white matter. Exp. Neurol., 104: 39-54.

David S. and Aguayo A.J. (1981) Axonal elongation into peripheral nervous system "bridges" after central nervous system injury in adult rats. Science, 214: 931-933.

Dawson T.R., Lazarus M.D., Hetzer M.W. and Wente S.R. (2009) ER membrane-bending proteins are necessary for de novo nuclear pore formation. J. Cell Biol., 184: 659-75.

Deng K., Gao Y., Cao Z., Graziani E.I., Wood A., Doherty P. and Walsh F.S. (2010) Overcoming amino-Nogo-induced inhibition of cell spreading and neurite outgrowth by 12-O-tetradecanoylphorbol-13-acetate-type tumor promoters. J. Biol. Chem., 285: 6425-33.

Dergham P., Ellezam B., Essagian C., Avedissian H., Lubell W.D. and McKerracher L. (2002) Rho signaling pathway targeted to promote spinal cord repair. J. Neurosci., 22: 6570-7.

Devanathan V., Jakovcevski I., Santuccione A., Li S., Lee H.J., Peles E., Leshchyns'ka I., Sytnyk V. and Schachner M. (2010) Cellular form of prion protein inhibits Reelin-mediated shedding of Caspr from the neuronal cell surface to potentiate Caspr-mediated inhibition of neurite outgrowth. J. Neurosci., 30: 9292-305.

Di Sano F., Fazi B., Tufi R., Nardacci R. and Piacentini M. (2007) Reticulon-1C acts as a molecular switch between endoplasmic reticulum stress and genotoxic cell death pathway in human neuroblastoma cells. J. Neurochem., 102: 345-53.

Dimou L., Schnell L., Montani L., Duncan C., Simonen M., Schneider R., Liebscher T., Gullo M. and Schwab M.E. (2006) Nogo-A-deficient mice reveal strain-dependent differences in axonal regeneration. J. Neurosci., 26: 5591-603.

Dodd D.A., Niederoest B., Bloechlinger S., Dupuis L., Loeffler J.P. and Schwab M.E. (2005) Nogo-A, -B, and -C are found on the cell surface and interact together in many different cell types. J. Biol. Chem., 280: 12494-502.

Domeniconi M., Cao Z., Spencer T., Sivasankaran R., Wang K., Nikulina E., Kimura N., Cai H., Deng K., Gao Y., He Z. and Filbin M. (2002) Myelin-associated glycoprotein interacts with the Nogo66 receptor to inhibit neurite outgrowth. Neuron, 35: 283-90.

Domeniconi M., Zampieri N., Spencer T., Hilaire M., Mellado W., Chao M.V. and Filbin M.T. (2005) MAG induces regulated intramembrane proteolysis of the p75 neurotrophin receptor to inhibit neurite outgrowth. Neuron, 46: 849-55.

Dupuis L., Gonzalez de Aguilar J.L., di Scala F., Rene F., de Tapia M., Pradat P.F., Lacomblez L., Seihlan D., Prinjha R., Walsh F.S., Meininger V. and Loeffler J.P. (2002) Nogo provides a molecular marker for diagnosis of amyotrophic lateral sclerosis. Neurobiol. Dis., 10: 358-65.

Eggert A., Grotzer M.A., Zuzak T.J., Wiewrodt B.R., Ho R., Ikegaki N. and Brodeur G.M. (2001) Resistance to tumor necrosis factor-related apoptosis-inducing ligand (TRAIL)-induced apoptosis in neuroblastoma cells correlates with a loss of caspase-8 expression. Cancer Res., 61: 1314-9.

Emerick A.J. and Kartje G.L. (2004) Behavioral recovery and anatomical plasticity in adult rats after cortical lesion and treatment with monoclonal antibody IN-1. Behav. Brain Res., 152: 315-25.

Eslamboli A., Grundy R.I. and Irving E.A. (2006) Time-dependent increase in Nogo-A expression after focal cerebral ischemia in marmoset monkeys. Neurosci. Lett., 408: 89-93.

Faivre-Sarrailh C., Gauthier F., Denisenko-Nehrbass N., Le Bivic A., Rougon G. and Girault J.A. (2000) The glycosylphosphatidyl inositol-anchored adhesion molecule F3/contactin is required for surface transport of paranodin/contactin-associated protein (caspr). J. Cell Biol., 149: 491-502.

Fatokun A.A, Stone T.W. and Smith R.A. (2008) Oxidative stress in neurodegeneration and available means of protection. Front. Biosci., 13: 3288-311.

Faulkner J.R., Herrmann J.E., Woo M.J., Tansey K.E., Doan N.B. and Sofroniew M.W. (2004) Reactive astrocytes protect tissue and preserve function after spinal cord injury. J. Neurosci., 24: 2143–2155.

Fazi B., Melino S., De Rubeis S., Bagni C., Paci M., Piacentini M. and Di Sano F. (2009) Acetylation of RTN-1C regulates the induction of ER stress by the inhibition of HDAC activity in neuroectodermal tumors. Oncogene, 28: 3814-24.

Filbin M.T. (2003) Myelin-associated inhibitors of axonal regeneration in the adult mammalian CNS. Nat. Rev. Neurosci., 4: 703-13.

Fontoura P., Ho P.P., DeVoss J., Zheng B., Lee B.J., Kidd B.A., Garren H., Sobel R.A., Robinson W.H., Tessier-Lavigne M. and Steinman L. (2004) Immunity to the extracellular domain of Nogo-A modulates experimental autoimmune encephalomyelitis. J. Immunol., 173: 6981-92.

Fouad K., Dietz V. and Schwab M.E. (2001) Improving axonal growth and functional recovery after experimental spinal cord injury by neutralizing myelin associated inhibitors. Brain Res. Rev., 36: 204-212.

Fouad K., Klusman I. and Schwab M.E. (2004) Regenerating corticospinal fibers in the Marmoset (Callitrix jacchus) after spinal cord lesion and treatment with the anti-Nogo-A antibody IN-1. Eur. J. Neurosci., 20: 2479-82.

Fournier A.E., Gould G.C., Liu B.P. and Strittmatter S.M. (2002) Truncated soluble Nogo receptor binds Nogo-66 and blocks inhibition of axon growth by myelin. J. Neurosci., 22: 8876-83.

Fournier A.E., GrandPré T. and Strittmatter S.M. (2001) Identification of a receptor mediating Nogo-66 inhibition of axonal regeneration. Nature, 409: 341-346.

Fournier A.E., Takizawa B.T. and Strittmatter S.M. (2003) Rho kinase inhibition enhances axonal regeneration in the injured CNS. J. Neurosci., 23: 1416-23.

Freund P., Schmidlin E., Wannier T., Bloch J., Mir A., Schwab M.E. and Rouiller E.M. (2006) Nogo-A-specific antibody treatment enhances sprouting and functional recovery after cervical lesion in adult primates. Nat. Med., 12: 790-2.

Gil V., Nicolas O., Mingorance A., Ureña J.M., Tang B.L., Hirata T., Sáez-Valero J., Ferrer I., Soriano E. and del Río J.A. (2006) Nogo-A expression in the human hippocampus in normal aging and in Alzheimer disease. J. Neuropathol. Exp. Neurol., 65: 433-44.

Gou X., Wang Q., Yang Q., Xu L. and Xiong L. (2010) TAT-NEP1-40 as a novel therapeutic candidate for axonal regeneration and functional recovery after stroke. J. Drug Target., 1-10, early online.

GrandPré T., Li S. and Strittmatter S.M. (2002) Nogo-66 receptor antagonist peptide promotes axonal regeneration. Nature, 417: 547-51.

GrandPré T., Nakamura F., Vartanian T. and Strittmatter S.M. (2000) Identification of the Nogo inhibitor of axon regeneration as a Reticulon protein. Nature, 403: 439-44.

Gregório S.P., Mury F.B., Ojopi E.B., Sallet P.C., Moreno D.H., Yacubian J., Tavares H., Santos F.R., Gattaz W.F. and Dias-Neto E. (2005) Nogo CAA 3'UTR Insertion polymorphism is not associated with Schizophrenia nor with bipolar disorder. Schizophr. Res., 75: 5-9.

Harel N.Y., Cudkowicz M.E., Brown R.H. and Strittmatter SM. (2009) Serum Nogo-A levels are not elevated in amyotrophic lateral sclerosis patients. Biomarkers, 14: 414-7.

Hasegawa Y., Fujitani M., Hata K., Tohyama M., Yamagishi S. and Yamashita T. (2004) Promotion of axon regeneration by myelin-associated glycoprotein and Nogo through divergent signals downstream of Gi/G. J. Neurosci., 24: 6826-32.

Hauben E., Ibarra A., Mizrahi T., Barouch R., Agranov E. and Schwartz M. (2001) Vaccination with a Nogo-A-derived peptide after incomplete spinal-cord injury promotes recovery via a T-cell-mediated neuroprotective response: comparison with other myelin antigens. Proc. Natl. Acad. Sci. USA, 98: 15173-8.

He X.L., Bazan J.F., McDermott G., Park J.B., Wang K., Tessier-Lavigne M., He Z. and Garcia K.C. (2003) Structure of the Nogo receptor ectodomain: a recognition module implicated in myelin inhibition. Neuron, 38: 177-85.

He W., Hu X., Shi Q., Zhou X., Lu Y., Fisher C. and Yan R. (2006) Mapping of interaction domains mediating binding between BACE1 and RTN/Nogo proteins. J. Mol. Biol., 363: 625-34.

He W., Lu Y., Qahwash I., Hu X.Y., Chang A. and Yan R. (2004) Reticulon family members modulate BACE1 activity and amyloid-beta peptide generation. Nat. Med., 10: 959-65.

Horresh I., Bar V., Kissil J.L. and Peles E. (2010) Organization of myelinated axons by Caspr and Caspr2 requires the cytoskeletal adapter protein 4.1B. J. Neurosci., 30: 2480-9.

Hou T., Shi Y., Cheng S., Yang X., Li L. and Xiao C. (2010) Nogo-A expresses on neural stem cell surface. Int. J. Neurosci., 120: 201-5.

Hsieh S.H., Ferraro G.B. and Fournier A.E. (2006) Myelin-associated inhibitors regulate cofilin phosphorylation and neuronal inhibition through LIM kinase and Slingshot phosphatase. J. Neurosci., 26: 1006-15.

Hu F. and Strittmatter S.M. (2008) The N-terminal domain of Nogo-A inhibits cell adhesion and axonal outgrowth by an integrin-specific mechanism. J. Neurosci., 28: 1262-9.

Hu F., Liu B.P., Budel S., Liao J., Chin J., Fournier A. and Strittmatter S.M. (2005) Nogo-A interacts with the Nogo-66 receptor through multiple sites to create an isoform-selective subnanomolar agonist. J. Neurosci., 25: 5298-304.

Huang D.W., McKerracher L., Braun P.E. and David S. (1999) A therapeutic vaccine approach to stimulate axon regeneration in the adult mammalian spinal cord. Neuron, 24: 639-47.

Huang J.K., Phillips G.R., Roth A.D., Pedraza L., Shan W., Belkaid W., Mi S., Fex-Svenningsen A., Florens L., Yates J.R. 3rd and Colman D.R. (2005) Glial membranes at the node of Ranvier prevent neurite outgrowth. Science, 310: 1813-1817.

Huber A.B., Weinmann O., Brösamle C., Oertle T. and Schwab M.E. (2002) Patterns of Nogo mRNA and protein expression in the developing and adult rat and after CNS lesions. J. Neurosci., 22: 3553-67.

Hunt D., Coffin R.S., Prinjha R.K., Campbell G. and Anderson P.N. (2003) Nogo-A expression in the intact and injured nervous system. Mol. Cell Neurosci., 24: 1083-102.

Hunt D., Mason M.R., Campbell G., Coffin R. and Anderson P.N. (2002) Nogo receptor mRNA expression in intact and regenerating CNS neurons. Mol. Cell Neurosci., 20: 537-52.

Ji B., Li M., Wu W.T., Yick L.W., Lee X., Shao Z., Wang J., So K.F., McCoy J.M., Pepinsky R.B., Mi S. and Relton J.K. (2006) LINGO-1 antagonist promotes functional recovery and axonal sprouting after spinal cord injury. Mol. Cell Neurosci., 33: 311-20.

Jokic N., Gonzalez de Aguilar J.L., Dimou L., Lin S., Fergani A., Ruegg M.A., Schwab M.E., Dupuis L. and Loeffler J.P. (2006) The neurite outgrowth inhibitor Nogo-A promotes denervation in an amyotrophic lateral sclerosis model. EMBO Rep., 7: 1162-7.

Josephson A., Trifunovski A., Widmer H.R., Widenfalk J., Olson L. and Spenger C. (2002) Nogo-receptor gene activity: cellular localization and developmental regulation of mRNA in mice and humans. J. Comp. Neurol., 453: 292-304.

Joset A., Dodd D.A., Halegoua S. and Schwab M.E. (2010) Pincher-generated Nogo-A endosomes mediate growth cone collapse and retrograde signaling. J. Cell Biol., 188: 271-85.

Jurewicz A., Matysiak M., Raine C.S. and Selmaj K. (2007) Soluble Nogo-A, an inhibitor of axonal regeneration, as a biomarker for multiple sclerosis. Neurology, 68: 283-7.

Karnezis T., Mandemakers W., McQualter J.L., Zheng B., Ho P.P., Jordan K.A., Murray B.M., Barres B., Tessier-Lavigne M. and Bernard C.C. (2004) The neurite outgrowth inhibitor Nogo A is involved in autoimmune-mediated demyelination. Nat. Neurosci., 7: 736-44.

Kilic E., ElAli A., Kilic U., Guo Z., Ugur M., Uslu U., Bassetti C.L., Schwab M.E. and Hermann D.M. (2010) Role of Nogo-A in neuronal survival in the reperfused ischemic brain. J. Cereb. Blood Flow Metab., 30: 969-84.

Kim J.E., Li S., GrandPré T., Qiu D. and Strittmatter S.M. (2003) Axon regeneration in young adult mice lacking Nogo-A/B. Neuron, 38: 187-99.

Kim J.E., Liu B.P., Park J.H. and Strittmatter S.M. (2004) Nogo-66 receptor prevents raphespinal and rubrospinal axon regeneration and limits functional recovery from spinal cord injury. Neuron, 44: 439-51.

Kiseleva E., Morozova K.N., Voeltz G.K., Allen T.D. and Goldberg M.W. (2007) Reticulon 4a/NogoA locates to regions of high membrane curvature and may have a role in nuclear envelope growth. J. Struct. Biol., 160: 224-35.

Koprivica V., Cho K.S., Park J.B., Yiu G., Atwal J., Gore B., Kim J.A., Lin E., Tessier-Lavigne M., Chen D.F. and He Z. (2005) EGFR activation mediates inhibition of axon regeneration by myelin and chondroitin sulfate proteoglycans. Science, 310: 106-10.

Kottis V., Thibault P., Mikol D., Xiao Z.C., Zhang R., Dergham P. and Braun P.E. (2002) Oligodendrocyte-myelin glycoprotein (OMgp) is an inhibitor of neurite outgrowth. J. Neurochem., 82: 1566-9.

Kuang E., Wan Q., Li X., Xu H., Liu Q. and Qi Y. (2005) ER Ca^{2+} depletion triggers apoptotic signals for endoplasmic reticulum (ER) overload response induced by overexpressed reticulon 3 (RTN3/HAP). J. Cell Physiol., 204: 549-59.

Kuang E., Wan Q., Li X., Xu H., Zou T. and Qi Y. (2006) ER stress triggers apoptosis induced by Nogo-B/ASY overexpression. Exp. Cell Res., 312: 1983-8.

Kume H., Murayama K.S. and Araki W. (2009) The two-hydrophobic domain tertiary structure of reticulon proteins is critical for modulation of beta-secretase BACE1. J. Neurosci. Res., 87: 2963-72.

Laurén J., Airaksinen M.S., Saarma M. and Timmusk T. (2003) Two novel mammalian Nogo receptor homologs differentially expressed in the central and peripheral nervous systems. Mol. Cell Neurosci., 24: 581-94.

Lee J.K., Chan A.F., Luu S.M., Zhu Y., Ho C., Tessier-Lavigne M. and Zheng B. (2009) Reassessment of corticospinal tract regeneration in Nogo-deficient mice. J. Neurosci., 29: 8649-54.

Lee J.K., Geoffroy C.G., Chan A.F., Tolentino K.E., Crawford M.J., Leal M.A., Kang B. and Zheng B. (2010) Assessing spinal axon regeneration and sprouting in Nogo-, MAG-, and OMgp-deficient mice. Neuron, 66: 663-70.

Lee J.K., Kim J.E., Sivula M. and Strittmatter S.M. (2004) Nogo receptor antagonism promotes stroke recovery by enhancing axonal plasticity. J. Neurosci., 24: 6209-17.

Lee J.T., Lee T.J., Kim C.H., Kim N.S. and Kwon T.K. (2009) Over-expression of Reticulon 3 (RTN3) enhances TRAIL-mediated apoptosis via up-regulation of death receptor 5 (DR5) and down-regulation of c-FLIP. Cancer Lett., 279: 185-92.

Li M., Li Y., Liao X., Liu J., Qin H., Xiao Z.C. and Song J. (2008) Rational design, solution conformation and identification of functional residues of the soluble and structured Nogo-54, which mimics Nogo-66 in inhibiting the CNS neurite outgrowth. Biochem. Biophys. Res. Commun., 373: 498-503.

Li M., Liu J. and Song J. (2006) Nogo goes in the pure water: solution structure of Nogo-60 and design of the structured and buffer-soluble Nogo-54 for enhancing CNS regeneration. Protein Sci., 15: 1835-41.

Li M., Shi J., Wei Z., Teng F.Y., Tang B.L. and Song J. (2004a) Structural characterization of the human Nogo-A functional domains. Solution structure of Nogo-40, a Nogo-66 receptor antagonist enhancing injured spinal cord regeneration. Eur. J. Biochem, 271: 3512-22.

Li M. and Song J. (2007) The N- and C-termini of the human Nogo molecules are intrinsically unstructured: bioinformatics, CD, NMR characterization, and functional implications. Proteins, 68: 100-8.

Li Q., Qi B., Oka K., Shimakage M., Yoshioka N., Inoue H., Hakura A., Kodama K., Stanbridge E.J. and Yutsudo M. (2001) Link of a new type of apoptosis-inducing gene ASY/Nogo-B to human cancer. Oncogene, 20: 3929-36.

Li S. and Strittmatter S.M. (2003) Delayed systemic Nogo-66 receptor antagonist promotes recovery from spinal cord injury. J. Neurosci., 23: 4219-27.

Li S., Liu B.P., Budel S., Li M., Ji B., Walus L., Li W., Jirik A., Rabacchi S., Choi E., Worley D., Sah D.W., Pepinsky B., Lee D., Relton J. and Strittmatter S.M. (2004b) Blockade of Nogo-66, myelin-associated glycoprotein, and oligodendrocyte myelin glycoprotein by soluble Nogo-66 receptor promotes axonal sprouting and recovery after spinal injury. J. Neurosci., 24: 10511-20.

Li W., Walus L., Rabacchi S.A., Jirik A., Chang E., Schauer J., Zheng B.H., Benedetti N.J., Liu B.P., Choi E., Worley D., Silvian L., Mo W., Mullen C., Yang W., Strittmatter S.M., Sah D.W., Pepinsky B. and Lee D.H. (2004c) A neutralizing anti-Nogo66 receptor monoclonal antibody reverses inhibition of neurite outgrowth by central nervous system myelin. J. Biol. Chem., 279: 43780-8.

Liao H., Duka T., Teng F.Y., Sun L., Bu W.Y., Ahmed S., Tang B.L. and Xiao Z.C. (2004) Nogo-66 and myelin-associated glycoprotein (MAG) inhibit the adhesion and migration of Nogo-66 receptor expressing human glioma cells. J. Neurochem., 90: 1156-62.

Liebscher T., Schnell L., Schnell D., Scholl J., Schneider R., Gullo M., Fouad K., Mir A., Rausch M., Kindler D., Hamers F.P. and Schwab M.E. (2005) Nogo-A antibody improves regeneration and locomotion of spinal cord-injured rats. Ann. Neurol., 58: 706-19.

Lindsey J.W., Crawford M.P. and Hatfield L.M. (2008) Soluble Nogo-A in CSF is not a useful biomarker for multiple sclerosis. Neurology, 71: 35-7.

Liu B.P., Fournier A., GrandPré T. and Strittmatter S.M. (2002a) Myelin-associated glycoprotein as a functional ligand for the Nogo-66 receptor. Science, 297: 1190-3.

Liu H., Ng C.E. and Tang B.L. (2002b) Nogo-A expression in mouse central nervous system neurons. Neurosci. Lett., 328: 257-60.

Liu J., Li M., Ran X., Fan J.S. and Song J. (2006) Structural insight into the binding diversity between the human Nck2 SH3 domains and proline-rich proteins. Biochemistry, 45: 7171-84.

Liu X., Wang Y., Zhang Y., Zhu W., Xu X., Niinobe M., Yoshikawa K., Lu C. and He C. (2009) Nogo-A inhibits necdin-accelerated neurite outgrowth by retaining necdin in the cytoplasm. Mol. Cell Neurosci., 41: 51-61.

Liu Y.Y., Jin W.L., Liu H.L. and Ju G. (2003) Electron microscopic localization of Nogo-A at the postsynaptic active zone of the rat. Neurosci. Lett., 346: 153-6.

Luo L. (2000) Rho GTPases in neuronal morphogenesis. Nat. Rev. Neurosci., 1: 173-80.

Lv J., Xu R.X., Jiang X.D., Lu X., Ke Y.Q., Cai Y.Q., Du M.X., Hu C., Zou Y.X., Qin L.S. and Zeng Y.J. (2010) Passive immunization with LINGO-1 polyclonal antiserum afforded neuroprotection and promoted functional recovery in a rat model of spinal cord injury. Neuroimmunomodulation, 17: 270-8.

Macleod M.R., Allsopp T.E., McLuckie J. and Kelly J.S. (2001) Serum withdrawal causes apoptosis in SHSY 5Y cells. Brain Res., 889: 308-15.

Madura T., Yamashita T., Kubo T., Fujitani M., Hosokawa K. and Tohyama M. (2004) Activation of Rho in the injured axons following spinal cord injury. EMBO Rep., 5: 412-7.

Marklund N., Fulp C.T., Shimizu S., Puri R., McMillan A., Strittmatter S.M. and McIntosh T.K. (2006) Selective temporal and regional alterations of Nogo-A and small proline-rich repeat protein 1A (SPRR1A) but not Nogo-66 receptor (NgR) following traumatic brain injury in the rat. Exp. Neurol., 197: 70-83.

Marklund N., Morales D., Clausen F., Hånell A., Kiwanuka O., Pitkänen A., Gimbel D.A., Philipson O., Lannfelt L., Hillered L., Strittmatter S.M. and McIntosh T.K. (2009) Functional outcome is impaired following traumatic brain injury in aging Nogo-A/B-deficient mice. Neuroscience, 163: 540-51.

Masliah E., Xie F., Dayan S., Rockenstein E., Mante M., Adame A., Patrick C.M., Chan A.F. and Zheng B. (2010) Genetic deletion of Nogo/Rtn4 ameliorates behavioral and neuropathological outcomes in amyloid precursor protein transgenic mice. Neuroscience, 169: 488-94.

McKeon R.J., Schreiber R.C., Rudge J.S. and Silver J. (1991) Reduction of neurite outgrowth in a model of glial scarring following CNS injury is correlated with the

expression of inhibitory molecules on reactive astrocytes. J. Neurosci., 11: 3398–3411.

McKerracher L., David S., Jackson D.L., Kottis V., Dunn R.J. and Braun P.E. (1994) Identification of myelin-associated glycoprotein as a major myelin-derived inhibitor of neurite growth. Neuron, 13: 805-11.

Meier S., Bräuer A.U., Heimrich B., Schwab M.E., Nitsch R. and Savaskan N.E. (2003) Molecular analysis of Nogo expression in the hippocampus during development and following lesion and seizure. FASEB J., 17: 1153-5.

Mi S., Lee X., Shao Z., Thill G., Ji B., Relton J., Levesque M., Allaire N., Perrin S., Sands B., Crowell T., Cate R.L., McCoy J.M. and Pepinsky R.B. (2004) LINGO-1 is a component of the Nogo-66 receptor/p75 signaling complex. Nat. Neurosci., 7: 221-8.

Mishra M., Akatsu H. and Heese K. (2010) The novel protein MANI modulates neurogenesis and neurite-cone growth. J. Cell Mol. Med., 2010 Aug 12. [Epub ahead of print]

Miyazaki K., Nagai M., Ohta Y., Morimoto N., Kurata T., Murakami T., Takehisa Y., Ikeda Y., Kamiya T. and Abe K. (2009) Changes of Nogo-A and receptor NgR in the lumbar spinal cord of ALS model mice. Neurol. Res., 31: 316-21.

Monti Graziadei G.A., Karlan M.S., Bernstein J.J. and Graziadei P.P. (1980) Reinnervation of the olfactory bulb after section of the olfactory nerve in monkey (Saimiri sciureus). Brain Res., 189: 343-354.

Moon L.D., Asher R.A., Rhodes K.E. and Fawcett J.W. (2001) Regeneration of CNS axons back to their target following treatment of adult rat brain with chondroitinase ABC. Nat. Neurosci., 4: 465-466.

Moreira E.F., Jaworski C.J. and Rodriguez I.R. (1999) Cloning of a novel member of the reticulon gene family (RTN3): gene structure and chromosomal localization to 11q13. Genomics, 58: 73-81.

Morris N.J., Ross S.A., Neveu J.M., Lane W.S. and Lienhard G.E. (1999) Cloning and characterization of a 22 kDa protein from rat adipocytes: a new member of the reticulon family. Biochim. Biophys. Acta., 1450: 68-76.

Morrison E.E. and Costanzo R.M. (1995) Regeneration of olfactory sensory neurons and reconnection in the aging hamster central nervous system. Neurosci. Lett., 198: 213-217.

Mukhopadhyay G., Doherty P., Walsh F.S., Crocker P.R. and Filbin M.T. (2002) A novel role for myelin-associated glycoprotein as an inhibitor of axonal regeneration. Neuron, 13: 757-67.

Müllner A., Gonzenbach R.R., Weinmann O., Schnell L., Liebscher T. and Schwab M.E. (2008) Lamina-specific restoration of serotonergic projections after Nogo-A antibody treatment of spinal cord injury in rats. Eur. J. Neurosci., 27: 326-33.

Murayama K.S., Kametani F., Saito S., Kume H., Akiyama H. and Araki W. (2006) Reticulons RTN3 and RTN4-B/C interact with BACE1 and inhibit its ability to produce amyloid beta-protein. Eur. J. Neurosci., 24: 1237-44.

Nagase T., Ishikawa K., Suyama M., Kikuno R., Hirosawa M., Miyajima N., Tanaka A., Kotani H., Nomura N. and Ohara O. (1998). Prediction of the coding sequences of unidentified human genes. XII. The complete sequences of 100 new cDNA clones from brain which code for large proteins in vitro. DNA Res., 5: 355–364.

Neumann S. and Woolf C.J. (1999) Regeneration of dorsal column fibers into and beyond the lesion site following adult spinal cord injury. Neuron, 23: 83-91.

Ni M., Zhou H., Wey S., Baumeister P. and Lee A.S. (2009) Regulation of PERK signaling and leukemic cell survival by a novel cytosolic isoform of the UPR regulator GRP78/BiP. PLoS One, 4: e6868.

Nie D.Y., Zhou Z.H., Ang B.T., Teng F.Y., Xu G., Xiang T., Wang C.Y., Zeng L., Takeda Y., Xu T.L., Ng Y.K., Faivre-Sarrailh C., Popko B., Ling E.A., Schachner M., Watanabe K., Pallen C.J., Tang B.L. and Xiao Z.C. (2003) Nogo-A at CNS paranodes is a ligand of Caspr: possible regulation of K(+) channel localization. EMBO J., 22: 5666-78.

Niederöst B., Oertle T., Fritsche J., McKinney R.A.and Bandtlow C.E. (2002) Nogo-A and myelin-associated glycoprotein mediate neurite growth inhibition by antagonistic regulation of RhoA and Rac1. J. Neurosci., 22: 10368-76.

Ng W.P., Cartel N., Roder J., Roach A. and Lozano A. (1996) Human central nervous system myelin inhibits neurite outgrowth. Brain Res., 720: 17-24.

Novak G. and Tallerico T. (2006) Nogo A, B and C expression in schizophrenia, depression and bipolar frontal cortex, and correlation of Nogo expression with CAA/TATC polymorphism in 3'-UTR. Brain Res., 1120: 161-71.

Novak G., Kim D., Seeman P. and Tallerico T. (2002) Schizophrenia and Nogo: elevated mRNA in cortex, and high prevalence of a homozygous CAA insert. Brain Res. Mol. Brain Res., 107: 183-9.

Nyatia E. and Lang D.M. (2007) Localisation and expression of a myelin associated neurite inhibitor, Nogo-A and its receptor Nogo-receptor by mammalian CNS cells. Res .Vet. Sci., 83: 287-301.

O'Neill P., Whalley K. and Ferretti P. (2004) Nogo and Nogo-66 receptor in human and chick: implications for development and regeneration. Dev. Dyn., 231: 109-21.

Oertle T., Huber C., van der Putten H. and Schwab M.E. (2003a) Genomic structure and functional characterisation of the promoters of human and mouse nogo/rtn4. J. Mol. Biol., 325: 299-323.

Oertle T., Klinger M., Stuermer C.A. and Schwab M.E. (2003b) A reticular rhapsody: phylogenetic evolution and nomenclature of the RTN/Nogo gene family. FASEB J., 17: 1238-1247.

Oertle T., Merkler D. and Schwab M.E. (2003c) Do cancer cells die because of Nogo-B? Oncogene, 22: 1390-9.

Oertle T., van der Haar M.E., Bandtlow C.E., Robeva A., Burfeind P., Buss A., Huber A.B., Simonen M., Schnell L., Brösamle C., Kaupmann K., Vallon R. and Schwab M.E. (2003d) Nogo-A inhibits neurite outgrowth and cell spreading with three discrete regions. J. Neurosci., 23: 5393-406.

Osborne S.L., Corcoran S.L., Prinjha R.K. and Moore S.E. (2004) Nogo A expression in the adult enteric nervous system. Neurogastroenterol. Motil., 16: 465-74.

Park J.B., Yiu G., Kaneko S., Wang J., Chang J., He X.L., Garcia K.C. and He Z. (2005) A TNF receptor family member, TROY, is a coreceptor with Nogo receptor in mediating the inhibitory activity of myelin inhibitors. Neuron, 45: 345-51.

Park J.H., Gimbel D.A., GrandPré T., Lee J.K., Kim J.E., Li W., Lee D.H. and Strittmatter S.M. (2006a) Alzheimer precursor protein interaction with the Nogo-66 receptor reduces amyloid-beta plaque deposition. J. Neurosci., 26: 1386-95.

Park J.H., Widi G.A., Gimbel D.A., Harel N.Y., Lee D.H. and Strittmatter S.M. (2006b) Subcutaneous Nogo receptor removes brain amyloid-beta and improves spatial memory in Alzheimer's transgenic mice. J. Neurosci., 26: 13279-86.

Pereira S., Zhang H., Takai T. and Lowell C.A. (2004) The inhibitory receptor PIR-B negatively regulates neutrophil and macrophage integrin signaling. J. Immunol., 173: 5757-65.

Pettigrew D.B., Shockley K.P. and Crutcher K.A. (2001) Disruption of spinal cord white matter and sciatic nerve geometry inhibits axonal growth in vitro in the absence of glial scarring. BMC Neurosci., 2: 8.

Pignot V., Hein A.E., Barske C., Wiessner C., Walmsley A.R., Kaupmann K., Mayeur H., Sommer B., Mir A.K. and Frentzel S. (2003) Characterization of two novel proteins, NgRH1 and NgRH2, structurally and biochemically homologous to the Nogo-66 receptor. J. Neurochem., 85: 717-28.

Peng X., Zhou Z., Hu J., Fink D.J. and Mata M. (2010) Soluble Nogo receptor down-regulates expression of neuronal Nogo-A to enhance axonal regeneration. J. Biol. Chem., 285: 2783-95.

Pot C., Simonen M., Weinmann O., Schnell L., Christ F., Stoeckle S., Berger P., Rülicke T., Suter U. and Schwab M.E. (2002) Nogo-A expressed in Schwann cells impairs axonal regeneration after peripheral nerve injury. J. Cell Biol., 159: 29-35.

Pradat P.F., Bruneteau G., Gonzalez de Aguilar J.L, Dupuis L., Jokic N., Salachas F., Le Forestier N., Echaniz-Laguna A., Dubourg O., Hauw J.J., Tranchant C., Loeffler J.P. and Meininger V. (2007) Muscle Nogo-A expression is a prognostic marker in lower motor neuron syndromes. Ann. Neurol., 62: 15-20.

Prinjha R., Moore S.E., Vinson M., Blake S., Morrow R., Christie G., Michalovich D., Simmons D.L. and Walsh F.S. (2000) Inhibitor of neurite outgrowth in humans. Nature, 403: 383-4.

Qi B., Qi Y., Watari A., Yoshioka N., Inoue H., Minemoto Y., Yamashita K., Sasagawa T. and Yutsudo M (2003) Pro-apoptotic ASY/Nogo-B protein associates with ASYIP. J. Cell Physiol., 196: 312-8.

Qin H., Pu H.X., Li M., Ahmed S. and Song J. (2008) Identification and structural mechanism for a novel interaction between a ubiquitin ligase WWP1 and Nogo-A, a key inhibitor for central nervous system regeneration. Biochemistry, 47: 13647-58.

Qu L., Huang S., Baltzis D., Rivas-Estilla A.M., Pluquet O., Hatzoglou M., Koumenis C., Taya Y., Yoshimura A. and Koromilas A.E. (2004) Endoplasmic reticulum stress induces p53 cytoplasmic localization and prevents p53-dependent apoptosis by a pathway involving glycogen synthase kinase-3beta. Genes Dev., 18: 261-77.

Ramón y Cajal S. (1928) Degeneration and regeneration of the nervous system. Translated by May R.M. Oxford Press, London.

Reier, P.J., Stensaas L.J. and Guth L. (1983) The astrocytic scar as an impediment to regeneration in the central nervous system. In Spinal Cord Reconstruction, editors Kao C.C., Bunge R.P., and Reier P.J. Raven Press, New York. pp. 163-195.

Reindl M., Khantane S., Ehling R., Schanda K., Lutterotti A., Brinkhoff C., Oertle T., Schwab M.E., Deisenhammer F., Berger T. and Bandtlow C.E. (2003) Serum and cerebrospinal fluid antibodies to Nogo-A in patients with multiple sclerosis and acute neurological disorders. J. Neuroimmunol., 145: 139-47.

Richardson P.M., McGuinness U.M. and Aguayo A.J. (1980) Axons from CNS neurons regenerate into PNS grafts. Nature, 284: 264-265.

Roebroek A.J., Contreras B., Pauli I.G. and Van de Ven W.J. (1998) cDNA cloning, genomic organization, and expression of the human RTN2 gene, a member of a gene family encoding reticulons. Genomics, 51: 98-106.

Roebroek A.J., van de Velde H.J., Van Bokhoven A., Broers J.L., Ramaekers F.C. and Van de Ven W.J. (1993) Cloning and expression of alternative transcripts of a novel neuroendocrine-specific gene and identification of its 135-kDa translational product. J. Biol. Chem., 268: 13439-13447.

Rudge J.S. and Silver J. (1990) Inhibition of neurite outgrowth on astroglial scars in vitro. J. Neurosci., 10: 3594-603.

Rutkowski D.T., Arnold S.M., Miller C.N., Wu J., Li J., Gunnison K.M., Mori K., Sadighi Akha A.A., Raden D. and Kaufman R.J. (2006) Adaptation to ER stress is mediated by differential stabilities of pro-survival and pro-apoptotic mRNAs and proteins. PLoS Biol., 4: e374.

Satoh J., Onoue H., Arima K. and Yamamura T. (2005) Nogo-A and nogo receptor expression in demyelinating lesions of multiple sclerosis. J. Neuropathol. Exp. Neurol., 64: 129-38.

Savio T. and Schwab M.E. (1990) Lesioned corticospinal tract axons regenerate in myelin-free rat spinal cord. Proc. Natl. Acad. Sci. USA, 87: 4130-3.

Schimmele B. and Plückthun A. (2005) Identification of a functional epitope of the Nogo receptor by a combinatorial approach using ribosome display. J. Mol. Biol., 352: 229-41.

Schwab M.E. and Caroni P. (1988) Oligodendrocytes and CNS myelin are nonpermissive substrates for neurite growth and fibroblast spreading in vitro. J. Neurosci., 8: 2381-93.

Schwab M.E. and Thoenen H. (1985) Dissociated neurons regenerate into sciatic but not optic nerve explants in culture irrespective of neurotrophic factors. J. Neurosci., 5: 2415-2423.

Senden N.H., van de Velde H.J., Broers J.L., Timmer E.D., Kuijpers H.J., Roebroek A.J., Van de Ven W.J. and Ramaekers F.C. (1994) Subcellular localization and supramolecular organization of neuroendocrine-specific protein B (NSP-B) in small cell lung cancer. Eur. J. Cell Biol., 65: 341-53.

Seymour A.B., Andrews E.M., Tsai S.Y., Markus T.M., Bollnow M.R., Brenneman M.M., O'Brien T.E., Castro A.J., Schwab M.E. and Kartje G.L. (2005) Delayed treatment with monoclonal antibody IN-1 1 week after stroke results in recovery of function and corticorubral plasticity in adult rats. J. Cereb. Blood Flow Metab., 25: 1366-75.

Sicotte M., Tsatas O., Jeong S.Y., Cai C.Q., He Z. and David S. (2003) Immunization with myelin or recombinant Nogo-66/MAG in alum promotes axon regeneration and sprouting after corticospinal tract lesions in the spinal cord. Mol. Cell Neurosci., 23: 251-63.

Silver J. and Miller J.H. (2004) Regeneration beyond the glial scar. Nature Rev. Neurosci., 5: 146–156.

Simonen M., Pedersen V., Weinmann O., Schnell L., Buss A., Ledermann B., Christ F., Sansig G., van der Putten H. and Schwab M.E. (2003) Systemic deletion of the

myelin-associated outgrowth inhibitor Nogo-A improves regenerative and plastic responses after spinal cord injury. Neuron, 38: 201-11.

Sinibaldi L., De Luca A., Bellacchio E., Conti E., Pasini A., Paloscia C., Spalletta G., Caltagirone C., Pizzuti A. and Dallapiccola B. (2004) Mutations of the Nogo-66 receptor (RTN4R) gene in schizophrenia. Hum. Mutat., 24: 534-5.

Shao Z., Browning J.L., Lee X., Scott M.L., Shulga-Morskaya S., Allaire N., Thill G., Levesque M., Sah D., McCoy J.M., Murray B., Jung V., Pepinsky R.B. and Mi S. (2005) TAJ/TROY, an orphan TNF receptor family member, binds Nogo-66 receptor 1 and regulates axonal regeneration. Neuron, 45: 353-9.

Shibata Y., Voss C., Rist J.M., Hu J., Rapoport T.A., Prinz W.A. and Voeltz G.K. (2008) The reticulon and DP1/Yop1p proteins form immobile oligomers in the tubular endoplasmic reticulum. J. Biol. Chem., 283: 18892-904.

Song X.Y., Zhong J.H., Wang X. and Zhou X.F. (2004) Suppression of p75NTR does not promote regeneration of injured spinal cord in mice. J. Neurosci., 24:542-6.

Sparkes I., Tolley N., Aller I., Svozil J., Osterrieder A., Botchway S., Mueller C., Frigerio L. and Hawes C. (2010) Five Arabidopsis reticulon isoforms share endoplasmic reticulum location, topology, and membrane-shaping properties. Plant Cell, 22: 1333-43.

Spillmann A.A., Bandtlow C.E., Lottspeich F., Keller F. and Schwab M.E. (1998) Identification and characterization of a bovine neurite growth inhibitor (bNI-22). J. Biol. Chem., 273: 19283-19293.

Su Y., Wang F., Teng Y., Zhao S.G., Cui H. and Pan S.H. (2009) Axonal regeneration of optic nerve after crush in Nogo66 receptor knockout mice. Neurosci. Lett., 460: 223-6.

Su Y., Wang F., Zhao S.G., Pan S.H., Liu P., Teng Y. and Cui H. (2008) Axonal regeneration after optic nerve crush in Nogo-A/B/C knockout mice. Mol. Vis., 14: 268-73.

Syken J., Grandpre T., Kanold P.O. and Shatz C.J. (2006) PirB restricts ocular-dominance plasticity in visual cortex. Science, 313: 1795-800.

Tagami S., Eguchi Y., Kinoshita M., Takeda M. and Tsujimoto Y. (2000) A novel protein, RTN-XS, interacts with both Bcl-XL and Bcl-2 on endoplasmic reticulum and reduces their anti-apoptotic activity. Oncogene, 19: 5736-46.

Takeda Y., Kamida T., Fujiki M. and Kobayashi H. (2007) Hippocampal Nogo-A and neo-Timm's staining in amygdala kindling rats. Neurol. Res., 29: 199-203.

Takei Y. (2009) Phosphorylation of Nogo receptors suppresses Nogo signaling, allowing neurite regeneration. Sci. Signal, 2: ra14.

Taketomi M., Kinoshita N., Kimura K., Kitada M., Noda T., Asou H., Nakamura T. and Ide C. (2002) Nogo-A expression in mature oligodendrocytes of rat spinal cord in association with specific molecules. Neurosci. Lett., 332: 37-40.

Tambe Y., Isono T., Haraguchi S., Yoshioka-Yamashita A., Yutsudo M. and Inoue H. (2004) A novel apoptotic pathway induced by the drs tumor suppressor gene. Oncogene, 23: 2977-87.

Thallmair M., Metz G.A., Z'Graggen W.J., Raineteau O., Kartje G.L. and Schwab M.E. (1998) Neurite growth inhibitors restrict plasticity and functional recovery following corticospinal tract lesions. Nat. Neurosci., 1: 124-131.

Thomas R., Favell K., Morante-Redolat J., Pool M., Kent C., Wright M., Daignault K., Ferraro G.B., Montcalm S., Durocher Y., Fournier A., Perez-Tur J. and Barker P.A. (2010) LGI1 is a Nogo receptor 1 ligand that antagonizes myelin-based growth inhibition. J. Neurosci., 30: 6607-12.

Tozaki H., Kawasaki T., Takagi Y. and Hirata T. (2002) Expression of Nogo protein by growing axons in the developing nervous system. Mol. Brain Res., 104: 111-9.

van de Velde H.J., Roebroek A.J., Senden N.H., Ramaekers F.C. and Van de Ven W.J. (1994) NSP-encoded reticulons, neuroendocrine proteins of a novel gene family associated with membranes of the endoplasmic reticulum. J. Cell Sci., 107: 2403-2416.

Vasudevan S.V., Schulz J., Zhou C. and Cocco M.J. (2010) Protein folding at the membrane interface, the structure of Nogo-66 requires interactions with a phosphocholine surface. Proc. Natl. Acad. Sci. USA., 107: 6847-51.

Voeltz G.K., Prinz W.A., Shibata Y., Rist J.M. and Rapoport T.A. (2006) A class of membrane proteins shaping the tubular endoplasmic reticulum. Cell, 124: 573-86.

Wakana Y., Koyama S., Nakajima K., Hatsuzawa K., Nagahama M., Tani K., Hauri H.P., Melançon P. and Tagaya M. (2005) Reticulon 3 is involved in membrane trafficking between the endoplasmic reticulum and Golgi. Biochem. Biophys. Res. Commun., 334: 1198-205.

Walmsley A.R., McCombie G., Neumann U., Marcellin D., Hillenbrand R., Mir A.K. and Frentzel S. (2004) Zinc metalloproteinase-mediated cleavage of the human Nogo-66 receptor. J. Cell Sci., 117: 4591-602.

Wan Q., Kuang E., Dong W., Zhou S., Xu H., Qi Y. and Liu Y. (2007) Reticulon 3 mediates Bcl-2 accumulation in mitochondria in response to endoplasmic reticulum stress. Apoptosis, 12: 319-28.

Wang B., Xiao Z., Chen B., Han J., Gao Y., Zhang J., Zhao W., Wang X. and Dai J. (2008) Nogo-66 promotes the differentiation of neural progenitors into astroglial lineage cells through mTOR-STAT3 pathway. PLoS One, 3: e1856.

Wang H., Yao Y., Jiang X., Chen D., Xiong Y. and Mu D. (2006) Expression of Nogo-A and NgR in the developing rat brain after hypoxia-ischemia. Brain Res., 1114: 212-220.

Wang K.C., Kim J.A., Sivasankaran R., Segal R. and He Z. (2002a) P75 interacts with the Nogo receptor as a co-receptor for Nogo, MAG and OMgp. Nature, 420: 74-8.

Wang K.C., Koprivica V., Kim J.A., Sivasankaran R., Guo Y., Neve R.L., He Z. (2002b) Oligodendrocyte-myelin glycoprotein is a Nogo receptor ligand that inhibits neurite outgrowth. Nature, 417: 941-4.

Wang X., Chun S.J., Treloar H., Vartanian T., Greer C.A. and Strittmatter S.M. (2002c) Localization of Nogo-A and Nogo-66 receptor proteins at sites of axon-myelin and synaptic contact. J. Neurosci., 22: 5505-15.

Wang Y., Khaing Z.Z., Li N., Hall B., Schmidt C.E. and Ellington A.D. (2010) Aptamer antagonists of myelin-derived inhibitors promote axon growth. PLoS One, 5: e9726.

Wanner I.B., Deik A., Torres M., Rosendahl A., Neary J.T., Lemmon V.P. and Bixby J.L. (2008) A new in vitro model of the glial scar inhibits axon growth. Glia, 56: 1691-709.

Weibel D., Cadelli D. and Schwab M.E. (1994) Regeneration of lesioned rat optic nerve fibers is improved after neutralization of myelin-associated neurite growth inhibitors. Brain Res., 642: 259-66.

Wieczorek D.F. and Hughes S.R. (1991) Developmentally regulated cDNA expressed exclusively in neural tissue. Brain Res., 10: 33-41.

Wiessner C., Bareyre F.M., Allegrini P.R., Mir A.K., Frentzel S., Zurini M., Schnell L., Oertle T. and Schwab M.E. (2003) Anti-Nogo-A antibody infusion 24 hours after experimental stroke improved behavioral outcome and corticospinal plasticity in normotensive and spontaneously hypertensive rats. J. Cereb. Blood Flow Metab., 23: 154-65.

Willi R., Weinmann O., Winter C., Klein J., Sohr R., Schnell L., Yee B.K., Feldon J. and Schwab M.E. (2010) Constitutive genetic deletion of the growth regulator Nogo-A induces schizophrenia-related endophenotypes. J. Neurosci., 30: 556-67.

Williams G., Wood A., Williams E.J., Gao Y., Mercado M.L., Katz A., Joseph-McCarthy D., Bates B., Ling H.P., Aulabaugh A., Zaccardi J., Xie Y., Pangalos M.N., Walsh F.S. and Doherty P. (2008) Ganglioside inhibition of neurite outgrowth requires Nogo receptor function: identification of interaction sites and development of novel antagonists. J. Biol. Chem., 283: 16641-52.

Wojcik S., Engel W.K. and Askanas V. (2006) Increased expression of Noga-A in ALS muscle biopsies is not unique for this disease. Acta. Myol., 25: 116-8.

Wong S.T., Henley J.R., Kanning K.C., Huang K.H., Bothwell M. and Poo M.M. (2002) A p75(NTR) and Nogo receptor complex mediates repulsive signaling by myelin-associated glycoprotein. Nat. Neurosci., 5: 1302-8.

Wu J., Yang H., Qiu Z., Zhang Q., Ding T. and Geng D. (2010) Effect of combined treatment with methylprednisolone and Nogo-A monoclonal antibody after rat spinal cord injury. J. Int. Med. Res., 38: 570-82.

Xiang R. and Zhao S. (2009) RTN3 inducing apoptosis is modulated by an adhesion protein CRELD1. Mol. Cell. Biochem., 331: 225-30.

Xiang R., Liu Y., Zhu L., Dong W. and Qi Y. (2006) Adaptor FADD is recruited by RTN3/HAP in ER-bound signaling complexes. Apoptosis, 11: 1923-32.

Xiaolei Y., Rongdi Y., Shuxing J. and Jian Y. (2009) The expression patterns of Nogo-A and NgR in the neonatal rat visual nervous system. Neurochem. Res., 34: 1204-8.

Xiong L., Rouleau G.A., Delisi L.E., St-Onge J., Najafee R., Rivière J.B., Benkelfat C., Tabbane K., Fathalli F., Danics Z., Labelle A., Lal S. and Joober R. (2005) CAA insertion polymorphism in the 3'UTR of Nogo gene on 2p14 is not associated with schizophrenia. Brain Res. Mol. Brain Res., 133: 153-6.

Yamashita T. and Tohyama M. (2003) The p75 receptor acts as a displacement factor that releases Rho from Rho-GDI. Nat. Neurosci., 6: 461-7.

Yamashita T., Tucker K.L. and Barde Y.A. (1999) Neurotrophin binding to the p75 receptor modulates Rho activity and axonal outgrowth. Neuron, 24: 585-93.

Yang J., Yu L., Bi A.D. and Zhao S.Y. (2000) Assignment of the human reticulon 4 gene (RTN4) to chromosome 2p14-->2p13 by radiation hybrid mapping. Cytogenet. Cell Genet., 88: 101-2.

Yang Y., Liu Y., Wei P., Peng H., Winger R., Hussain R.Z., Ben L.H., Cravens P.D., Gocke A.R., Puttaparthi K., Racke M.K., McTigue D.M. and Lovett-Racke A.E. (2010) Silencing Nogo-A promotes functional recovery in demyelinating disease. Ann. Neurol., 67: 498-507.

Yang Y.S. and Strittmatter S.M. (2007) The reticulons: a family of proteins with diverse functions. Genome Biol., 8: 234.

Yang Y.S., Harel N.Y. and Strittmatter S.M. (2009) Reticulon-4A (Nogo-A) redistributes protein disulfide isomerase to protect mice from SOD1-dependent amyotrophic lateral sclerosis. J. Neurosci., 29: 13850-9.

Yick L.W., Wu W., So K.F., Yip H.K. and Shum D.K. (2000) Chondroitinase ABC promotes axonal regeneration of Clarke's neurons after spinal cord injury. Neuroreport, 11: 1063-1067.

Yiu G. and He Z. (2006) Glial inhibition of CNS axon regeneration. Nat. Rev. Neurosci., 7: 617-27.

Yu P., Huang L., Zou J., Yu Z., Wang Y., Wang X., Xu L., Liu X., Xu X.M. and Lu P.H. (2008) Immunization with recombinant Nogo-66 receptor (NgR) promotes axonal regeneration and recovery of function after spinal cord injury in rats. Neurobiol. Dis., 32: 535-42.

Yu W., Guo W. and Feng L. (2004) Segregation of Nogo66 receptors into lipid rafts in rat brain and inhibition of Nogo66 signaling by cholesterol depletion. FEBS Lett., 577: 87-92.

Zander H., Hettich E., Greiff K., Chatwell L. and Skerra A. (2007) Biochemical characterization of the recombinant human Nogo-A ectodomain. FEBS J., 274: 2603-13.

Zhang D., Vjestica A. and Oliferenko S. (2010) The cortical ER network limits the permissive zone for actomyosin ring assembly. Curr. Biol., 20: 1029-34.

Zhang H., Meng F., Chu C.L., Takai T. and Lowell C.A. (2005) The Src family kinases Hck and Fgr negatively regulate neutrophil and dendritic cell chemokine signaling via PIR-B. Immunity, 22: 235-46.

Zhang Z., Xu X., Zhang Y., Zhou J., Yu Z. and He C. (2009) LINGO-1 interacts with WNK1 to regulate nogo-induced inhibition of neurite extension. J. Biol. Chem., 284: 15717-28.

Zheng B., Atwal J., Ho C., Case L., He X.L., Garcia K.C., Steward O. and Tessier-Lavigne M. (2005) Genetic deletion of the Nogo receptor does not reduce neurite inhibition in vitro or promote corticospinal tract regeneration in vivo. Proc. Natl. Acad. Sci. USA, 102: 1205-10.

Zheng B., Ho C., Li S., Keirstead H., Steward O. and Tessier-Lavigne M. (2003) Lack of enhanced spinal regeneration in Nogo-deficient mice. Neuron, 38: 213-24.

Zhou Z.M., Sha J.H., Li J.M., Lin M., Zhu H., Zhou Y.D., Wang L.R., Zhu H., Wang Y.Q. and Zhou K.Y. (2002) Expression of a novel reticulon-like gene in human testis. Reproduction, 123: 227-34.

Zörner B. and Schwab M.E. (2010) Anti-Nogo on the go: from animal models to a clinical trial. Ann. N.Y. Acad. Sci., 1198: E22-34.

Primers used for DNA constructs Appendix 1

Primer name	Primer sequence	FW/RV	RE
A-P1	5’ GGTCCTCGAGGAAGACCTGGACCAGTCTCCTCTGG 3’	FW	Xho1
A-P2	5’ GGGCACGGTCGACGACACCGGGCTC 3’	RV	Sal1
A-P3	5’ GCAGATGGAGGAGCTCAGTACTGC 3’	FW	Sac1
A-P4	5’ GCCGTAGAGCTCGCGGCCGCTCACTGATGCCGTTCATA AATAAC 3’	RV	Not1
A-P5	5’ CCTCTCTCTAGAAGTCTTCTTAATGTCTTCC 3’	RV	Xba1
A-P6	5’ CTAGTGTCTAGAAGGATATACAAGGGTGTGATC 3’	Fw	Xba1
A-P7	5’ GAGCTCGCGGCCGCATCAGCGCTT 3’	RV	Not1
A-P8	5’ CTAAATGAGCTCGCGGCCGCTCACTTCAGAGAATCAACT AAATC 3’	RV	Not1
A-P9	5’ CCTCTCTCTAGATCAAGTCTTCTTAATGTCTCTCC 3’	RV	Xba1
A-P10	5’ GTTCGAATTCGATTTCCCATCTGTCCTGCTTG 3’	FW	EcoR1
A-P11	5’ GCTCCTCGAGTCAACTATCTTTCACTTCCCATACTCG 3’	RV	Xho1
A-P12	5’ CGGGAATTCAGGATATACAAGGGTGTGATCCAAGC 3’	FW	EcoR1
A-P13	5’ CGATCTCGAGTCACTGAACCAACTCCTCAGATATAGC 3’	RV	Xho1
A-P14	5’ CCCGCTCGAGTCAAGAATTACTGTACTTCTGAACC 3’	RV	Xho1
A-P15	5’ CATCTCGAGTCACTTCAGAGAATCAACTAAATCATC 3’	RV	Xho1
B-P1	5’ GGGAGAATTCAGAAGACCTGGACCAGTCTCCTCTGG 3’	FW	EcoR1
B-P2	5’ TGAGCCCGAGGAGCCCCTGCGCTTGGG 3’	RV	-
B-P3	5’ GTGGTTGTTGACCTCCTGTACTGGAGAG 3’	FW	-
B-P4	5’ CCTAGCGGCCGCTCATTCAGCTTTGCGCTTCAATCC 3’	RV	Not1
B-P5	5’ GGTCGAATTCATGGAAGACCTGGACCAGTCTCCTCTGG 3’	FW	EcoR1
B-P6	5’ CCTCTGCGGCCGCTCACACTCCAGTCTTCTTAATGTCTCTCC 3’	RV	Not1
B-P7	5’ GGTAGCGGCCGCTCACTTGTATATCCTAAAGCTGATGG 3’	RV	Not1
C-P1	5’ GAGGGAATTCAACCATGGACGGTCAGAAGAAAAATT GGAAGGACAAGGTTGTTGACCTCCTGTACTGGAG 3’	FW	EcoR1
C-P2	5’ GAGGAATTCAGACGGTCAGAAGAAAAATTGGAAGGACA AGGTTGTTGACCTCCTGTACTGGAG 3’	FW	EcoR1
1-P1	5’ CTAGCTCGAGGCCGCACCGCCGGATC 3’	FW	Xho1
1-P2	5’ GCGGGTCGACCTACTCAGCGTGCCTCTTGGCG 3’	RV	Sal1
2-P1	5’ CTTCCTCGAGGGGCAGGTCCTGCCGGTCTTC 3’	FW	Xho1
2-P2	5’ CCTAGTCGACTCATTCGGCTTTGGCTTTGGATCC 3’	RV	Sal1
3-P1	5’ CCTGGAATTCAACCATGGCGGAGTCGTCAGCGGCCACTC AGTCC 3’	FW	EcoR1
3-P2	5’ CGTTGTCGACTTATTCTGCCTTTTTTTTGGCGATTCCA GGAAGCTTTGC 3’	RV	Sal1
3-P3	5’ GGTTGAATTCAGTGAAGAAGACTGGGTTTGTCTTTGG 3’	FW	EcoR1
3-P4	5’ CTAAGAGCTCAGTCTTCTTCACATCTCGCCAGAAAATC 3’	RV	Sac1
3-P5	5’ GTGTGAGCTCAGAGTCTATAAGTCTGTCATTCAAGCTGTG 3’	FW	Sac1
3-P6	5’ GACCGAGCTCCTTCAAGGAGTCAACCAAGTCTTCTACCA G 3’	RV	Sac1
3-P7	5’ GTTAGAGCTCACACAGATTGACCACTATGTTGGGATTG 3’	FW	Sac1
Caspr-P1	5’ CCATGAATTCAATCATCGCTATAAGGGCTCCTACC 3’	FW	EcoR1
Caspr-P2	5’ CTTGCTCGAGTCAGATCTGGGGTAGGTTC 3’	RV	Xho1
Caspr2-P1	5’ CGGGAATTCCGGTACATGTTCCGCCACAAGGGC 3’	FW	EcoR1
Caspr2-P2	5’ CTTTCTCGAGTCAAATGAGCCATTCCTTTTTGCTTTC 3’	RV	Xho1

Note: Underlined bases – RE site. FW – forward. RV – reverse.

Primary antibodies used in western blotting Appendix 2

Antigen	Antibody's cat no. (Co.)	Dilution
AIF	sc-13116	1:1000
p-Akt (thr308)	9275 (Cell Signaling Tech)	1:1000
p-Akt (ser473)	9277 (Cell Signaling Tech)	1:1000
Akt	9272 (Cell Signaling Tech)	1:2000
AR2	a gift (refer to section 2.7.1)	1:5000
Bax (activated)	sc-493	1:1000
Bax (total)	sc-20067	1:500
Bcl-2	551107 (BD Biosciences)	1:500
Bcl-xL	2762 (Cell Signaling Tech)	1:1000
Bid	sc-6538	1:500
Caspr	-	1:1000
Caspr 2	-	1:1000
c-myc (9E10)	sc-40	1:1000
Cu/Zn-SOD	07-403 (Upstate)	1:1000
p-EIF2α	9721 (Cell Signaling Tech)	1:1000
EIF2α	9722 (Cell Signaling Tech)	1:1000
p-Erk1/2 (thr202/tyr204)	9101 (Cell Signaling Tech)	1:1000
Erk1/2	4696 (Cell Signaling Tech)	1:2000
GRP78	sc-13968	1:500
GRP94	sc-1794	1:1000
p-GSK3α/β (ser21/9)	9331 (Cell Signaling Tech)	1:1000
GSK3α	9338 (Cell Signaling Tech)	1:2000
GSK3β	9315 (Cell Signaling Tech)	1:2000
HA (12CA5)	-	1:1000
NF-κB p65	sc-8008	1:500
Ng1V2	-	1:2000
Nogo	sc-11027	1:2000
PARP	9532 (Cell Signaling Tech)	1:5000
RTN3	AB72814 (Abcam)	1:2000
Tuj	T8660 (Sigma-Aldrich)	1:1000
γ-tubulin	T6557 (Sigma-Aldrich)	1:5000

Note: Upstate (Charlottesville, Virginia, USA).
Cell Signaling Technology (Danvers, Masachusetts, USA).
(-) refers to “homemade”.